Composites: Mechanics, Computations, Applications
An International Journal

YURY G. YANOVSKY
EDITOR-IN-CHIEF

AIMS AND SCOPE

Composites: Mechanics, Computations, Applications, An International Journal seeks to provide a central vehicle for exchange of basic ideas in the mechanics of composite materials and structures between the research workers and engineers located throughout the world. Only those papers that convey original unpublished research of permanent interest will be accepted for publication. In all cases, the highest priority will be given to those contributions which increase our basic understanding of the mechanics of composite materials and structures and of its application to computational and engineering problems. The subjects covered in this journal include, but are not limited to: the mechanics of structured, homogeneous, and heterogeneous media with complex rheological properties and phase transitions; thermodynamics, physicochemical mechanics and micromechanics of composite materials; the properties of fibers, matrices, and of an interphase layer; methods of averaging; numerical methods in the mechanics of heterogeneous media and composites; computer simulation of the behavior of composites; diagnostics and accumulation of faults; strength, rigidity, durability, and mechanics of disintegration of composites; composite plates and shells; methods for calculation of composite structures; static and dynamic problems; interaction with the environment; intellectual (active, adaptive) materials and structures; natural composites and biocomposites; technological mechanics of composites; methods of experimental study of composites and composite structures.

Yu.G.Yanovsky
Editor-in-Chief

Printed February 28, 2010

Composites: Mechanics, Computations, Applications, An International Journal

PROCEDURES TO BUILD PLATE MICROMECHANICAL MODELS FOR COMPOSITES LIKE PERIODIC BRICKWORKS: A CRITICAL REVIEW

Antonella Cecchi

Università IUAV di Venezia, Facoltà di Architettura,
Dorsoduro 2206 - 30123 Venezia, ITALIA; cecchi@iuav.it

Procedures for constructing plate models to describe the out-of-plane mechanical behavior of regular brickwork are proposed. Both asymptotic homogenization procedures and direct identification procedures — methods based on balance by internal work in the discrete model and in the continuous model for a class of regular motions — have been proposed to obtain relations between the 3D discrete model and the 2D plate continuum model. A crucial problem, with the choice of identification procedures, is how kinematic, dynamic, and constitutive prescriptions of a discrete system are transferred to the continuous one. Hence, constitutive functions of the plate may be different. A Love–Kirchhoff plate model based on standard homogenization, for linear elastic periodic brickwork, has been already proposed by Cecchi and Sab (2002b). This model has been also developed in the case both of infinitely rigid blocks and of elastic blocks connected by elastic interfaces taking into account shear effects leading to the identification of a new Mindlin–Reissner homogenized plate model (Cecchi and Sab, 2004, 2006). In this case, the identification between the 3D block discrete model and the 2D plate continuum model is based on a relation at the order 1 in the displacement and at the order 0 in the rotation. The Mindlin–Reissner model when blocks are rigid blocks based on a compatible identification at the order 1 both in the displacement and in the rotation has been performed by Cecchi and Rizzi (2003, 2005). Here these models have been implemented also in the case of elastic blocks. The idea is to critically analyze the accuracy of these identification models by comparison with a 3D F.E. model for some meaningful case.

KEY WORDS: *periodic brickwork, Love–Kirchhoff plate, Mindlin–Reissner plate, asymptotic homogenization, equivalent compatible method*

1. INTRODUCTION

Modelling composite materials like brickwork is a difficult task. If a composite brickwork-like material is modelled as a "molecular skeleton", hence the number of degrees of freedom is finite. The interactions between the molecules (rigid blocks) that, across interfaces, mutually exchange forces and moments depend on the geometric microstructure of the composite (Bazant et al., 1990; Lofti and Shing, 1994; Schlangen and Garbozci, 1996; Markov, 1999; Lourenço and Rots, 1997).

The out-of-plane behavior of masonry may be of interest in the case of scarf joint masonry panels. The masonry skeleton can be reasonably represented by a 3D discrete system of blocks that interact through elastic mortar thin joints. However, the high number of degrees of freedom in the 3D case represents a not negligible drawback. As a consequence, many researchers are led to use equivalent continuum models; in particular, 2D models resulted to be reliable to describe the behavior of masonry panels subject to both in-plane and out-of-plane actions (Salerno and de Felice, 1999, 2000; Masiani et al., 1995; Trovalusci and Masiani, 1996; Cecchi and Sab, 2002a,b; de Felice, 1995).

In the case of historical masonries, rigid body systems (the blocks — brick blocks or stone blocks) interacting by elastic interfaces (the mortar thin joints) may be assumed as a first reliable model. In fact here the ratio between the elastic coefficient block/mortar is sufficiently high (Cecchi and Sab, 2002a,b) and the mortar joint thickness is sufficiently small if compared to the block size. A second model, where the blocks are elastic bodies that interact by elastic interfaces, has been built. This latter model may be predictive on the masonry behavior under service loads.

When a 3D discrete system is modelled as a continuum, a crucial question is how the kinematic, static descriptors and constitutive prescriptions are transferred to the continuum model. In particular, the former question is which continuum model has to be used to represent the discrete system, the latter question is which procedure has to be used to characterize the continuum model starting from the discrete system.

Here the attention is focused on the case of out-of-plane actions. Hence the 2D continuum is a plate model, that signifies a continuum with a rigid internal microstructure.

Therefore the answer to the first question may be twofold: the Love–Kirchhoff plate model or the Mindlin–Reissner plate model. It is well known that when the ratio of the thickness of a homogeneous plate over its overall size goes to zero, then the 3D solution converges to the Love–Kirchhoff solution. Caillerie (1984) has extended this result to periodic plates. More precisely, on the basis of the theoretical homogenization results of Caillerie (1984), it can be shown that the 3D discrete system may be accurately approximated by the Love–Kirchhoff homogeneous plate model, under the following three assumptions: 1) the 3 dimensions of the block that constitute the periodic brickwork [a — weight of the block, b — height of the block, and t — thickness of the block] are of the same order, 2) the considered structure is large enough and 3) the applied actions are smooth enough. In the other cases, the Mindlin–Reissner model may be more consistent.

The second question requires some preliminary remarks. The transfer of constitutive prescriptions from a heterogeneous body to a homogeneous continuum one is often performed by reference to standard homogenization methods (Sanchez-Palencia, 1980; Suquet, 1987); procedures based on homogenization methods are used to provide constitutive prescriptions for masonry panels subject to in plane and out of

plane actions, see (Lourenço and Rots, 1997; Zuccini and Lourenço, 2002; Anthoine, 1995; Cecchi and Sab, 2002b). A suitable field problem is defined and solved, on a representative elementary volume (R.E.V.), before using average operations, to determine the constitutive homogenized functions.

Other procedures may be found in the literature, as methods based on equivalence relations between discrete system and continuum model proposed in (Salerno and de Felice, 1999, 2000; Masiani et al., 1995; Trovalusci and Masiani, 1996; Cecchi and Rizzi, 2003, 2005), not necessarily based on the solution of an elastic field problem. In order to link the behavior on the micro (discrete) level to the macro (continuum) level, the internal work of the discrete system has to be written as a function of the deformation variables for the continuum. This requires, in principle, the choice of a kinematic correspondence between the motion in the two models and the writing of the internal work of the discrete system in terms of the strain in the continuum. Alternatively, in a dual form, the internal work of the discrete system may be written in terms of the stress in the continuum, by selecting an appropriate correspondence between the stress in the two systems. Therefore, both approaches generally are based on an approximation, due respectively to equilibrium or compatibility assumptions and depending on the correspondence postulated. As is well known the choice of uniform strain or uniform stress, in the discrete system, corresponds to the well-known Voigt and Reuss bounds in homogenization.

The principal aim of this paper is to compare the results of an asymptotic homogenization method with the results obtained from a compatible equivalent procedure both at the constitutive level and at a structural level for some meaningful cases.

2. ASYMPTOTIC MULTIPARAMETER MODEL FOR REGULAR BRICKWORK

A masonry panel may be represented by a regular system of blocks connected by elastic joints. A characteristic module, called in the literature R.E.V. (representative elementary volume) may be found. This module must be chosen such as is able to contain, in a small scale, all the kinematic, dynamic and constitutive descriptors of the body as a whole.

A first simplification of the 3D blocks discrete system is to model the elastic mortar joints as linear interfaces of zero thickness. Hence a φ parameter — the ratio between the mortar joint size (s^h = bed joint and s^v = head joint) and the characteristic size of the module (a = weight of the block and b = height of the block): $\varphi = s^h/a = s^v/(kb)$ is introduced. k is a further parameter which takes into account the possibility that head and bead joints may have not the same thickness ratio. The obtained continuum depends, when $\varphi \to 0$, also on the ratio between the $\mathbf{a}^B$ constitutive function of the block and the $\mathbf{a}^M$ constitutive function of the mortar. If, for simplicity, block and mortar are both isotropic, then a parameter ξ is defined by $\xi = \dfrac{E^M}{E^B}$, where E is the Young modulus of the two materials. Hence,

it may be written: $\mathbf{a}^M = \xi\mathbf{a}$, where $\mathbf{a}$ is the isotropic elasticity tensor with the Young modulus of the block and the Poisson ratio of the mortar.

In this study, for fixed elastic tensors (Cecchi and Sab, 2002a,b) $\mathbf{a}^B$ and $\mathbf{a}$, and for fixed geometric parameters a, b, t, and k, the focus is on the asymptotic case:

$$\xi \to 0 \qquad \varphi \to 0 \ .$$

In fact, if φ tends to zero, then the mortar joint becomes an interface (such problem has been studied by Klarbring (1991) by means of perturbative techniques). If ξ tends to zero, then the mortar becomes infinitely deformable with respect to the block. Therefore, the asymptotic problem depends on how ξ and φ parameters tend to zero. Considering $\xi = \xi(\varphi)$, Cecchi and Sab (2202a) have pointed out three relevant cases.

- **case 1:**

$$\lim_{\varphi \to 0} \xi(\varphi)\varphi^{-1} = +\infty$$

the joint is perfectly cohesive, φ tends to zero more quickly than ξ. Hence, there is a perfect continuity between the blocks, i.e., the displacement at the interface $u^+ = u^-$ (monolithic body), which may be assumed as one single homogeneous material. Then

$$\lim_{\substack{\xi\varphi^{-1}\to\infty \\ \varphi\to 0}} (\mathbf{A}^{\xi\varphi}) = (\mathbf{a}^B) \ ,$$

where $\mathbf{A}^{\xi\varphi}$ is the homogenized elastic tensor and $\mathbf{a}^B$ is the elastic tensor of the block

- **case 2:**

$$\lim_{\varphi \to 0} \xi(\varphi)\varphi^{-1} = \omega \neq 0 \ .$$

The obtained asymptotic problem exhibits a cohesive zero thickness interface between the blocks with a possible jump of the displacement. The constitutive function of the interface is a linear relation between the tractions on the block surfaces and the jump of the displacement field. If I is the interface, $\mathbf{u} = [[\mathbf{u}(y)]]$ is the jump of the displacement field at I. The $\mathbf{K}$ constitutive function at the interface is given by:

$$\mathbf{K}_{ij} = \frac{1}{s} \, a^M_{iklj} \, \mathbf{n}_k \mathbf{n}_l \ . \tag{1}$$

Here s is the thickness of the real joint and $\mathbf{n}$ is the normal to the interface. In the isotropic case, the above expression becomes:

$$\mathbf{K} = \frac{1}{s} \, (\mu^M \mathbf{I} + (\mu^M + \lambda^M) \, (\mathbf{n} \otimes \mathbf{n})) \ , \tag{2}$$

where μ^M and λ^M are the Lamé constants of the mortar (Klarbring, 1991; Avila-Pozos et al., 1999). Note that $\mathbf{K}$ tensor has a diagonal form in this case. This is a consistent simplification, in fact the transversal contraction, due to the zero thickness of the joint, is not taken into account. Moreover, in what follows $\mathbf{K} = \mathbf{K}^h$ is used for the horizontal interfaces and $\mathbf{K} = \mathbf{K}^v$ for the vertical interfaces.

The limit relation between the homogenized elastic tensors $\mathbf{A}^{\xi\varphi}$ and the asymptotic homogenized elastic tensors $\mathbf{A}^H$ is

$$\lim_{\substack{\xi\varphi^{-1}\to\omega \\ \varphi\to 0}} (\mathbf{A}^{\xi,\varphi}) = \lim_{\xi\varphi^{-1}\to\omega} (\mathbf{A}^H) \ ,$$

- **case 3:**

$$\lim_{\varphi\to 0} \xi(\varphi)\varphi^{-2} = \omega \neq 0 \ .$$

This condition corresponds to infinitely rigid blocks connected by elastic interfaces. It means that the strain $\in = 0$ in the blocks and that the stress σ remains undetermined inside the blocks.

The limit relation between these asymptotic homogenized elastic tensor and the already introduced elastic tensor, when blocks are rigid, is

$$\lim_{\substack{\xi\varphi^{-2}\to\omega \\ \varphi\to 0}} \varphi^{-1} (\mathbf{A}^{\xi\varphi}) = \lim_{\substack{\varphi\to 0 \\ \xi\varphi^{-2}\to\omega}} \varphi^{-1} (\mathbf{A}^H) = \lim_{\xi\varphi^{-2}\to\omega} \varphi^{-1} (\mathbf{A}^F) \ .$$

In what follows, cases 2 and 3 are studied, hence two models for the masonry panel are considered: the former corresponds to case 3 — rigid blocks connected by linear elastic interfaces; the latter corresponds to case 2 — elastic blocks connected by linear elastic interfaces.

3. RIGID BLOCKS CONNECTED BY LINEAR INTERFACES — Case 3 of Section 2

The idea is to propose two procedures to identify the 3D discrete system with 2D continuous plate models. In particular, the first approach proposed is an asymptotic multi-parameter homogenization procedure (Cecchi and Sab, 2002b), the second is a compatible equivalent procedure (Cecchi and Rizzi, 2003, 2005). In both the approaches, an R.E.V. is defined, such as shown in Fig. 1. The module must be chosen such as it contains in a small scale all the mechanical and geometrical information to describe the body as a whole. It must be noted that the two R.E.V. chosen in Fig. 1 for the two adopted procedures show some differences that depend on technical motivation in the solution of two methods (i.e., imposition of boundary conditions). It must also be noted that the dimension of the module is the same ($a \times b \times t$).
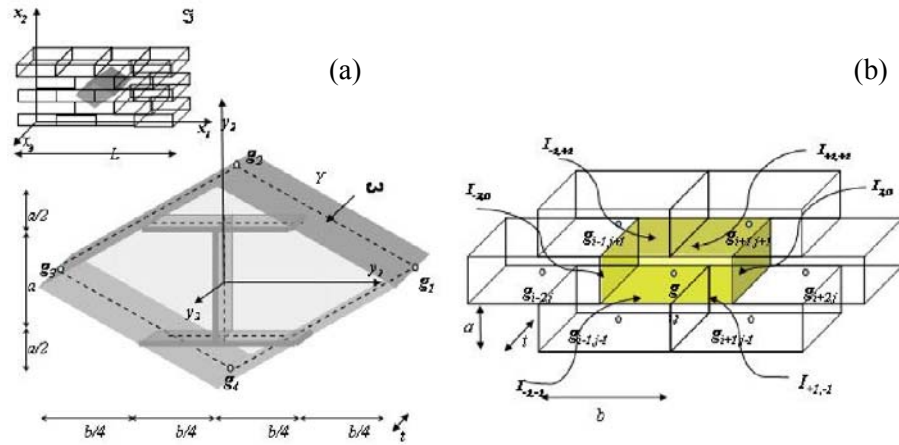
FIG. 1: a) R.E.V. used in the homogenization procedure; b) R.E.V. used in the compatible procedure

3.1 3D Discrete System

By defining by ε the three-dimensional Euclidean manifold of the body and by ν its translation space, the motion of a generic block B_i may be described by means of the relationships

$$\mathbf{u}^i \in \nu, \quad \omega^i \in \mathrm{Skw}\nu , \tag{3}$$

where $\mathbf{u}^i$ and ω^i are, respectively, the displacement of the centre of the block and its rotation. Hence the rigid motion of the generic i-block is:

$$\mathbf{u}^i(y) = \mathbf{u}^i + \omega^i \Lambda (y - \mathbf{y}^i) , \tag{4}$$

where $\mathbf{y}^i$ is the center of the i-block, $\mathbf{u}^i$ is its translation, and ω^i is its rotation vector.

Additionally, the interaction of a couple of blocks (B_i, B_{i+1}) has been taken into account. Let p be the center of the I interface between B_i and B_{i+1} (Fig. 2). The displacement of the material points of B_i and B_{i+1} in contact in a place $\xi \in I$ may be written as

$$\mathbf{u}^i(\xi) = \mathbf{u}^i(p) + \omega^i(\xi - p) ,$$

$$\tag{5}$$

$$\mathbf{u}^{i+1}(\xi) = \mathbf{u}^{i+1}(p) + \omega^{i+1}(\xi - p) ,$$

The jump of the displacement, for a generic point $\xi \in I$ is assumed as a local deformation measure, hence
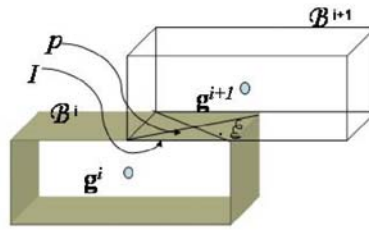
FIG. 2: The interactionn between the couple of blocks

$$[[\mathbf{u}]](\xi)]] = \mathbf{u}^{i+1}(\xi) - \mathbf{u}^{i}(\xi)$$

$$= \mathbf{u}^{i+1}(p) - \mathbf{u}^{i}(p) + \omega^{i+1}(\xi - p) - \omega^{i}(\xi - p) \qquad (6)$$

$$= \mathbf{u}_p + \omega_p(\xi - p) \ ,$$

where

$$\mathbf{u}_p = \mathbf{u}^{i+1}(p) - \mathbf{u}^{i}(p), \ \omega_p = \omega^{i+1} - \omega^{i}.$$

Setting a spatial field $\mathbf{t}^{i}(\xi)$ and $\mathbf{t}^{i+1}(\xi)$ of the contact force, respectively with the B_i and B_{i+1} blocks, for the dynamic balance $\mathbf{t}^{i}(\xi) = -\mathbf{t}^{i+1}(\xi)$.

3.2 Continuous Models

In this phase, separately respect the discrete model, the definition of two plate continuous models are proposed. The following notations are used: Greek index α, β = 1, 2; Latin index i, j = 1, 2, 3. Here, the term plate is used to describe a bi-dimensional continuum, identified by an S plane middle surface of the plate in which the points are characterized by a microstructure represented by a $\mathbf{e}_3$ unit vector which in the reference configuration is orthogonal to S (Fig. 3).

The kinematics is described by the fields $\mathbf{u}$ that represent the displacement of the points of S and ω that represent the rotation of the associated unit vectors. The
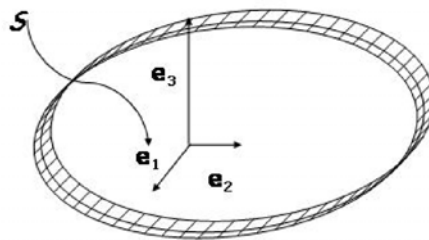
FIG. 3: Plate geometric definition

dynamics is described by the fields $\mathbf{N}$ and $\mathbf{M}$ that represent the stress tensor and the couple stress tensor, respectively. If the Love–Kirchhoff model is considered, then $\mathbf{N} = (N_{\alpha,\beta})$ is the macroscopic in-plane (membranal) stress field for the homogenized plate; $\mathbf{M} = (M_{\alpha,\beta})$ is the macroscopic out-of-plane (flexural) stress field for the homogenized plate; $\mathbf{E} = (E_{\alpha,\beta})$ is the corresponding in-plane strain field; $\mathbf{\chi} = (\chi_{\alpha,\beta})$ is the corresponding out-of-plane strain field; $\mathbf{u} = (u_i)$ is a displacement field. The displacement fields are defined in terms of the components: $u_1(x_1, x_2)$, $u_2(x_1, x_2)$, and $u_3(x_1, x_2)$ and the corresponding strains are: $E_{\alpha,\beta} = \frac{1}{2}(u_{\alpha,\beta} + u_{\beta,\alpha})$, $E_{i3} = 0$, $\chi_{\alpha\beta} = -u_{3,\alpha\beta}$, and $\chi_{i3} = 0$. The plate constitutive law is

$$\mathbf{N} = \mathbf{AE} + \mathbf{B\chi} \tag{7}$$

$$\mathbf{M} = {}^{T}\mathbf{BE} + \mathbf{D\chi} \tag{8}$$

In the case of the central symmetry of the plate $\mathbf{B} = 0$, then the in-plane plate constitutive functions take the following form

$$\begin{cases} N_{11} = A_{1111}E_{11} + A_{1122}E_{22}, \\ N_{22} = A_{1122}E_{11} + A_{2222}E_{22}, \\ N_{12} = 2A_{1212}E_{12}, \end{cases} \tag{9}$$

and out-of-plane ones are:

$$\begin{cases} M_{11} = D_{1111}\chi_{11} + D_{1122}\chi_{22}, \\ M_{22} = D_{1122}\chi_{11} + D_{2222}\chi_{22}, \\ M_{12} = 2D_{1212}\chi_{12}. \end{cases} \tag{10}$$

Shear effects are not taken into account in the Love–Kirchhoff model. In order to enhance this model, the Mindlin–Reissner plate model may be considered. The strain tensors are related to displacement and rotation field components as follows: $E_{\alpha\beta} = \frac{1}{2}(u_{\alpha,\beta} + u_{\beta,\alpha})$, $\gamma = (\gamma_\alpha)$, $\gamma_\alpha = u_{3,\alpha} + \theta_\alpha$, $\chi_{\alpha\beta} = \frac{1}{2}(\theta_{\alpha,\beta} + \theta_{\beta,\alpha})$. The stress tensors are $\mathbf{N} = (N_{\alpha\beta}(x_1, x_2))$, $\mathbf{M} = (M_{\alpha\beta}(x_1, x_2))$ and the shear stress vector is $\mathbf{T} = (T_\alpha(x_1, x_2))$. The normal and bending elastic constants must be the same as those of the Love–Kirchhoff model (9)–(10) because these two models are asymptotically equivalent when the ratio $\frac{t}{L}$ goes to zero. The shear elastic constants $\mathbf{F} = F_{\alpha\beta}$ relate the shear vector $\mathbf{T}$ to the shear strain vector γ as follows:

$$T_1 = F_{11}\gamma_1, \quad T_2 = F_{22}\gamma_2, \quad F_{12} = 0 \,.$$

3.2.1 *Asymptotic homogenization procedure: the Love–Kirchhoff plate model*

Assumed a R.E.V., an auxiliary field problem is formulated in it. The solution of this problem provides the homogenized constitutive functions that must be used in the macroscopic solution of the field problem. In particular, if the idea is to model the 3D discrete system as a plate model and if the study is focused on the actions characterized by wavelength much larger than the one of the size of the blocks, the generic masonry wall may be identified with the Love–Kirchhoff plate, as it has been demonstrated by Caillerie (1984).

Given a reference system ($\mathbf{x}$) for the global description of the body $\mathfrak{I}$ (macroscopic scale) and a reference system ($\mathbf{y}$) for the elementary module Y which is defined as (Fig. 1a):

$$Y = \omega \times \left]-\frac{t}{2}, \frac{t}{2}\right[\, ,$$

where $Y \subset \mathfrak{R}^3$ and $\omega \subset \mathfrak{R}^2$; the boundary of Y is denoted:

$$\partial Y = \partial Y_l \cup \partial Y_3^+ \cup \partial Y_3^- \, , \quad \partial Y_3^\pm = \omega \times \pm \frac{t}{2}$$

Then, the following definitions are proposed:

$$\varepsilon = \frac{a}{L} \qquad \zeta = \frac{t}{L} \, .$$

Here L is the overall length of the plate, a is the in plane dimension of the module, ζ is the ratio between the thickness of the module t, and L.

The constitutive law of masonry modelled as the Love–Kirchoff plate can be expressed in terms of its 3D characteristics when the asymptotic problem exhibits cohesive zero thickness interfaces between the blocks with a possible jump of the displacements. The constitutive function of the interface is a linear relation between the tractions on the block surfaces and the jump of the displacement field. The following field problem is formulated on the unit cell with zero thickness joints:

$$\begin{cases} \text{div } \boldsymbol{\sigma}^H & = \ 0 \\ \varepsilon & = \mathbf{E} + y_3 \boldsymbol{\chi} + sym(grad\mathbf{u}^{per}) \\ \boldsymbol{\sigma}^H \mathbf{e}_3 & = 0 \ \text{on } \partial Y_3^+ \ \text{and } \partial Y_3^- \\ \boldsymbol{\sigma}^H \mathbf{n} & \quad \text{antiperiodic on } \partial Y_l \\ \mathbf{u}^{per} & \quad \text{periodic on } \partial Y_l \\ \boldsymbol{\sigma}^H \mathbf{n} & = \mathbf{Ku} \ \text{interface constitutive relation on } I \end{cases} \qquad (11)$$

where I is the interface, $\mathbf{u} = [[\mathbf{u}(y)]]$ is the jump of displacement field at I, and $\mathbf{K}$ is given by (2); σ^H is the Cauchy stress tensor; $\mathbf{u}^{per}$ is an ω-periodic displacement

field; $\mathbf{E}$ is the macroscopic in-plane strain tensor of the plate (membranal strain); $\boldsymbol{\chi}$ is the out-of-plane strain tensor (curvature tensor). The macroscopic tensors are related to the macroscopic displacement field components $u_1(x_1, x_2)$, $u_2(x_1, x_2)$, and $u_3(x_1, x_2)$ as follows: $\mathbf{E}_{\alpha\beta} = \frac{1}{2}(u_{\alpha,\beta} + u_{\beta,\alpha})$, $\mathbf{U}_{i3} = 0$, $\chi_{\alpha\beta} = -u_{3,\alpha\beta}$, and $\chi_{i3} = 0$ with the Greek index $\alpha, \beta = 1, 2$, while the Latin index $i, j = 1, 2, 3$; $\langle t \rangle^* = \frac{1}{S}\int_Y f(y_1, y_2, y_3)$ $\times dy_1 dy_2 dy_3$; S is the area of ω.

The case

$$\lim_{\varphi \to 0} \xi(\varphi)\varphi^{-2} = \omega \neq 0$$

is now taken into account. This condition corresponds to infinitely rigid blocks connected by an elastic interface. It means that $\varepsilon = 0$ in (11) and that σ remains undetermined inside the blocks. Since $\varepsilon = 0$ and $\mathbf{u}$ is discontinuous at the interfaces, then $\mathbf{u}$ is a rigid body displacement on each block. The rigid motion on the generic i-block is 4. By reference to the chosen R.E.V., the displacement field corresponding to ε in (11) is defined by

$$sym(grad(\mathbf{u})) = \mathbf{E} + y_3\boldsymbol{\chi} + sym(grad(\mathbf{u}^{per})) , \tag{12}$$

where $\mathbf{E}$ is the macroscopic membranal strain tensor and $\boldsymbol{\chi}$ is the macroscopic curvature tensor. Therefore, up to a rigid body motion, the displacement field is given by:

$$\mathbf{u} = \begin{pmatrix} E_{11}y_1 + E_{12}y_2 + y_3(\chi_{11}y_1 + \chi_{12}y_2) + u_1^{per} \\ E_{12}y_1 + E_{22}y_2 + y_3(\chi_{12}y_1 + \chi_{22}y_2) + u_2^{per} \\ -(\frac{1}{2}\chi_{11}y_1^2 + \chi_{12}y_1y_2 + \frac{1}{2}\chi_{22}y_2^2) + u_3^{per} \end{pmatrix}. \tag{13}$$

It must be noted the periodicity condition in the displacement field impose that all the blocks have same rotation.

The asymptotic constitutive law of the plate becomes:

$$\mathbf{N} = \langle \boldsymbol{\sigma}^H \rangle^* = \mathbf{A}^H\mathbf{E} + \mathbf{B}^H\boldsymbol{\chi} = \mathbf{A}^F\mathbf{E} + \mathbf{B}^F\boldsymbol{\chi} \tag{14}$$

$$\mathbf{M} = \langle y_3 \boldsymbol{\sigma}^H \rangle^* = {}^T\mathbf{B}^H\mathbf{E} + \mathbf{D}^H\boldsymbol{\chi} = {}^T\mathbf{B}^F\mathbf{E} + \mathbf{D}^F\boldsymbol{\chi} \tag{15}$$

The asymptotic homogenized plate tensors are defined in the following variational form:

$$\mathbf{E}\cdot(\mathbf{A}^F\mathbf{E}) + 2\boldsymbol{\chi}\cdot(\mathbf{B}^F\mathbf{E}) + \boldsymbol{\chi}\cdot(\mathbf{D}^F\boldsymbol{\chi}) = \min_{u^{per}\ \omega-periodic,\ \varepsilon=0} \frac{1}{|S|}\int_I [[\mathbf{u}]]\cdot\mathbf{K}[[\mathbf{u}]]\,ds.$$

The limit relation between these asymptotic homogenized elastic plate tensors and the elastic plate tensors is:

$$\lim_{\substack{\xi\varphi^{-2}\to\omega \\ \varphi\to 0}} \varphi^{-1}\begin{pmatrix} \mathbf{A}^{\xi\varphi} & \mathbf{B}^{\xi\varphi} \\ {}^{T}\mathbf{B}^{\xi\varphi} & \mathbf{D}^{\xi\varphi} \end{pmatrix} = \lim_{\substack{\varphi\to 0 \\ \varphi^{-2}\to\omega}} \varphi^{-1}\begin{pmatrix} \mathbf{A}^{H} & \mathbf{B}^{H} \\ {}^{T}\mathbf{B}^{H} & \mathbf{D}^{H} \end{pmatrix} = \lim_{\xi\varphi^{-2}\to\omega} \varphi^{-1}\begin{pmatrix} \mathbf{A}^{F} & \mathbf{B}^{F} \\ {}^{T}\mathbf{B}^{F} & \mathbf{D}^{F} \end{pmatrix}.$$

By reference to the characteristic module shown in Fig. 1a that exhibits a central symmetry ($\mathbf{B}^{F} = 0$) the elastic homogenized membranal constants are:

$$A_{1111}^{F} = \frac{\partial^2 W}{\partial E_{11}^2} = t\,\frac{4K'_v\,\dfrac{s^h}{a} + \dfrac{b}{a}K''_h\,\dfrac{s^v}{a}}{4\,\dfrac{s^h}{a}\dfrac{s^v}{b}}, \tag{16}$$

$$A_{1122}^{F} = 0, \tag{17}$$

$$A_{2222}^{F} = \frac{\partial^2 W}{\partial E_{22}^2} = t\,\frac{K'_h}{\dfrac{s^h}{a}}, \tag{18}$$

$$A_{1212}^{F} = \frac{\partial}{2\partial E_{12}}\frac{\partial W}{2\partial E_{12}} = t\,\frac{K''_h\left(K'_h\,\dfrac{s^v}{b} + \dfrac{4a}{b}K''_v\,\dfrac{s^h}{b}\right)}{\dfrac{s^h}{a}\left(K'_h\,\dfrac{s^v}{b} + \dfrac{4a}{b}K''_h\,\dfrac{s^h}{b} + \dfrac{4a^2}{b^2}K''_v\,\dfrac{s^v}{b}\right)}. \tag{19}$$

These 3D results coincide with those of the 2D model used by de Felice (1995).

The homogenized bending constants are given by:

$$D_{1111}^{F} = \frac{\partial^2 W}{\partial \chi_{11}^2} = \frac{t}{12}\,\frac{\left[4K'_v\,\dfrac{s^h}{a} + \dfrac{b}{a}K''_h\,\dfrac{s^v}{a}\right]t^2 + \dfrac{b}{4a}\dfrac{s^v}{a}K''_h b^2}{4\,\dfrac{s^h}{a}\dfrac{s^v}{b}}, \tag{20}$$

$$D_{1122}^{F} = 0, \tag{21}$$

$$D_{2222}^{F} = \frac{\partial^2 W}{\partial \chi_{22}^2} = \frac{t^3}{12}\,\frac{K'_h}{\dfrac{s^h}{a}}, \tag{22}$$

$$D_{1212}^{F} = \frac{\partial}{2\partial \chi_{12}}\frac{\partial W}{2\partial \chi_{12}} = \frac{t}{192}\,\frac{K''_v\left(\dfrac{4s^h}{a}(a^2 + t^2)\right) + K''_h\left(\dfrac{4s^v}{b}\left(\dfrac{b^2}{4} + t^2\right)\right) + K'_h\,\dfrac{b}{a}\dfrac{s^v}{a}t^2}{\dfrac{s^h}{a}\dfrac{s^v}{b}}, \tag{23}$$

where a, b, and t are the weight, height, and the thickness of the block, the subscripts h and v identify the horizontal and vertical joints, s their width, $K' = 2\mu + \lambda$ and $K'' = \mu$.

Remark: Cecchi and Sab (2004) propose the Mindlin–Reissner plate model, where the flexural constants are the ones obtained through the Love–Kirchhoff homogenized model and the shear elastic constants are obtained through an identification with a 3D discrete model. It is demonstrated that both the Love–Kirchhoff model and Mindlin–Reissner model coincide asymptotically with the discrete 3D model as $\zeta \approx \varepsilon$ tends to zero.

3.2.2 *Compatible equivalent procedure: the Mindlin–Reissner plate model*

The basic idea of this procedure is to describe separately the 3D discrete system and the 2D plate model, then a correspondence between the kinematic descriptors is assigned *a priori*. Here the case of the Mindlinn–Reissner plate model is carried out. This corresponds to obtaining of the well-known Voight upper bound. The discrete system has been already performed in Section 3.1. Hence, it is possible to define the internal work of the contact actions at the interface as follows:

$$\pi = \int_I \mathbf{t}^i(\xi) \cdot \mathbf{u}^i(\xi) + \mathbf{t}^{i+1}(\xi) \cdot \mathbf{u}^{i+1}(\xi) \tag{24}$$

For simplicity, the following notation is introduced: $\mathbf{t}^{i+1}(\xi) = \mathbf{t}(\xi)$:

$$\pi = \int_I \mathbf{t}(\xi) \cdot [\mathbf{u}^{i+1}(\xi) - \mathbf{u}^i(\xi)] = \mathbf{t}_p \cdot \mathbf{u}_p \cdot \boldsymbol{\omega}_p \cdot \int_I \text{skw } \mathbf{t} \otimes (\xi - p) \ , \tag{25}$$

hence, the internal work may be written with the equation

$$\pi_p = \mathbf{t}_p \cdot \mathbf{u}_p + \frac{1}{2} \mathbf{M}_p \cdot \boldsymbol{\omega}_p \ , \tag{26}$$

where $\mathbf{t}_p = \int_I \mathbf{t}(\xi)$, $\mathbf{M}_p = 2\int_I \text{skw } \mathbf{t}(\xi) \otimes (\xi - p)$. Hence, at this stage, the 2D plate model is introduced separately and independently from the discrete 3D model according to Section 3.2, the Mindlin–Reissner model. Hence, the internal work evaluated on S may be written as

$$\pi = \mathbf{N} \cdot \text{sym grad } \mathbf{u} + (\mathbf{N}\mathbf{e}_3 \otimes \mathbf{e}_3) \cdot \boldsymbol{\omega} + \mathbf{M} \cdot \text{sym grad } (\boldsymbol{\omega}\mathbf{e}_3) \ , \tag{27}$$

where grad is the gradient operator on S. By indicating with an upper line the projection on S, the previous equation becomes

$$\pi = \overline{\mathbf{N}} \cdot \text{sym grad } \overline{\mathbf{u}} + \mathbf{N}\mathbf{e} \cdot (\text{grad } u_3 + \boldsymbol{\omega}\mathbf{e}_3) + \mathbf{M} \cdot \text{sym grad } (\boldsymbol{\omega}\mathbf{e}_3) \ . \tag{28}$$

In particular, $\overline{\mathbf{N}}$ are the membrane actions in the plate $\mathbf{N}\mathbf{e}_3 = \mathbf{T}$ are the shear actions in the plate, and $\mathbf{M}$ are the bending actions in the plate. The following definition is used:

$$(\boldsymbol{\omega}) = \begin{pmatrix} 0 & 0 & \omega_2 \\ 0 & 0 & -\omega_1 \\ -\omega_2 & \omega_1 & 0 \end{pmatrix}.$$

Furthermore, having assumed $\boldsymbol{\omega}\mathbf{e}_3 = \boldsymbol{\theta}$, where $\boldsymbol{\theta}$ is the plate rotation:

$$\text{grad } \boldsymbol{\omega}\mathbf{e}_3 = \begin{pmatrix} \omega_{1,2} & \omega_{2,2} \\ -\omega_{1,1} & -\omega_{1,2} \end{pmatrix} = \begin{pmatrix} \theta_{1,1} & \theta_{1,2} \\ \theta_{2,1} & \theta_{2,2} \end{pmatrix}.$$

Hence the membrane actions spend work in the membrane strain (sym grad $\overline{\mathbf{u}}$) = $\mathbf{E} \rightarrow E_{\alpha\beta} = \frac{1}{2}(u_{\alpha,\beta} + u_{\beta,\alpha})$; the shear actions spend work in the strain component orthogonal to S (grad $u_3 + \boldsymbol{\omega}\mathbf{e}_3$) = $\boldsymbol{\gamma} \rightarrow \gamma_{3\alpha} = (u_{3,\alpha} + \theta_\alpha)$, and the bendings spend work in the plate curvature (sym grad $(\boldsymbol{\omega}\mathbf{e}_3)$) = $\boldsymbol{\chi} \rightarrow \chi_{\alpha\beta} = \frac{1}{2}(\theta_{\alpha,\beta} + \theta_{\beta,\alpha})$.

A portion of the P panel equal to the R.E.V. has been considered; this portion has been chosen so that its center x^i coincides with the center of block B^i. A portion of the plate, H, with the same edge is considered, so that the x point of H coincides with x^i (Fig. 4). A correspondence between a class of regular motions in P and H is assigned

$$\mathbf{u}^i = \mathbf{u}(x), \quad \boldsymbol{\omega}^i = \boldsymbol{\omega}(x) \tag{29}$$
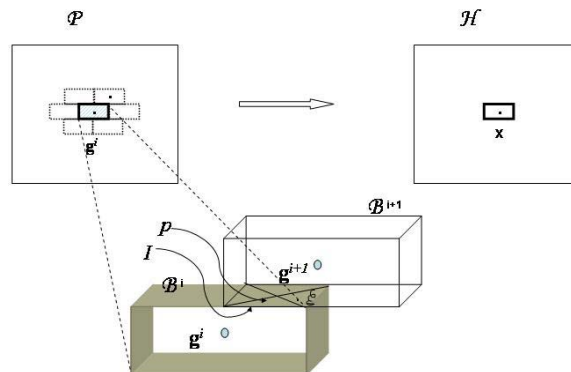
while

FIG. 4: Identification between the 3D blocks system and the plate

$$\mathbf{u}^{i+1} = \mathbf{u}(x) + \text{grad } \mathbf{u}(x)(x^{i+1} - x) \tag{30}$$

$$\boldsymbol{\omega}^{i+1} = \boldsymbol{\omega}(x) + \text{grad } \boldsymbol{\omega}(x)(x^{i+1} - x)$$

where x^{i+1} is the center of $B^{i+1} \in P$ generic block.

Let us define $\mathbf{t}_p = \bar{\mathbf{t}}_p + t_{3p}$, where the upper line identifies the projection on S of $\mathbf{t}_p$ and t_{3p} is the component orthogonal to S of $\mathbf{t}_p$. Let us consider correspondent motion tests, from Eqs. (29) and (30), Eq. (26) may be written as

$$\mathbf{t}_p \cdot \mathbf{u}_p = \bar{\mathbf{t}}_p \otimes (x^{i+1} - x^i) \cdot \text{grad}\bar{\mathbf{u}} + t_{3p}(x^{i+1} - x^i) \cdot (\text{grad}u_3 + \boldsymbol{\omega}\mathbf{e}_3)$$

$$-t_{3p}(p - x^{i+1}) \otimes (x^{i+1} - x^i) \cdot \text{grad}(\boldsymbol{\omega}\mathbf{e}_3), \tag{31}$$

$$\frac{1}{2}\mathbf{M}_p \cdot \boldsymbol{\omega}_p = \int_I (\mathbf{t}_p \otimes \mathbf{v}_p - \mathbf{v}_p \otimes \mathbf{t}_p) \cdot \text{grad}\boldsymbol{\omega}(x^{i+1} - x^i)$$

$$= \frac{1}{2}\int_I (v_{3p}\bar{\mathbf{t}}_p - t_{3p}\bar{\mathbf{v}}_p) \otimes (x^{i+1} - x^i) \cdot \text{grad}(\boldsymbol{\omega}\mathbf{e}_3), \tag{32}$$

where $\mathbf{v}_p = (\xi - p)$ and $\xi \in I$.

At this point, for a chosen R.E.V. and a chosen class of regular motions (Cecchi and Rizzi, 2003, 2005), we impose that the internal work of the contact actions on P and H coincides. Under these assumptions, the measures of stress $\mathbf{N}$ and $\mathbf{M}$ in the plate may be expressed as a function of the measures of the stress in the panel

$$\bar{\mathbf{N}} = \frac{1}{2A}\sum_n \text{sym}\bar{\mathbf{t}}_p \otimes (x^{i+1} - x^i), \tag{33}$$

$$\mathbf{T} = \frac{1}{2A}\sum_n t_{3p}(x^{i+1} - x^i), \tag{34}$$

$$\mathbf{M} = \frac{1}{2A}[\sum_n \int_I \text{sym}(v_{3p}\bar{\mathbf{t}}_p - t_{3p}\bar{\mathbf{v}}_p) \otimes (x^{i+1} - x^i)$$

$$+ \sum_n t_{3p}\text{sym}(p - x^{i+1}) \otimes (x^{i+1} - x^i)], \tag{35}$$

where A is the area of the chosen R.E.V. and the symbol Σ_n is the summation extended to all of the interfaces to which the chosen R.E.V. is in contact. It must be noted that the part of π which is associated to skw grad $\bar{\boldsymbol{\omega}}$ and to skw grad ($\boldsymbol{\omega}\mathbf{e}_3$) is not identified. In fact, in the adopted plate model these kinematic fields characterize neutral (rigid) motions. The 1/2 coefficient which appears in the above ex-

pressions for $\overline{\mathbf{N}}$, $\mathbf{T}$, $\mathbf{M}$ depends on the fact that the work expended at the interface between a generic couple of blocks (B^i, B^{i+1}) provides a contribution to both blocks.

By assuming the constitutive function (2) in Eqs. (33)–(35) the constitutive equivalent functions are obtained. This constitutive function gives the response functions of the actions in the middle surface $\overline{\mathbf{N}}$, of the actions orthogonal to the middle surface $\mathbf{T}$ and of the couples $\mathbf{M}$.

For the R.E.V., only one block was chosen. The single block (Fig. 1b) is in contact with six blocks by means of four horizontal interfaces and two vertical interfaces.

The coefficients different from zero are listed hereafter:

$$A_{1111}^{\text{comp}} = \frac{4K_v'\dfrac{s^h}{a} + \dfrac{b}{a}K_h''\dfrac{s^v}{a}}{4\dfrac{s^h}{a}\dfrac{s^v}{b}}, \tag{36}$$

$$A_{2222}^{\text{comp}} = \frac{K_h'}{\dfrac{s^h}{a}}, \tag{37}$$

$$A_{1212}^{\text{comp}} = \frac{1}{2}[K_h''\frac{a}{2s^h} + \frac{b}{4a}K_h'\frac{b}{2s^h} + K_v''\frac{b}{2s^v}], \tag{38}$$

$$F_{11}^{\text{comp}} = [K_h''\frac{b}{s_h}t\frac{b}{4a} + K_v''\frac{b}{s_v}t], \tag{39}$$

$$F_{22}^{\text{comp}} = K_h''t\frac{a}{s_h}, \tag{40}$$

$$D_{1111}^{\text{comp}} = \frac{t}{12}\frac{[4K_v'\dfrac{s^h}{a} + \dfrac{b}{a}K_h''\dfrac{s^v}{a}]t^2 + \dfrac{b}{4a}\dfrac{s}{a}K_h''b^2}{4\dfrac{s^h}{a}\dfrac{s^v}{b}}$$

$$+ \frac{t}{32}\frac{b^2[\dfrac{b}{a}\dfrac{s^v}{a}K_h'' + 4K_h''\dfrac{s^h}{a}]}{4\dfrac{s^h}{a}\dfrac{s^v}{b}}, \tag{41}$$

$$D_{2222}^{\text{comp}} = \frac{t^3}{12}\frac{K_h'}{\dfrac{s^h}{a}} + \frac{t}{16}\frac{K_h''a^2}{\dfrac{s^h}{a}}, \tag{42}$$

$$D_{1212}^{\text{comp}} = \frac{t}{192} \frac{K''_v \dfrac{4s^h}{a}(a^2+t^2) + K''_h \dfrac{4s^v}{b}(\dfrac{b^2}{4}+t^2) + K'_h \dfrac{b}{a}\dfrac{s^v}{a}t^2}{\dfrac{s^h}{a}\dfrac{s^v}{b}}$$

$$+ \frac{t}{128} \frac{K''_h \dfrac{b}{a}\dfrac{s^v}{a}a^2}{\dfrac{s^h}{a}\dfrac{s^v}{b}}, \tag{43}$$

where $F_{\alpha\alpha}$ are the shear constants:

$$T_\alpha = F_{\alpha\alpha}(u_{3,\alpha} + \theta_\alpha) . \tag{44}$$

It must be stressed that coefficients (36)–(38) are the same that have been found by Salerno and de Felice (1999, 2000). Coefficients (39)–(40) coincide with those obtained by Cecchi and Sab (2004). Coefficients (41)–(43) coincide with the corresponding ones (20)–(23) unless the terms in the second row of (41) and (43).

This difference can be explained by considering that the shear forces at an interface expend work even in the relative rotation of the blocks facing one another. Given that the rotation field in the R.E.V. is assumed to be constant in the homogenization procedure and linear in the compatible identification.

4. ELASTIC BLOCKS CONNECTED BY ELATIC INTERFACES —
Case 2 of Section 2

In this section, the homogenized membranal and bending constants are found when the blocks are isotropic linear elastic bodies connected by linear interfaces made with isotropic mortar. In this case, as already written

$$\lim_{\varphi \to 0} \xi(\varphi)\varphi^{-1} = \omega \neq 0 .$$

The asymptotic constitutive law of the plate becomes

$$\mathbf{N} = \langle \boldsymbol{\sigma}^H \rangle^* = \mathbf{A}^H \mathbf{E} + \mathbf{B}^H \boldsymbol{\chi} , \tag{45}$$

$$\mathbf{M} = \langle y_3 \boldsymbol{\sigma}^H \rangle^* = {}^T\mathbf{B}^H \mathbf{E} + \mathbf{D}^H \boldsymbol{\chi} , \tag{46}$$

and the limit relation between the homogenized elastic plate tensors $\mathbf{A}^{\xi\varphi}$, $\mathbf{B}^{\xi\varphi}$, and $\mathbf{D}^{\xi\varphi}$ and the asymptotic homogenized elastic plate tensors $\mathbf{A}^H$, $\mathbf{B}^H$ and $\mathbf{D}^H$ is

$$\lim_{\substack{\xi\varphi^{-1} \to \infty \\ \varphi \to 0}} \begin{pmatrix} \mathbf{A}^{\xi,\varphi} & \mathbf{B}^{\xi,\varphi} \\ {}^T\mathbf{B}^{\xi,\varphi} & \mathbf{D}^{\xi,\varphi} \end{pmatrix} = \lim_{\xi\varphi^{-1} \to \infty} \begin{pmatrix} \mathbf{A}^H & \mathbf{B}^H \\ {}^T\mathbf{B}^H & \mathbf{D}^H \end{pmatrix} .$$

In the case of central symmetry of the unit cell, $\mathbf{B}^H = 0$ and the asymptotic homogenized plate tensors can be equivalently defined in the following variational form:

$$\max_{\substack{\operatorname{div}_y \sigma = 0,\, \sigma e_3 = 0 \text{ on } \partial Y_3^\pm \\ \sigma n-\text{antiperiodic on } \partial Y_1}} 2\mathbf{E} \cdot \langle \sigma \rangle^* - \langle \sigma \cdot [(\mathbf{a}^B)^{-1} \sigma] \rangle^* - \frac{1}{|S|} \int_\Sigma (\sigma n) \cdot \mathbf{K}^{-1}(\sigma n) ds$$

$$= \mathbf{E} \cdot (\mathbf{A}^H \mathbf{E}) = \tag{47}$$

$$\min_{\substack{u^{per} \\ \omega-\text{periodic}}} \langle [E + \operatorname{sym}(\operatorname{grad}_y \mathbf{u}^{per})] \cdot [\mathbf{a}^B [\mathbf{E} + \operatorname{sym}(\operatorname{grad}_y \mathbf{u}^{per})]] \rangle^* + \frac{1}{|S|} \int_\Sigma \mathbf{u} \cdot \mathbf{K} \mathbf{u} ds$$

and

$$\max_{\substack{\operatorname{div}_y \sigma = 0,\, \sigma e_3 = 0 \text{ on } \partial Y_3^\pm \\ \sigma n-\text{antiperiodic on } \partial Y_1}} 2\boldsymbol{\chi} \cdot \langle y_3 \sigma \rangle^* - \langle \sigma \cdot [(\mathbf{a}^B)^{-1} \sigma] \rangle^* - \frac{1}{|S|} \int_\Sigma (\sigma n) \cdot \mathbf{K}^{-1}(\sigma n) ds$$

$$= \boldsymbol{\chi} \cdot (\mathbf{D}^H \boldsymbol{\chi}) = \tag{48}$$

$$\min_{\substack{u^{per} \\ \omega-\text{periodic}}} \langle [y_3 \boldsymbol{\chi} + \operatorname{sym}(\operatorname{grad}_y \mathbf{u}^{per})] \cdot [\mathbf{a}^B [y_3 \boldsymbol{\chi} + \operatorname{sym}(\operatorname{grad}_y \mathbf{u}^{per})]] \rangle^* + \frac{1}{|S|} \int_\Sigma \mathbf{u} \cdot \mathbf{K} \mathbf{u} ds$$

For the chosen R.E.V., the evaluation of the $D_{\alpha\beta\gamma\delta}$ constants is based on a numerical F.E.M. procedure. Besides, the variational formulation enables us to build analytical upper and lower bounds. Here for the two models an upper bound on the flexural constants is evaluated.

4.1 Bound on $\mathbf{D}^H$

Bounds for the bending constants may be built. In particular, an upper bound may be obtained by superposition of the rigid block kinematics of the form (4) to a homogenous plate kinematics, hence:

$$\boldsymbol{\chi} \cdot (\mathbf{D}^H \boldsymbol{\chi}) \leq \boldsymbol{\chi} \cdot (\mathbf{D}^R \boldsymbol{\chi}) , \tag{49}$$

where

$$(\mathbf{D}^R) = (\frac{t^3}{12} \mathbf{a}^{B*})^{-1} + (\mathbf{D}^F)^{-1} \tag{50}$$

where $\mathbf{a}^{B*}$ is the plane stress elasticity tensor of blocks and $\mathbf{D}^F$ is the homogenized membranal tensor for rigid blocks connected by elastic interfaces. Note that this procedure may be also used for the compatible equivalent model.

In the case of the homogenization method, the expression of D^R moduli may be obtained in an explicit form as follows:

$$D_{1111}^R = \frac{t^3}{12} \frac{\frac{s^h}{a} 4\mu^B (\lambda^{*B} + \mu^B) + K'(2\mu^B + \lambda^{*B}))(4t^2(4K'\frac{s^h}{a} + \frac{b}{a}K''\frac{s^v}{a}) + b^2 K''\frac{s^v}{a}\frac{b}{a})}{(64t^2\frac{s^{h^2}}{a^2}\frac{s^v}{b}\mu^B(\mu^B + \lambda^{*B}) + 4(2\mu^B + \lambda^{*B})\frac{s^h}{a}(t^2 C + b^2 K''\frac{b}{4a}\frac{s^v}{a}) + 4K'(t^2 D + b^2 K''\frac{b}{4a}\frac{s^v}{a})},$$

(51)

$$D_{1122}^R = \frac{t^3}{12} \frac{4K'\lambda^{*B}(t^2(4K'\frac{s^h}{a} + \frac{b}{a}K''\frac{s^v}{a}) + b^2 K''\frac{b}{4a}\frac{s^v}{a})}{64t^2\frac{s^{h^2}}{a^2}\frac{s^v}{b}\mu^B(\mu^B + \lambda^{*B}) + 4(2\mu^B + \lambda^{*B})\frac{s^h}{a}(t^2 C + b^2 K''\frac{b}{4a}\frac{s^v}{a}) + 4K'(t^2 D + b^2 K''\frac{b}{4a}\frac{s^v}{a})},$$

(52)

$$D_{2222}^R = \frac{t^3}{12} K' \frac{(64\mu^B \frac{s^h}{a}\frac{s^v}{b}(\lambda^{*B} + \mu^B) + [4t^2(\frac{b}{a}K''\frac{s^v}{a} + 4K'\frac{s^h}{a}) + b^2 K''\frac{b}{a}\frac{s^v}{a}](2\mu^B + \lambda^{*B}))}{64t^2\frac{s^{h^2}}{a^2}\frac{s^v}{b}\mu^B(\mu^B + \lambda^{*B}) + 4(2\mu^B + \lambda^{*B})\frac{s^h}{a}(t^2 C + b^2 K''\frac{b}{4a}\frac{s^v}{a}) + 4K'(t^2 D + b^2 K''\frac{b}{4a}\frac{s^v}{a})},$$

(53)

$$D_{1212}^R = \frac{t^3}{12}\mu^B \frac{4K''[\frac{s^v}{b}(\frac{b^2}{4} + t^2) + \frac{s^h}{a}(a^2 + t^2)] + \frac{b}{a}K'\frac{s^v}{a}t^2}{16\frac{s^v}{b}\frac{s^h}{a}\mu^B t^2 + 4K''[\frac{s^v}{b}(\frac{b^2}{4} + t^2) + \frac{s^h}{a}(a^2 + t^2)] + \frac{b}{a}K'\frac{s^v}{a}t^2},$$

(54)

where

$$\mathbf{C} = \frac{b}{a}K''\frac{s^v}{a} + 4K'\frac{s^h}{a} + 4K'\frac{s^v}{b},$$

$$\mathbf{D} = \frac{b}{a}K''\frac{s^v}{a} + 4K'\frac{s^h}{a},$$

while in the case of the compatible equivalent method an explicit expression is too onerous to write symbolically, but the values of the coefficients may be obtained analytically.

4.2 Analytical Evaluation of $\mathbf{F}^H$

An analytical approximation of $\mathbf{F}^H$ may be obtained in analogy with the procedure proposed for the bending constants (see Eq. (50)). Hence also in this case this procedure is adopted so as rigid blocks displacement is superimposed to a displacement field corresponding to a homogeneous plate kinematics in the block. More precisely, the discontinuous rigid body kinematics in the blocks and the continuous

part are uncoupled. The discontinuous part leads to $(F_{\alpha\alpha}^F)^{-1}$, see Eqs. (39)–(40), while the continuous part leads to $\left(\dfrac{5t}{6}\mu^B\right)^{-1}$, where μ^B is the shear constant of the block. Hence a reasonable approximation may be defined as:

$$(\mathbf{F}^R)^{-1} = \left(\frac{5t}{6}\mu^B\right)^{-1} + (\mathbf{F}^F)^{-1} \tag{55}$$

Hence

$$F_{11}^R = \frac{5t}{6}\mu^B \frac{3[K_h''\dfrac{b}{s_h}t\dfrac{b}{4a}+K_v''\dfrac{b}{s_v}t]}{3[K_h''\dfrac{b}{s_h}t\dfrac{b}{4a}+K_v''\dfrac{b}{s_v}t]+\dfrac{5}{2}\mu^B}, \tag{56}$$

$$F_{22}^R = \frac{5t}{6}\mu^B \frac{K_h''t\dfrac{a}{s_h}}{K_h''t\dfrac{a}{s_h}+\dfrac{5}{6}\mu^B}. \tag{57}$$

5. NUMERICAL COMPARISON

The results obtained in the preceding Sections 2 and 3 are analyzed. The two sets of coefficients in the case of rigid and elastic blocks are compared at the constitutive level. The two models are then used to analyze the structural behavior of simply supported square masonry panels subjected to a load condition of pure bending. The same panels are finally analyzed via the F.E. approach and the results are compared with those obtained using the plate models.

5.1 The Constitutive Coefficients

In order to make a quantitative comparison between the coefficients obtained in Section 2.1.1 (D_{ijkl}^F) and those obtained in Section 2.1.2 (D_{ijkl}^{comp}) a block of $55 \times 120 \times 250$ mm has been chosen. The elastic constants for the joint material have been assumed as in Cecchi and Sab (2002b). Then the two textures reported in Fig. 5 as cases a) and b) have been analyzed, obtaining the following results when the block is assumed as rigid bodies:

case a)

$$D_{1111}^{\text{comp}} = 1.714 D_{1111}^F$$

$$D_{2222}^{\text{comp}} = 1.063 D_{2222}^F$$
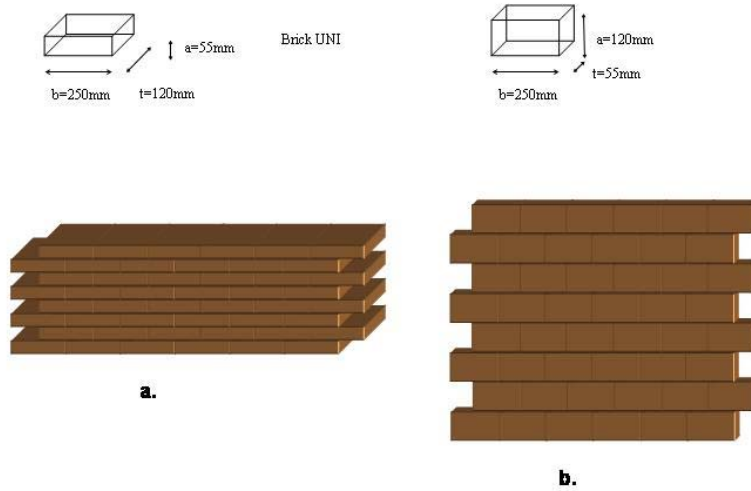
$$D_{1212}^{\text{comp}} = 1.076 D_{1212}^F$$

FIG. 5: Brick UNI geometric characteristics: panel with two different dispositions of the blocks with respect to the thickness t of the plate
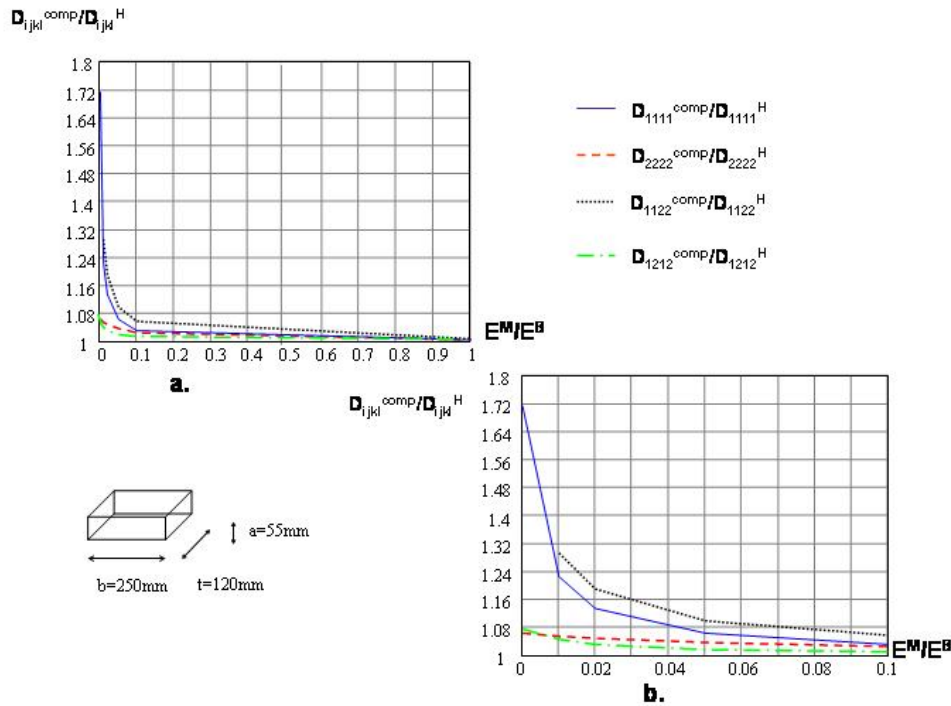

FIG. 6: a) $D_{ijkl}^{\text{comp}}/D_{ijkl}^{H}$ modulus versus E^M/E^B for $0 \leq E^M/E^B \leq 1$; b) details of Fig. 6a for $0 \leq E^M/E^B \leq 0.1$

case b)

$$D_{1111}^{\text{comp}} = 3.063 D_{1111}^{F}$$

$$D_{2222}^{\text{comp}} = 2.428 D_{2222}^{F}$$

$$D_{1212}^{\text{comp}} = 1.317 D_{1212}^{F}$$

It can easily be seen that the two approaches lead to differences which are very huge. As the values reported before are referred to the coefficients that characterize the flexural behavior of the panel, it must be guessed that the two models give very different results when used to solve current problems, even though nothing can be said, at this stage, on their accuracy.

The consistent difference between the two models is evident. Furthermore it must be noted that the model here proposed is a compatible model, so as is based on a compatible solution that is not necessarily equilibrated. As is well known in this approach an upper bound of the constitutive functions may be obtained.

In the following Figs. 6 and 7 for cases a) and b) of Fig. 5 the trend of the ratio between the flexural constants obtained from the compatible equivalent method D_{ijkl}^{comp} and the homogenization method D_{ijkl}^{H} is reported when $0 \leq E^{M}/E^{B} \leq 1$. As expected the difference between the two models is maximum in the case of rigid block assumption (in this case, the evaluated ratio is $D_{ijkl}^{\text{comp}}/D_{ijkl}^{H}$), while is negligible when $E^{M}/E^{B} = 1$ (homogeneous case).
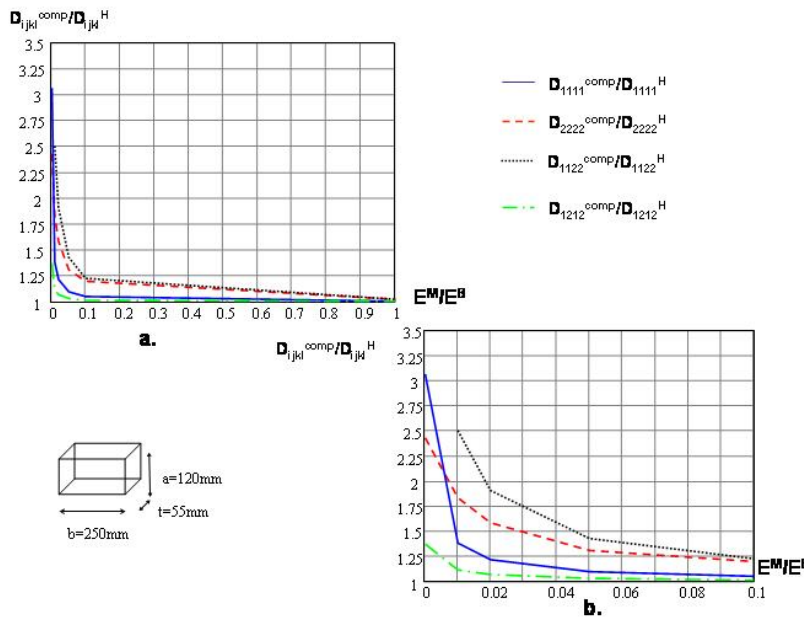

FIG. 7: a) $D_{ijkl}^{\text{comp}}/D_{ijkl}^{H}$ modulus versus E^{M}/E^{B} for $0 \leq E^{M}/E^{B} \leq 1$; b) details of Fig. 7a for $0 \leq E^{M}/E^{B} \leq 0.1$

5.2 Structural Analysis

A number of square panels with different side lengths have been considered.

The panels are made up by the same blocks described in the preceding subsection ($55 \times 120 \times 250$ mm) and arranged as in Fig. 5a, with joints of 4-mm width.

5.2.1 *Pure bending*

The load condition of pure bending has been analyzed. The motivation in the choice of this loading condition depends on the independence of the shear constants of the solution of the field in the plate. Hence, the Mindlin–Reissner and Love–Kirchhoff models coincide.

Figure 8 shows the loading and boundary conditions assumed here. As is well known, in this case the deflection surface may be obtained in a closed form and reads

$$w_3(x_1, x_2) = \frac{D_{2222}M_{11} - D_{1122}M_{22}}{D_{1111}D_{2222} - (D_{1122})^2} x_1^2 + \frac{D_{1111}M_{22} - D_{1122}M_{11}}{D_{1111}D_{2222} - (D_{1122})^2} x_2^2. \tag{58}$$

The problem being linear, the effect of the bending couples M_{11} and M_{22} have been evaluated separately.

The two 2D plate models are compared with a 3D numerical model. The 3D non-homogeneous body with blocks and joints in their real dimensions is studied. The 3D problems have been solved using the F.E. code. Also the mortar joints are modelled in their effective dimension. In order to simulate the rigid block conditions, their Young modulus has been assumed to be 10^6 greater than that of the joints.

Let us denote the deflection of the plate center obtained using the constitutive coefficients obtained from the compatible equivalent method, the constitutive coefficients obtained from the homogenization method, and the 3D F.E. solution by w_{comp}, w_H, w, respectively. Then the following error measures have been calculated:

$$e_{\text{comp}} = \frac{w - w_{\text{comp}}}{w} \cdot 100, \tag{59}$$

$$e_H = \frac{w - w_H}{w} \cdot 100 \tag{60}$$

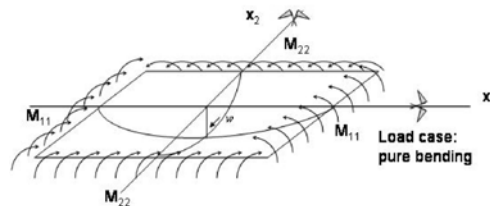**FIG. 8:** The plate under pure bending

and it is found, when the blocks are rigid bodies, that

$$e_H = -26\% \text{ while } e_{comp} = 8\%, \text{ in the case } M_{11} \neq 0 \text{ and } M_{22} = 0$$

$$e_H = -7 \text{ while } e_{comp} = 3\%, \text{ in the case } M_{11} = 0 \text{ and } M_{22} \neq 0.$$

The following error measures have been calculated when $E^B = 10E^M$:

$$e_H = -3 \text{ while } e_{comp} = 1.7\%, \text{ in the case } M_{11} \neq 0 \text{ and } M_{22} = 0$$

$$e_H = -1.1 \text{ while } e_{comp} = 0.8\%, \text{ in the case } M_{11} = 0 \text{ and } M_{22} \neq 0.$$

The following remarks must be pointed out:

- e_{comp}, e_H, strongly depend on the ratio E^M/E^B;
- the compatible equivalent model is stiffer than the 3D F.E. model which, in turn, is stiffer than the one obtained from the homogenization procedure;
- e_{comp}, e_H do not depend on the ratio t/L (in the numerical experimentation the ratio t/L varies from 1/5 to 1/25);
- Figure 9 shows that, even in the case of pure bending, the 3D F.E. solution exhibits shear stress components which are different from zero. In particular, the presence of shear actions is maximum when the blocks are rigid bodies. This may be a reason of a better accord of 3D F.E. with the compatible equivalent method that overestimates the shear actions.
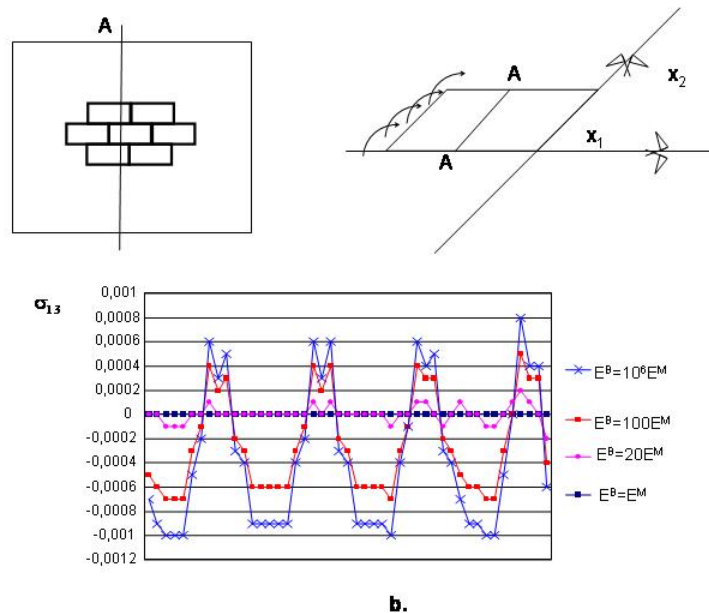

FIG. 9: The stress σ_{13} along the A–A section for $x_3 = t/2$ under only M_{11} bending

5.2.2 *Transverse bending*

The loading condition assumed here (a concentrated force applied at the plate center) is shown in Fig. 10.

The following two boundary conditions have been taken into account:

b_1) the edges $x_1 = 0$ and $x_1 = L$ are simply supported while the edges $x_2 = 0$ and $x_2 = L$ are free (see Fig. 10a);

b_2) the edges $x_2 = 0$ and $x_2 = L$ are simply supported while the edges $x_1 = 0$ and $x_1 = L$ are free (see Fig. 10b).

In this case, the shear is constant piecewise while the bending varies linearly. The balance equation if the Mindlin–Reissner model is considered is

$$D_{1111}\theta_{1,11} + D_{1212}\theta_{1,22} + (D_{1122} + D_{1212})\theta_{2,12} - F_{11}(\theta_1 + w_{3,1}) = 0, \tag{61}$$

$$(D_{1122} + D_{1212})\theta_{1,12} + D_{1212}\theta_{2,11} + D_{2222}\theta_{2,22} - F_{22}(\theta_2 + w_{3,2}) = 0, \tag{62}$$

$$F_{11}(\theta_{1,1} + w_{3,11}) + F_{22}(\theta_{2,2} + w_{3,22}) - p(x_1, x_2) = 0 \tag{63}$$

with the boundary conditions

$$w_3 = 0; \quad \theta_2 = 0; \quad \theta_{1,1} = 0 \quad \text{in the case } b_1 \tag{64}$$

$$w_3 = 0; \quad \theta_1 = 0; \quad \theta_{2,2} = 0 \quad \text{in the case } b_2 . \tag{65}$$

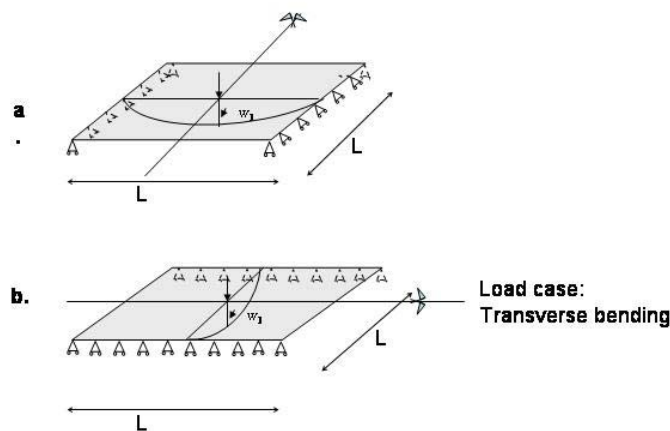The functions that satisfy Eqs. (61)–(63) are (Dobyns, 1981)

FIG. 10: The plate simply supported along two parallel edges with concentrated load: a) supported edges $x_1 = \pm l/2$; b) supported edges $x_2 = \pm l/2$}

$$w_3(x_1, x_2) = \sum_{m=1}^{\infty} \sum_{n=1}^{\infty} S_{mn} \sin\frac{m\pi x_1}{L} \sin\frac{n\pi x_2}{L}, \tag{66}$$

$$\theta_1(x_1, x_2) = \sum_{m=1}^{\infty} \sum_{n=1}^{\infty} A_{mn} \cos\frac{m\pi x_1}{L} \sin\frac{n\pi x_2}{L}, \tag{67}$$

$$\theta_2(x_1, x_2) = \sum_{m=1}^{\infty} \sum_{n=1}^{\infty} B_{mn} \sin\frac{m\pi x_1}{L} \cos\frac{n\pi x_2}{L}, \tag{68}$$

$$p(x_1, x_2) = \sum_{m=1}^{\infty} \sum_{n=1}^{\infty} p_{mn} \sin\frac{m\pi x_1}{L} \sin\frac{n\pi x_2}{L}, \tag{69}$$

where S_{nm} are unknown constants that must be evaluated, m and n are integers; and p_{nm} is:

$$p_{mn} = \frac{4P}{L^2} \frac{\sin m\pi \frac{L}{2}}{L} \frac{\sin n\pi \frac{L}{2}}{L}. \tag{70}$$

It is clear that the solution to Eqs. (66)–(69) depends only on x_1, in case b_1, and on x_2 in case b_2. By substituting these functions in Eqs. (61)–(63) it is possible to determine the displacement field $w_3(x_1, x_2)$ and the rotations $\theta_\alpha(x_1, x_2)$ of the plate.

The results obtained show that

$$e_H = -32\%, \quad e_{\text{comp}} = 12\% \text{ in the case } b_1$$

$$e_H = -11\%, \quad e_{\text{comp}} = 5\% \text{ in the case } b_2.$$

The comments made in the case of pure bending apply also in this case. It must be stressed, however, that the relevance of the shear components being greater, the difference in the results is bigger.

6. CONCLUSIONS

The analysis of the homogeneous deformation patterns of brickwork has shown that the 2D plate Mindlin–Reissner model, obtained from the compatible equivalent procedure, provides consistent results. In particular, this model allows one to take into account two crucial aspects of the problems investigated: the heterogeneity that induces the presence of actions that do not exist in the homogeneous model, the effect of the shear stress. This latter aspect was already discussed by Cecchi and Sab (2004).

It must also be stressed that the compatible equivalent procedure expects the possibility that the blocks, when are modelled as rigid bodies, have different rotations, while in the case of the homogenization procedure the only periodic field admissible imposes that all the blocks have the same rotations. Hence, also if the

compatible equivalent model is rough and overestimates the elastic moduli, this model provides an accurate description of the discrete system.

REFERENCES

Anthoine, A., Derivation of in plane elastic characteristic of masonry through homogenization theory, *Int. J. Solids Struct.*, vol. 32, pp. 137–163, 1995.

Avila-Pozos, O., Klarbring, A., and Movchan, A. B., Asymptotic model of orthotropic highly inhomogeneous layered structure, *Mech. Mater.*, vol. 31, pp. 101–115, 1999.

Bazant, Z. P., Tabbara, M. R., and Kazemi, M. T., Random particle model for fracture of aggregate or fiber composites, *ASCE J. Eng. Mech.*, vol. 116, pp. 1686–1705, 1990.

Caillerie, D., Thin elastic and periodic plates, *Math. Meth. Appl. Sci.*, vol. 6, pp. 159–191, 1984.

Cecchi, A. and Rizzi, N. L., Analisi in piu' parametri perturbativi per murature a struttura regolare: identificazione 3D con modelli 2D di piastra, *Proc. XVI Congresso AIMETA di Meccanica Teorica e Applicata*, Ferrara 9–12, 2003.

Cecchi, A. and Sab, K., A comparison between a 3D discrete model and two homogenised plate models for periodic elastic brickwork, *Int. J. Solids Struct.*, vol. 41, nos. 9–10, pp. 2259–2276, 2004.

Cecchi, A. and Sab, K., A multi-parameter homogenization study for modelling elastic masonry, *Eur. J. Mech., A Solids*, vol. 21, pp. 249–268, 2002a.

Cecchi, A. and Sab, K., Corrigendum to "A comparison between a 3D discrete model and two homogenized plate models for periodic elastic brickwork" [Int. J. Solids Struct., vol. 41, nos. 9–10, pp. 2259–2276, 2004], *Int. J. Solids Struct.*, vol. 43, no. 2, pp. 390–392, 2006.

Cecchi, A. and Sab, K., Out of plane model for heterogeneous periodic materials: the case of masonry, *Eur. J. Mech., A Solids*, vol. 21, pp. 249–268, 2002b.

Cecchi, A. and Sab, K., Corrigendum to "A comparison between a 3D discrete model and two homogenised plate models for periodic elastic brickwork" [*Int. J. Solids Struct.*, vol. 41, nos. 9–10, pp. 2259–2276], *Int. J. Solids Struct.*, vol. 43, no. 2, pp. 390–392, 2006.

Cecchi, A. and Rizzi, N. L., Modelli 2D con microstruttura per pannelli di muratura in 3D, *Proc. XVII Congresso AIMETA di Meccanica Teorica e Applicata*, Firenze 11–15, 2005.

de Felice, G., Détermination des coefficients d'élasticité de la maçonnerie par une méthode d'homogénéisation, *Actes du 12ème Congrès Français de Mécanique*, vol. 1, pp. 393–396, Strasbourg, 1995.

Dobyns, A. L., The analysis of simply supported orthotropic plates subject to static and dynamic loads, *AIAA J.*, May, pp. 642–650, 1981.

Klarbring, A., Derivation of model of adhesively bounded joints by the asymptotic expansion method, *Int. J. Eng. Sci.*, vol. 29, pp. 493–512, 1991.

Lofti, H. R. and Benson Shing, P., Interface model applied to fracture of masonry structures, *ASCE J. Struct. Eng.*, vol. 120, pp. 63–80, 1994).

Lourenço, P. B. and Rots, J. G., On the use of homogenisation techniques for the analysis of masonry structures, *Masonry Int.*, vol. 11, no. 1, pp. 26–32, 1997.

Markov, K. Z., Elementary micromechanics of heterogeneous solids, in: K. Z. Markov and L. Preziosi (Eds.), *Heterogeneous Media: Micromechanics Modeling Methods and Simulations*, Boston: Birkhauser, pp. 1–162, 1999.

Masiani, R., Rizzi, N., and Trovalusci, P., Masonry as structured continuum, *Meccanica*, vol. 30, pp. 673–683, 1995.

Salerno, G. and de Felice, G., Continuum modelling of periodic brickwork, Report no. 206 Collana LABMEC, Dipartimento di Strutture, Università della Calabria, 1999.

Salerno, G. and de Felice, G., Continuum modelling of discrete systems: a variational approach, *Proc. Eur. Congress on Computational Methods in Applied Sciences and Engineering*, ECCOMAS 2000, Barcelona, 2000.

Sanchez-Palencia, E., Nonhomogeneous media and vibration theory, *Lecture Notes in Physics*, vol. 127, Berlin: Springer-Verlag, 1980.

Schlangen, E. and Garbozci, E., New method for simulationg fracture using an elastically uniform random geometry lattice, *Int. J. Eng. Sci.*, vol. 34, no. 10, pp. 1131–1144, 1996.

Suquet, P., Elements of homogenization for inelastic solid mechanics, in: *Homogenization Techniques for Composite Media*, *Lecture Notes in Physics*, vol. 272, Berlin: Springer-Verlag, pp. 193–279, 1987.

Trovalusci, P. and Masiani, R., Cosserat and Cauchy materials as continuum models of brick masonry, *Meccanica*, vol. 31, pp. 421–432, 1996.

Zucchini, A. and Lourenço, P. B., A micro-mechanical model for homogenisation of masonry, *Int. J. Solids Struct.*, vol. 39, pp. 3233–3255, 2002.

MODELING OF DEGRADATION OF THE COMPOSITE PROPERTIES ON CRACKING AND DELAMINATION WHEN SUBJECTED TO STATIC AND CYCLIC LOADING

Doan Chuck Luat[1], *S. A. Lurie*[2*], *& A. A. Dudchenko*[1]

[1]*Moscow Aviation Institute (Technical University), Moscow, Russia*

[2]*Institute of Applied Mechanics, Russian Academy of Sciences, Moscow, Russia*

[*]Address all correspondence to S. Lurie E-mail: lurie@ccas.ru; salurie@mail.ru

The model of damage accumulation and the model of degradation of the mechanical properties of layered composites due to the defects of the type of transversal cracking and interlayer cracks have been developed. An analysis of the increase in the defectiveness is made, and the model of degradation of properties is suggested. An algorithm of the refinement of the stress-strain state with account for the increase in the defectiveness is presented; its implementation is possible with the use of the finite-element method.

KEYWORDS: *layered composites, accumulation of damages, degradation of properties, transversal cracking, delamenation*

1. INTRODUCTION

Real structural elements from composite materials always have structural defects at different dimensional levels acquired in the process of fabrication, transportation, or other actions. These can be longitudinal and transverse microcracks in the layer between the fibers, an incomplete contact between the layers, between a fiber and the matrix, defects in individual fibers, etc. Being loaded, all the types of microdefects cause perturbation of the stressed state and deformations, and exert their influence on the effective characteristics of the material. Under certain conditions, microdefects initiate the growth of macrocracks and destruction of the material on quasistatic or cyclic loading, when in service.

It is known that in the case of the tension loading, even when there is a small value of strain across the fibers (≈0.2%), there occurs the failure of the matrix.

Thus, in an orthogonally reinforced composite of longitudinal-transverse structure, in the 90$^\text{o}$-oriented layer cracking occupies its entire length with the same step between transverse micorcracks. In this case, the layer will fall out, entirely or partially, from the operation of the structure, which leads to deterioration of the rigidity characteristics. With increase in loading, additional cracking of the matrix can occur with simultaneous formation of an additional system of microcracks, with the general defectiveness of the layered system changing by jumps. If transverse microcracks are the source of the appearance of the delamination cracks of certain initial length, the additional defectiveness due to the delamination also changes jumpwise. The delamination cracks have a tendency to grow on quasistatic and cyclic loading, determining in the main the defectiveness of the layered composite and leading to a substantial influence on its effective properties.

2. ON MODELING THE ACCUMULATION OF DAMAGES

We will formulate the essential features required of the models of accumulation of damages with the use of micromechanical approaches (Lurie et al., 2005, 2006; Movchan, 1989, 1990):

1. The parameters of the models are to be determined in terms of micromechanical parameters that avoid measurements on a damaged composite with the aid of corresponding procedures.
2. It is necessary to account simultaneously for two processes being the reason of the increase in the micromechanical defectiveness: a) the process of the origination of new defects and b) the process of the growth of the available microdefects.

As the measure of the defectiveness S we take a scalar parameter that can be interpreted as the measure of the increment in the entropy density. As the real time of the process t we may take the number of the cycles of loading, duration of quasistatic loading, determined by the level of stresses, the length of the deformation arc, etc. Let the function $P(t)$ define the density of microdefects in a unit of the representative volume of the test material and $s(t)$ — the local measure of defectiveness connected with a fixed (typical) microdefect. The value of $s(t)$ can carry information on the shape of microdefects and their size. In the case of differently oriented microdefects one may introduce a local measure of defectiveness — the tensor of defectiveness $s(t)$ in the representative volume that describes also local irreversible phenomena of nonmechanical origin. Since each of the processes (the origination of microdefects and their growth) is responsible for the increment in the defectiveness ΔS, we may write: $\Delta S = \Delta S_s + \Delta S_p$, where ΔS_s represents the increments in the defectiveness (increments in the entropy density) caused by the increase in the local measure of defectiveness s; ΔS_p is the increment of defectiveness caused by the change in the number of microdefects. Let in time Δt the num-

ber of microdefects with the local characteristic $s(t)$ change by the value ΔN and the total microdefectiveness on the available defects P increase by the value $\Delta\Omega$. Then $\Delta S_s = P\Delta\Omega = s'(t)P\Delta t$, $\Delta S_p = s(t)\Delta N = s(t)P'\Delta t$, $s'(t)$, $P'(t)$ are the derivatives of the functions $s(t)$ and $P(t)$ with respect to the parameter t. For what follows it is necessary to determine the character of each of the two processes: the generation of defects and their growth. For this purpose, we prescribe the functions of the speeds of each of the processes: $\dfrac{dP}{dt} = v(t)$, $s' = \dfrac{ds}{dt} = \varphi(t, s, S)$. Then the system of the kinetic equations of defectiveness acquires the form [3, 4]

$$\frac{dS}{dt} = s(t)v(t) + P\varphi(t,s,S), \quad \frac{dP}{dt} = v(t), \quad s' = \frac{ds}{dt} = \varphi. \tag{1}$$

This system of equations should be supplemented with the initial conditions:

$$S\big|_{t=t_0} = S_0, \quad P\big|_{t=t_0} = P_0, \quad s\big|_{t=t_0} = s_0. \tag{2}$$

Equations (1) and (2) form a closed system of kinetic equations that describe the increase in the defectiveness of the investigated medium with account for the processes of the origination of microdefects and of their growth.

Note that the equation of the growth of microdefects can be interpreted as the description of the Poisson process. In particular, the increment of the local defectiveness $s(t, \tau)$ can be written in the form

$$s(t,\tau) = s_0 + \Delta s\left(1 - e^{-b(t-\tau)}\right).$$

Here s_0 is the local increment of the defectiveness due to the microdefect originated at the moment $t = \tau$, $t \geq \tau$. The quantities b and Δs are the parameters of the Poisson process, whereas the equation for S can be written in the form of the Langevin stochastic equation.

3. INFLUENCE OF TRANSVERSAL CRACKING
ON THE PROPERTIES OF A COMPOSITE

We will consider a composite material with a symmetric structure (Fig. 1). Let the orthotropic layer with the symmetric structure be extended by the force P. We assume that the layered composite can be represented as a three-layered structure consisting of two extreme layers of identical thicknesses h_1 each and of the inner layer of thickness $2h_2$.

The technique of calculation of the stressed state in the vicinity of the through cut in the transverse (relative to the extending loading) monolayer for cross-reinforced composite was suggested in (Vasiliev et al., 1970). It is hypothized in that work that the inner layer, which is the monolayer with transverse reinforcement
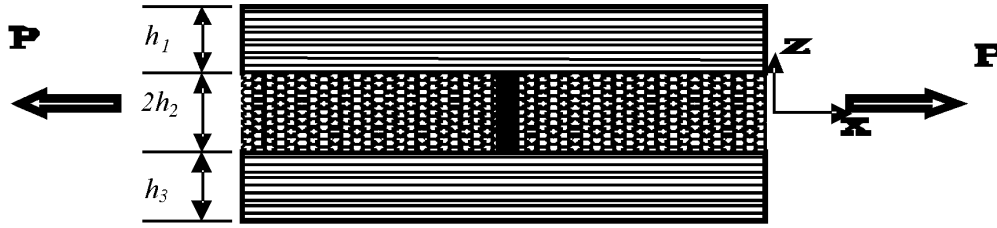
FIG. 1: Transversal cracking

relative to the extending component of normal stresses, undergoes cracking. This allows one to generalize the technique of (Vasiliev et al., 1970) to the case of cracking of any layer in the structure. The system of coordinates connected with the inner layer of thickness $2h_2$ is used. The remaining laminated structure is described by the characteristics B_{ij}. Its total thickness is equal to $2h_1$. Let relative to the selected monolayer of thickness $2h_2$ there exist such loading that the stress σ_x^0 determines the extension in this monolayer.

We will briefly consider the algorithm of the solution construction and the results of this solution. According to (Vasiliev et al., 1970), the solution is constructed in stresses which are considered constant over the thickness of the layers. Taking into account that in the zone of the crack the transverse layer gets unloaded and the longitudinal layers receive additional loading, we use the expansion: $\sigma_{x1} = \sigma_{x3} = \sigma_{10} + \tilde{\sigma}_{x1}(x)$, $\sigma_{x2} = \sigma_{20} - \sigma_{x2}(x)$, where σ_{10} and σ_{20} are the stresses constant over the coordinates in the nonperturbed layers, the variable stresses of the perturbed state $\tilde{\sigma}_{x1}$ and $\tilde{\sigma}_{x2}$ must be self-balanced over their thickness: $\tilde{\sigma}_{x1}h_1 = \tilde{\sigma}_{x2}h_2$. Here the coordinate x is along the length of the plate and the z coordinate is along the plate height. Using the equations of equilibrium and boundary conditions at $z = \pm h_2$, $z = \pm(h_1 + h_2)$, all the components of stresses can be expressed in terms of one unknown component of the perturbed state stress $\tilde{\sigma}_{x2}$:

$$\sigma_{x1} = \sigma_{x3} = \sigma_{10} + \tilde{\sigma}_{x2}\frac{h_2}{h_1}; \ \sigma_{x2} = \sigma_{20} - \tilde{\sigma}_{x2}(x); \ \tau_2 = \tilde{\sigma}'_{x2}\, y;$$

$$\sigma_{z2} = -\frac{1}{2}\tilde{\sigma}''_{x2}\Big[y^2 - h_2(h_1 + h_2)\Big]; \ \tau_i = -\frac{h_2}{h_1}\tilde{\sigma}_{x2}\big[y \mp (h_1 + h_2)\big],$$

$$\sigma_{zi} = \frac{h_2}{2h_1}\tilde{\sigma}''_{x2}\Big[y \mp (h_1 + h_2)\Big]^2, (i = 1; 3).$$

The function $\tilde{\sigma}_{x2}$ is determined from the condition of the minimum of the additional potential energy:

$$U = \int\limits_{0}^{1} \sum\limits_{i=1}^{3} \int\limits_{h_i} \left[\frac{\sigma_{xi}^2}{2E_{xi}} + \frac{\sigma_{zi}^2}{2E_{zi}} - \frac{1}{2}\left(\frac{\mu_{xzi}}{E_{xi}} + \frac{\mu_{zxi}}{E_{zi}} \right) \sigma_{xi}\,\sigma_{zi} + \frac{\tau_i^2}{2G_i} \right] dx\,dz. \qquad (3)$$

As a result, the solution of the problem takes the form

$$\sigma_{x2} = \sigma_{20}\left[1 - e^{-k_1 x}\left(\frac{k_1}{k_2}\sin k_2 x + \cos k_2 x \right) \right],$$

$$(4)$$

$$\tau_2 = \sigma_{20}\frac{k_1^2 + k_2^2}{k_2}e^{-k_1 x}\left(\sin k_2 x \right)y, \quad k_{1,2} = \sqrt{\frac{b^2 \pm a^2}{2}},$$

where k_1 and k_2 are the roots of the characteristic equation $\sigma^{IV} - 2a^2\sigma^{II} + b^4\sigma = 0$ and they depend on the geometric parameters h_1 and h_2 and on the mechanical properties of each of the layers of the three-layered structure E_{xi}, E_{yi}, E_{zi}, and G_i.

Let for the sake of definiteness the material be defined by the following parameters: $\varphi_1 = -\varphi_3 = 45^\circ$; $\varphi_2 = \pi/2$, $h_2 = 0.5h_1$, and $h_3 = h_1 = 0.001$ m. The properties of the layer are prescribed by elasticity moduli: along the fibers $E_1 = 120.000$
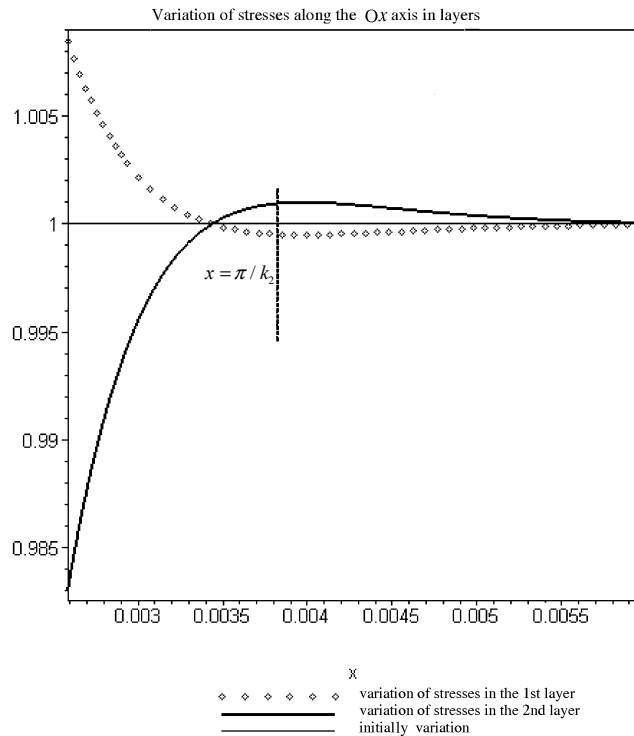

FIG. 2: Variation of the relative stresses σ_x^2/σ_{20}^2 along the length
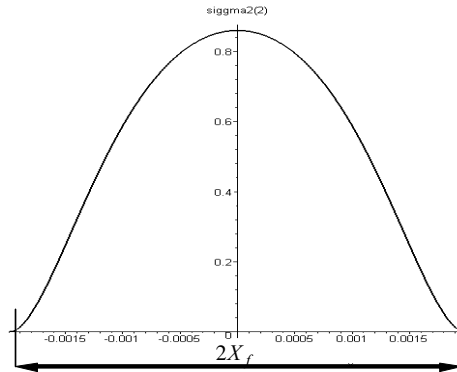
FIG. 3: Transverse stress in the transverse layer between cracks

MPa, across them E_2 = 9000 MPa, the shear modulus G_{12} = 6000 MPa. For the indicated parameters we will obtain the following changes in the relative stresses σ_x^2/σ_{20}^2 along the length (the superscript indicates the number of the layer) (Fig. 2). The stress σ_{x2} attains a maximum at $x = l_1 = \pi/k_2$. At this point τ_2 = 0, with this stress being greater than the ultimate strength $(\sigma_{x2})_{\max} > \sigma_{b2}$. After this, a system of cracks spaced π/k_2 apart is formed in the middle layer (Vasiliev et al., 1970). In this case, the transverse stress between the cracks in the transverse layer takes the form (Fig. 3)

$$\sigma_{x2} = \frac{\sigma_{20}}{sh(\pi k_1/2k_2)}\left(sh\frac{\pi k_1}{2k_2} - \frac{k_1}{k_2}ch(k_1 x)\cos(k_2 x) - sh(k_1 x)\sin(k_2 x) \right). \qquad (5)$$

After the first cracking with the formation of a system of microcracks spaced $2X_f$ apart [5] a second system of microcracks can be formed. If the loading is such that σ_2 exceeds the limiting value $[\sigma_2]$, another system of microcracks with the distance between the latter $2X_f'$, $X_f' = X_f/2$, is formed [5].

3.1 Determination of the Characteristics of the Composite after Cracking

We propose that from the system of transversal microcracks, in the layer only its transverse elasticity modulus E_2 undergoes a change. To determine the effective local transverse modulus $E_2 = E_{2\text{ave}(k)}$ in the destroyed zone, we will avail ourselves of the following approximate relations:

$$E_{2\text{ave}(k)} = \frac{\sigma_{\text{ave}(k)}}{\varepsilon_{2\text{ave}}}, \quad \sigma_{\text{ave}(k)} = \frac{1}{2X_f}\int_{-X_f}^{X_f} \sigma_2 dx,$$

$$\varepsilon_{2\text{ave}(k)} = 2W/\sigma_{2\text{ave}}, \quad \sigma_{2\text{ave}} = 0,5P/(h_1 + h_{2(k)}), \quad \varepsilon_{2\text{ave}(k)} = \varepsilon_{2\text{ave}}. \qquad (6)$$

The value of the specific average energy of deformation W is calculated from Eq. (3). The stresses under the integration sign are calculated with account for Eq. (4). Approximately we may consider that $\tau_i = 0$.

To determine the effective rigidities of the composite material the equations of the mechanics of composites are used with account for the fact that for the layers where the cracking occurred the transverse elasticity modulus is calculated by Eq. (6).

We will consider a specific example of a composite with the 0° and 90° laying of fibers for three different ratios of the thickness h_1 of the longitudinal layer and thickness h_2 of the transverse layer, with the thickness h_1 remaining unchanged. The composite is under the conditions of uniaxial tension. The following mechanical parameters of the unidirectional layer are adopted: the modulus along the direction of fibers $E_1 = 120$ GPa, the modulus across the fibers $E_2 = 9$ GPa, the shear modulus $G_{12} = 6$ GPa, the Poisson coefficient $\mu_{21} = 0.28$, the ultimate strength along the direction of fibers $\sigma_{b1} = 1200$ MPa, and across the fibers $\sigma_{b2} = 40$ MPa. At the base computational thickness equal to $h_6 = 1$ mm, the following variants have been calculated: $h_1 = h_2 = h_b$, $h_1 = 0.5h_2 = 0.5h_b$, $h_2 = 0.25\ h_1$.

Figure 4 presents the graphs of the deformation of the transverse layer in the process of its operation together with the longitudinal layer where the sequence of its destruction is seen. Along the vertical the forces (in Newtons) received by the transverse layers are given. It is seen from the graphs that after the second cracking the transverse layer actually drops out of operation. Then it should be adopted
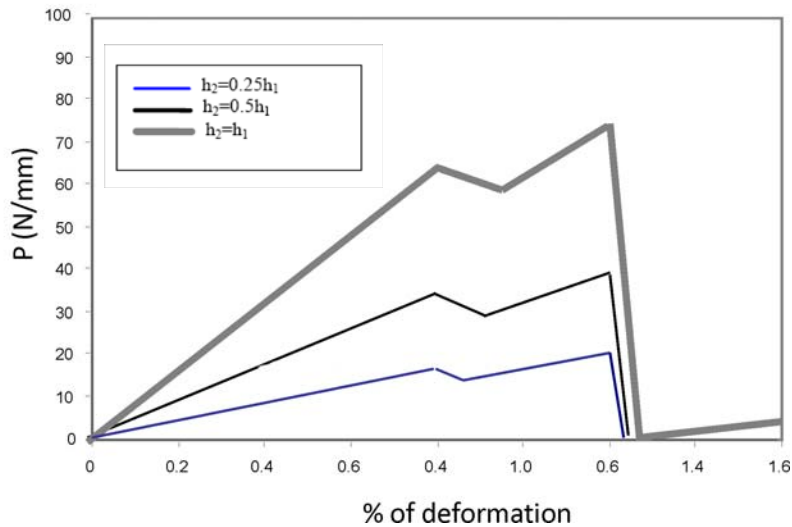

FIG. 4: Diagrams of the tension of a transverse layer for three types of structures with allowance for the appearance of the first and second system of transverse microcracks in the 90° layer
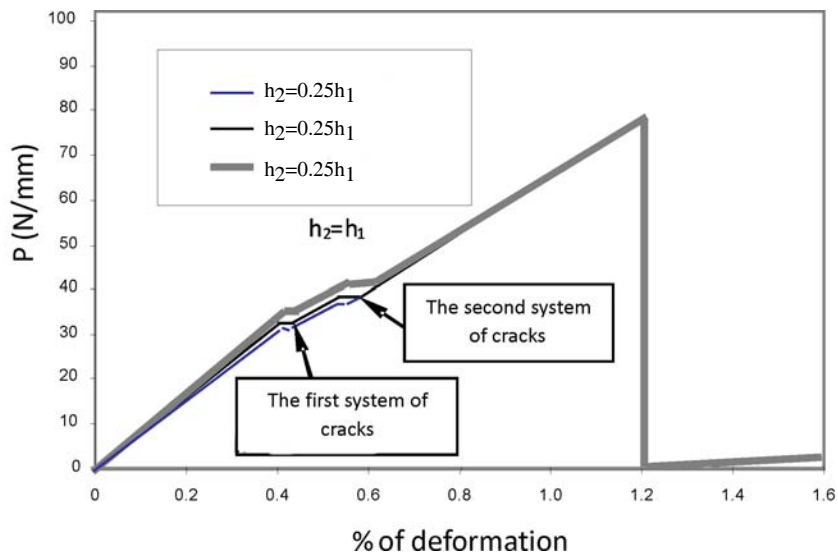
FIG. 5: Diagram of the deformation of a three-layered composite material with allowance for the appearance of the first and second system of transverse microcracks in the 90° layer

that $E_{2(k)} = 0$. Henceforth we consider that after the appearance of the second system of microcracks the transverse rigidity of the transverse layer is equal to zero.

We will consider the same structure. We will plot the diagram of deformation of the entire laminated composite with account for the appearance of the first and second system of cracks in the transverse layer (Fig. 5). The forces (in Newtons) are plotted along the ordinate and deformation — along the abscissa axis. The first of the structures mentioned ($h_2 = h_1$) is shown dotted boldly, the next in thickness is the second structure ($h_1 = 0.5h_2$), and then goes the third structure ($h_2 = 0.25h_1$). The graphs reflect the sequence of the destruction of each structure. In all of the cases, there occur two successive crackings of the transverse layer, with its entire drop-out from operation, after which only the longitudinal layer continues to operate until its entire breakdown.

The last portion of the sloping part of the diagram (Fig. 5) corresponds to the case, where the transverse layer is entirely destroyed $E_{2ave(k)} = 0$, and the rigidity of the structure is determined only by the rigidity of the fibers. This is in full agreement with the graphs of Fig. 4.

4. DEVELOPMENT OF INTERLAYER CRACKS

Usually, by virtue of the concentration of stresses the transversal cracking is the reason for the appearance of a system of microcracks of interlayer delamination
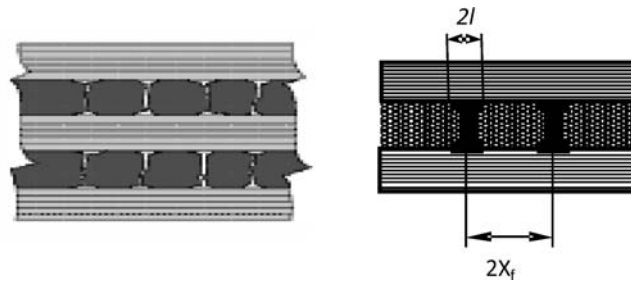
FIG 6: Development of delaminations

(Fig. 6). Local interlayer cracks appear in the vicinity of transverse microcracks. The influence of transversal cracking on the effective characteristics of layered composites is substantial especially on their shear characteristics. A detailed analysis of the influence of transversal cracking on the properties of layered composite materials is given in (Kashtalyan and Soutis, 2002a,b, 2005). It is significant that this mechanism of defectiveness continues to develop in the process of loading, i.e., the interlayer cracks that originated in the vicinity of the zones of transversal cracking begin to grow, and they depend on the time of the process. The process of the development of such kind of damages in the mentioned works (Kashtalyan and Soutis, 2002a,b, 2005) has not been studied, even though for the majority of composite materials precisely this character of defectiveness is determining. We will consider the variant of the model of degradation of the properties of a composite due to the delamination-controlled defectiveness. The main idea is that it is sufficient to write the model of degradation for a monolayer. The model of degradation of effective properties is determined directely by the relations of the mechanics of composites for effective characteristics.

Let E_0 and G_{120} be the characteristics of a monolayer with transverse cracks. We consider the layers to be thin enough, so that the stresses are distributed uniformly over the depth. Part of the layer corresponding to the interlayer cracking of length $2l$ drops out of operation. We may assume that with account for the compatibility of the deformations the following equalities hold: $E_1 F = E_{10}(F - \Delta F)$, $F = 2X_f h$, $\Delta F = k^E 2lh$. The quantity k^E determines the part of the layer, in the vicinity of a crack, that drops out of operation. The quantity $E_1 = E_{10}(1 - k^E \Delta)$, where $\Delta = l/X_f$, $2l$ is the crack length, $2X_f = \pi/k_2$ is the distance between two cracks. A similar equality is obrained for the shear modulus. As a result we have: $E_1^{(1)} = E_{10}$, $E_2^{(1)} = E_{20}$, $G_{12}^{(1)} = G_{120}$, $E_1^{(2)} = E_{10}(1 - k^E \Delta)$, $G_{12}^{(2)} = G_{120}(1 - k^G \Delta)$. Similar reasoning yields the following relation for the transverse elasticity modulus of the layer:

$$E_2^2 = \frac{[\sigma_{20}^{(2)}]^2 X_f h_2}{[\int_{-h_2/2}^{h_2/2} \frac{[\sigma_2^{(2)}]^2}{2E_{20}^2} dxdy}. \tag{7}$$

The parameters k^E and k^G can be found later from a comparison with experimental data for a monolayer or from a comparison with more precise results of investigations. Generally, one should use the following model of degradation:

$$E_1^{(1)} = E_{10}, \qquad E_2^{(1)} = E_{20}, \qquad G_{12}^{(1)} = G_{120},$$

$$E_1^{(2)} = K_E E_{10}(1 - k^E \Delta), \qquad G_{12}^{(2)} = K_G G_{120}(1 - k^G \Delta). \tag{8}$$

The values of $K_E E_{10}$ and $K_G G_{120}$ correspond to the "real" (damaged by transversal cracking) values of the effective elasticity moduli by the start of the growth of delamination-caused defectiveness.

The further algorithm of the account for interlayer delamination is reduced to the recalculation of the effective characteristics of a laminated packet. In the monolayers where transversal cracking occurred, the characteristics are determined from Eqs. (6)–(8). As a result, we find the characteristics of rigidity b_{ij} and B_{ij} as functions of the parameter Δ. Thereafter the effective mechanical (technical) characteristics of the structure are calculated. For the orthotropic structure we have

$$E_x = E_x(\Delta) = B_{11}(\Delta) - \frac{B_{12}^2(\Delta)}{B_{22}(\Delta)}, \quad E_y = E_y(\Delta) = B_{11}(\Delta) - \frac{B_{12}^2(\Delta)}{B_{11}(\Delta)}, \tag{9}$$

$$G_{xy} = G_{xy}(\Delta) = B_{33}(\Delta).$$

We will show that the applied model of the degradation of properties (8) allows one to rather accurately predict the change in the effective characteristics of a composite. For this purpose, we will avail ourselves of the results of refined investigations (Kashtalyan and Soutis, 2002a,b, 2005) devoted to the study of the influence of microdelaminations on the properties of layered composites. We will show that for a specific structure, by selecting the parameters in the model of degradation of the properties of monolayers, one can successfully model the degradation of effective properties.

We will consider the T300/5208 composite (Kashtalyan and Soutis, 2002a,b, 2005) having the structure [O$_2$/90$_4$]. The following characteristics of a layer of the material are adopted: $E_{10} = 134$ GPa, $E_{20} = 10.5$ GPa, $G_{120} = 5.5$ GPa, $\mu_{21} = 0.28$, and the monolayer thickness $t = 0.14$ mm.

We will calculate the effective mechanical (technical) characteristics of the structure (from the well-known equations of the mechanics of composites). Using the relations that model the degradation of the properties of monolayers and relations (9), we find

$$G_{xy} = B_{33} = \frac{G_{120}[h_1 + K_{G0}(1 - k^G \Delta)h_2]}{(h_1 + h_2)},$$

$$E_x = \frac{\overline{E}_1 + E_2^{(2)}}{3} - (\mu_{12})^2 \frac{[\overline{E}_1 + 2K_E \overline{E}_1 (1 - k^E \Delta)]}{[\overline{E}_2 + 2K_E \ \overline{E}_1 \ (1 - k^E \Delta)]}. \tag{10}$$

We will compare the results found with the aid of Eq. (10) with those obtained for the same structure by the refined model of (Kashtalyan and Soutis, 2002a,b, 2005) and, using the results of the comparison, we determine the parameters in the model of degradation (8). We obtain

$$K_E = 0.9852, \quad k^E = 0.855, \quad K_G = 0.8875, \quad k^G = 2.197.$$

It can be easily seen that for these values of the parameters the graphs of the change in the effective properties actually accurately agree with the results of more exact investigations [6–8]. This allows us to state that the model of degradation (6)–(8) ensures factually accurate prediction of the degradation of effective properties depending on the length of delaminantion. The parameters k^G, k^E, $(1 - k^G \Delta)$ ≥ 0, $(1 - k^E \Delta) \geq 0$ indicate which part of the matrix in the destroyed monolayer drops out of operation. The values of $K_E E_{10}$ and $K_G G_{120}$ yield "real" values of the effective elasticity moduli by the start of the growth of delamination-caused defectiveness. These values of the effective properties account for the degradation of the properties on the previous stages of the process of accumulation of defectiveness.

5. ALGORITHM OF THE ACCOUNT FOR DEFECTIVENESS

The algorithm of the account for the defectiveness with consideration of the transversal cracking and the cracking on quasistatic loading is reduced to the following successive steps:

1. Determination of the stressed state of an element of constructions and singling out the zones of the concentration of stresses that potentially are dangerous from the viewpoint of destruction.
2. Calculation of stresses in the local layers of a composite using the relations of the mechanics of composites and the checking of the validity of the local criteria of destruction (i.e., with the aid of the Hill strength criterion). Revealing of the zones where the strength criterion over the transverse tension stresses and shear-strength criteria is violated.
3. If the shear-strength criterion is violated in a monolayer, then it is assumed that the local shear modulus in the monolayer is equal to zero.
4. If the strength criterion is violated over transversal tension stresses, it is checked how many systems of transverse microcracks appear in the given monolayer. If two systems of microcracks appear, then in the monolayer subjected to tension we should assume that $E_2 = 0$. Two systems of microcracks appear on violation of the strength criterion $\sigma_{x2}^+ \geq [\sigma_2]$, where

$$\sigma_{x2} = \frac{\sigma_{20}}{sh(\pi k_1/2k_2)} \left(sh\frac{\pi k_1}{2k_2} - \frac{k_1}{k_2}ch(k_1 x)\cos(k_2 x) - sh(k_1 x)\sin(k_2 x) \right).$$

5. In the found zones of the concentrations of stresses the characteristics of the composite are calculated. If there is cracking with one system of transverse cracks, the transverse elasticity moduli of monolayers are calculated by Eqs. (6). If two systems of cracks are formed, then in the monolayer considered $E_2 = 0$. If the strength criterion is violated by the shift in the monolayer, then it is adopted that the local shear modulus in the monolayer is equal to zero. The effective properties of the damaged composite are determined; they take into account the cracking-caused defectiveness and determine the values of the damaged moduli $K_E E_{10}$ and $K_G G_{120}$ in relations (7) and (8).

6. In the element of the construction, in the zones, where microdestruction occurred, the original material is replaced by the damaged one with the characteristics found by the above-given algorithm. As a result, a construction element with altered (generally variable over the coordinates) mechanical characteristics is obtained. In the general case, the property of the orthotropy of the material (if initially the composite was orthotropic) is violated.

7. Again the stresses in an element of the construction are calculated, and the entire procedure of calculation from Item 1 to Item 6 is repeated. Such kind of algorithm should be realized with the aid of the numerical method, say the method of finite elements.

Thus, a model of the accumulation of damages by the mechanism of transversal cracking and subsequent delamination of lamellar composites is suggested. Precisely this mechanism mainly determines the degradation of the properties of real composites. Actually, a model of the defectiveness is suggested that accounts for the two-stage character of the increase in defectiveness, when the transversal cracking is replaced by interlayer delamination on quasistatic loading.

We will give an example of calculation for a multilayered composite, and we will take into account the change in the stressed state in the region of cracking and delamination. We will estimate the influence of the accumulation of damages due to the delamination on the change in the characteristics of the material and, consequently, on the stressed state of the construction as a whole. For this purpose we will use the method of finite elements and the procedure of successive refinement, if required.

We will carry out calculations using as an example a strengthened panel (Fig. 7).

In the figures given below (Fig. 8), the distributions of stresses in the construction for an undamaged damaged material of the elements of the construction with different levels of damages ($\Delta \neq 0$, $\Delta = 0.1$) are given. The superscripts at the stresses designate the number of the layer (three layers: 1 – (45), 2 – (–45), 3 – (90)) and the subscripts denote the kind of stresses in the local coordinates of the
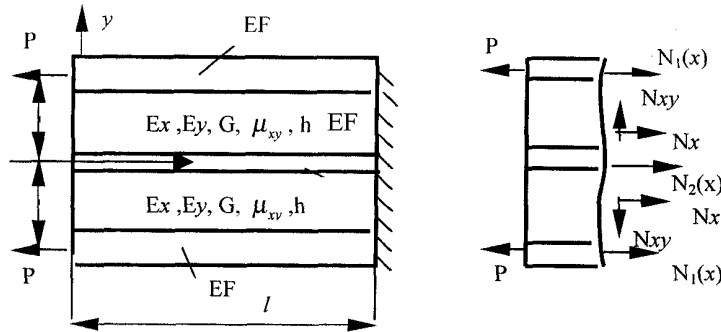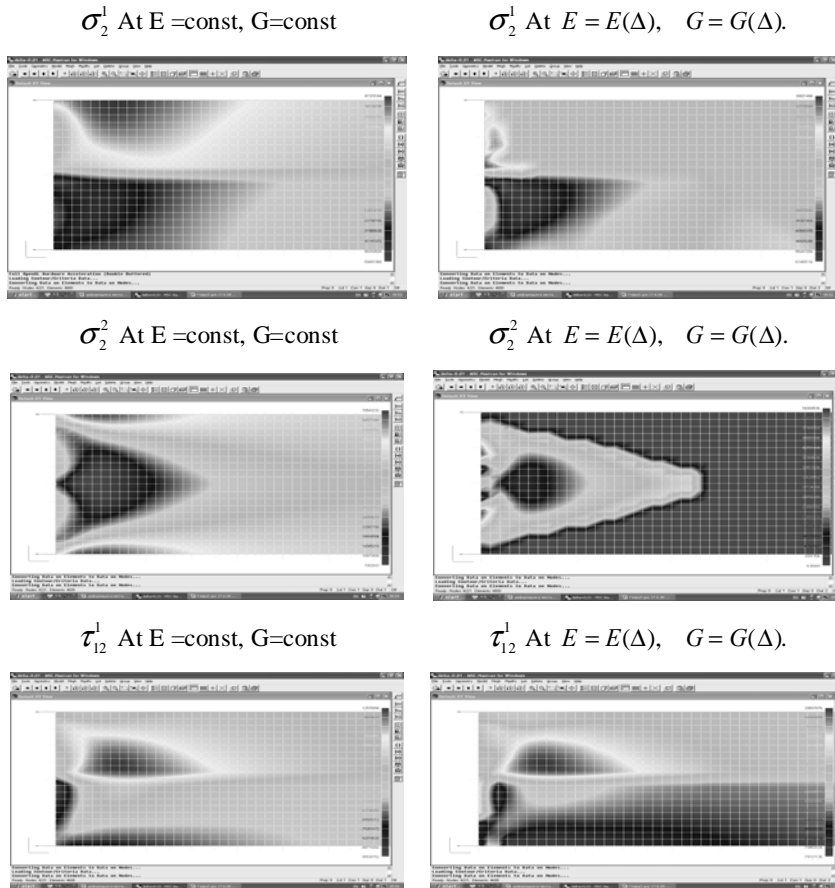
FIG. 7: Strengthened composite panel

σ_2^1 At E =const, G=const

σ_2^1 At $E = E(\Delta), \quad G = G(\Delta)$.

σ_2^2 At E =const, G=const

σ_2^2 At $E = E(\Delta), \quad G = G(\Delta)$.

τ_{12}^1 At E =const, G=const

τ_{12}^1 At $E = E(\Delta), \quad G = G(\Delta)$.

FIG. 8: Variation of stresses in the panel with allowance for the accumulation of damages from the transversal cracking and delamination

layer. It is shown that the character of the distribution of stresses can change substantially with an increase in the defectiveness, which should be taken into account in estimation of the capacity for work of the construction.

6. ACCOUNT FOR TRANSVERSAL CRACKING
AND DELAMINATION ON CYCLIC LOADING

We shall give a model of the increase in the defectiveness which is controlled by cracking and delamination on a pulsed change in loading.

The following hypotheses are adopted:

1. It is assumed that the number of the cracks of the delamination is fully dictated by the transversal cracking, i.e., by the value of the parameter X_f. We consider that each of the monolayers is internal for the structure investigated and we relate the delamination defects precisely to each of such monolayers assuming that these defects decrease the effective volume of the layer material participating in the deformation of the laminated packet of the composite. The number of the delamination defects is determined by the fact whether there is cracking in the given layer or not. It there is one system of transverse microcracks, then the number of delamination defects is proportional to $1/X_f$; if there are two transverse systems — to $1/2X_f$.
2. The delamination defects originating in different layers of the composite system do not interact between themselves.
3. The local parameter of defectiveness is determined as the length of a delamination microcrack.
4. The dependence of the speed of growth of a crack on the number of cycles of loading obeys the Paris law.

The model of the accumulation of damages is written in this case in the form

$$v(t) = v(N) = 0, \quad \frac{ds}{dt} = \frac{ds}{dN} = \frac{dl}{dN} = C(\Delta K)^m = C(\Delta\sigma)^m (\pi l)^{m/2}.$$

(see Eqs. (1) and (2))

Here N is the number of the cycles of loading, $\Delta\sigma$ is the amplitude of a stress in a cycle, l is the length of the delamination microcrack, and C and m are the parameters of the model.

$$S_e = \frac{\Delta}{3}\left[2 + \left(1 + \frac{N}{N_*^0}\left(\sqrt[3]{\frac{3S_*}{\Delta}} - 2 - 1\right)\left(1 - \frac{\sigma_2}{\left[\sigma_{b2}\right]}\right)^{-4}\right)^3\right],$$

$$S_g = \frac{\Delta}{3}\left[2 + \left(1 + \frac{N}{N_*^0}\left(\sqrt[3]{\frac{3S_*}{\Delta}} - 2 - 1\right)\left(1 - \frac{\tau_{12}}{\left[\tau_{12}\right]}\right)^{-4}\right)^3\right]$$

(11)

As a result, we will obtain the following models of the accumulation of damages for transversal directions of a monolayer with account for the level of loading: Here N_*^0 is the base number of cycles.

The limiting numbers of cycles in the ratio of the transversal characteristics of loading N_*^E and N_*^G (N_*^E is the limiting number of cycles prior to the destruction in the layer in the transverse direction and N_*^G is the number of cycles before the

$$N_*^E = \left(1 - \frac{\sigma_2}{[\sigma_{b2}]}\right)^{\alpha} N_*^0, \qquad N_*^G = \left(1 - \frac{\tau_{12}}{[\tau_{12}]}\right)^{\alpha} N_*^0,$$

shear-caused destruction in the layer) are determined by the level of loading and by the value of limiting stresses:

where α is the parameter of the model taken to be equal to four, $\alpha = 4$. The model of the degradation of the properties on cyclic loading which is in complete conjugation with the model of accumulation of damages on quasistatic loading ($N = 0$) has the form
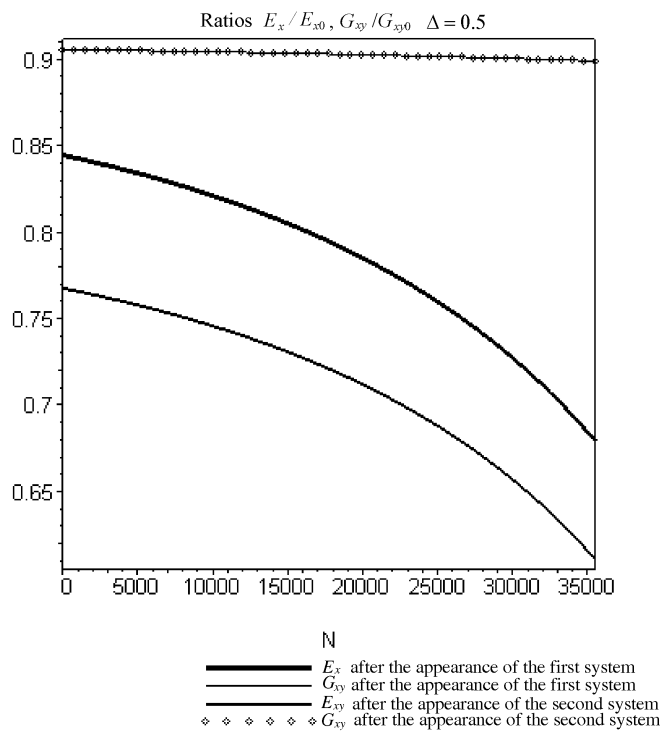
FIG. 9: Degradation of the properties after the appearance of the first and second systems of microcracks with delamination ($\Delta = 0.5$)

$$E_2 = E_{20}[1 - K_E^i S_e(N)], \qquad G_{12} = G_{120}[1 - K_G^i S_g(N)],$$

$$E_1 = K_E E_{10}(1 - k^E \Delta), \qquad G_{12} = K_G G_{120}(1 - k^G \Delta), \tag{12}$$

$$E_{20} = \frac{1}{X_f} \frac{1}{[\sigma_{20}^{(2)}]^2} \int_{-(X_f - l)}^{(X_f - l)} \frac{[\sigma_2^{(2)}(x)]^2}{2E_{20}} dx.$$

This algorithm of calculation of the stressed state and of the modeling of the process of degradation of properties entirely coincides with the above-described algorithm. It also envisages the procedure of successive refinement.

We will give an example of modeling of defectiveness with account for relations (11) and (12), when in one layer or in several layers of the composite the defectiveness connected with one or two systems of transverse cracks, depending on the level of loading, can be realized. A comparison of the defectiveness in these two cases will be carried out using as an example a strengthened panel in the case of $F = 4.5$ cm^2, assuming that in the casing one or two systems of cracks may form depending on the level of loading. The first case precedes the complete transversal destruction of the layer. The second signifies its actual destruction relative to the modulus E_2. The curves of Fig. 9 demonstrate the influence of the defectiveness on the effective properties of the panel (E_x and G_{xy}) depending on the number of cycles of loading after the appearance of the first system of transverse microcracks and of the second system of transverse microcracks. In this case, the defectiveness caused by both the transversal cracking and subsequent delamination is taken into account. Thus, the proposed technique makes it possible to obtain estimates of the influence of accumulated defectiveness on the effective properties and the stressed-strained state. It turns out to be very efficient as allows one to carry out a comparative analysis of various scenarios of defectiveness.

7. CONCLUSIONS

A model of degradation and an algorithm of calculation of the properties of monolayers and effective moduli of the elasticity of a composite on cracking and interlayer delamination for the cases of static and cyclic loading with account for the level of loading in individual monolayers of structure are suggested. The algorithm of the account for the cracking-delamination defectiveness has been developed and an applied model of the degradation of the mechanical properties in calculation of the stressed state by numerical methods has been proposed. The algorithm foresees the use of the procedure of successive refinement.

REFERENCES

1. Kashtalyan, M. and Soutis, C., Analysis of composite laminates with intra- and interlaminar damage, *Progr. Aerosp. Sci.*, vol. 41, pp. 152–173, 2005.
2. Kashtalyan, M. and Soutis, C.,, Analysis of local delaminations in composite laminates with angle–ply matrix cracks, *Int. J. Solids Struct.*, vol. 39, pp. 1515–1537, 2002a.
3. Kashtalyan, M. and Soutis, C., Mechanisms of internal damage and their effect on the behavior and properties of cross–ply composite laminates, *Int. J. Appl. Mech.*, vol. 38, no. 6, pp. 641–657, 2002b.
4. Lurie, S. A., Dudchenko, A. A., Halim, K., and Semerin, A. V., An algorithm of accounting for the defectiveness in the mechanics of materials, *Mekh. Kompoz. Mat. Konstr.*, vol. 12, no. 4, pp. 498–510 2006.
5. Lurie, S. A., Dudchenko, A. A., Halim, K., and Semerin, A. V., On modeling of the degradation of the mechanical characteristics of composite material due to the accumulation of damages, in: *Proc. Conf. "Modern Problems of the Mechanics of Heterogeneous Media,"* RAN Press, pp. 202–219, 2005.
6. Movchan, A. A., A micromechanical approach to the problem of describing the accumulation of anisotropic scattered damages, *Izv. Akad. Nauk SSSR, Mekh. Tverd. Tela*, vol. 3, pp. 115–123, 1990.
7. Movchan, A. A., *Problemy prochnosti tonkostennykh konstruktsii* (Problems of the Strength of Thin-Walled Constructions), MEI Press, pp. 20–24, 1989.
8. Vasiliev, V. V., Dudchenko, A. A., and Elpatievskii, A. N., On the specific features of deformation of orthotropic glass-plastics composite on extension, *Mekh. Polimerov*, vol. 1, pp. 144–147, 1970.

THE ALGORITHM OF SEARCHING FOR CONSTANTS IN A MODEL OF THE MECHANICAL BEHAVIOR OF RUBBER

A. G. Pelevin,[1*] *A. L Svistkov,*[1] *A. A. Adamov,*[1] *Lauke Bernd,*[2] *& Heinrich Gert*[2]

[1]*Institute of Continuum Mechanics, Ural Branch of the Russian Academy of Sciences, Perm, Russia*

[2]*Leibniz Institut für Polymerforschung, Dresden e.V., Dresden, Germany*

[*]Address all correspondence to A. G. Pelevin E-mail: pelevin@icmm.ru

A model of the mechanical behavior of rubber is considered. For constructing the governing equation, a scheme whose points are connected by elastic, viscous, plastic, and transmission elements is used. To describe the properties of each of the elements, the well-known equations of the nonlinear theory of elasticity, of the theory of nonlinear viscous fluids, and of the theory of plastic flow of a material under the conditions of the finite deformations of a medium are employed. An algorithm for obtaining the constants of the model is suggested. The search for these constants is arranged in steps. The constants in the governing equations determined at the previous step do not change at subsequent ones. The experiments (cyclic loadings with relaxation and creep) allow one to obtain more information on the viscoelastic properties of rubber.

KEY WORDS: *governing equations, finite deformations, viscoelasticity, softening, model, rubber*

1. INTRODUCTION

Rubbers are nanocomposites formed by an elastomer matrix and aggregates of technical carbon particles. The introduction of a filler into a polymer substantially changes the mechanical properties of the elastomer and leads to the appearance of new effects such as the softening of a material after the first deformation (the Patrikeev–Mullins effect), the dependence of the complex modulus on the amplitude of small deformations (the Pane effect), strength increase, etc. Wide application of rubbers in industry and the necessity of carrying out calculations for articles made from them have led to the appearance of mathematical models of elastomer nanocomposites. Great attention in literature is paid to modeling the viscoelastic behav-

NOMENCLATURE

c_h	thermal conductivity		$\mathbf{W_R}$	spin
$c_n^{(j)}$	scalar		w	volume density of free energy
$\mathbf{D}, ..., \mathbf{D}_i, ..., \mathbf{D}_k^{\text{left}}, \mathbf{D}_k^{\text{right}}$	tensors of			of the material
	deformation rates			
F	deformation gradient		**Greek symbols**	
	of a medium		η_k	viscosity coefficient
h	heat flux		$\eta_k^{(j)}$	scalar
g_n	scalar		θ	temperature
I_V, I_{V7}	scalars		κ_n	proportionality factor
$\mathbf{n}_1^i, \mathbf{n}_2^i, \mathbf{n}_3^i$	orthonormalized triplet		$\kappa_k^{(j)}$	scalar
	of the eigenvectors		λ_j^i	extension ratio of the ith elastic
	of extension vectors			element
$\mathbf{R}$	turning tensor		ν_k	scalar
s	material entropy		$\nu_k^{(j)}$	scalar
$\mathbf{T}_i, ..., \mathbf{T}_k^{\text{left}}, \mathbf{T}_k^{\text{right}}$	Cauchy stress		ξ_n	scalar
	tensors		ρ	mass density of the medium
$\mathbf{V}, \mathbf{V}_i$	extension tensors		Φ_n	scalar

ior of the material. For this purpose, internal tensor variables are used in equations. They are ascribed with the physical sense of stresses (Govindjee and Simo, 1992; Holzapfel and Simo, 1996; Holzapfel, 1996; Simo, 1987) or strains (Govindjee and Reese, 1997; Haupt et al., 2000; Lion, 1997a,b, 1998; Miehe and Keck, 2000; Reese and Govindjee, 1998). In constructing models, use is often made of the multiplicative decomposition of the deformation gradient into the elastic and inelastic ones. Another approach is the use of the additive representation of the strain rate tensor of the medium by the rate tensors of elastic and inelastic deformations (Palmov, 2000, 2001). We use this approach in the present work.

To construct a system of phenomenological equations use is often made of the notions of physical processes occurring on the structural level of the material. The concept of transition grids made it possible to construct a model, which describes experimental dependences with a high accuracy (Drozdov and Dorfman, 2002, 2004). A model of cluster–cluster aggregation was suggested (Klüppel, 2003; Meier and Klüppel, 2008). Based on the kinematics of superposition of small elastic and inelastic deformations on finite elastic–inelastic ones, a general form of evolution governing relations with objective derivatives coordinated with these equations was constructed (Novokshanov and Rogovoi, 2005; Rogovoi, 2005).

The method of constructing a system of governing equations for complex media operating under the conditions of finite deformations was suggested by Svistkov and Lauke (2009). In the present paper we consider its concrete use for describing the softening effect and the viscoelastic behavior of rubbers. An algorithm of a successive search for the model's constants has been suggested.

2. THE MODEL OF MECHANICAL BEHAVIOR OF RUBBER

To describe the mechanical behavior of rubber, we use the model presented in Fig. 1. Each element in the scheme conventionally represents a group of governing equations. From the scheme of the material one can see in which way the non-linear tensor equations are united into a full system of equations that makes it possible to model a complex viscoelastic behavior of the medium in the case of an arbitrary deformation of the material. The details of the algorithm for construct-ing governing equations from individual groups of constitutive relations (elastic, viscous, plastic, transmission ones) are described by Svistkov and Lauke (2009). The model was based on the approach that relies on the additive decomposition of the strain rate tensor of a medium into the strain rate tensors of individual ele-ments of the scheme. For the internal points of the scheme the fulfillment of the condition of the coordination of the Cauchy stress tensors is required (Svistkov and Lauke, 2009). The scheme of the mechanical behavior of the material demon-strates the transmitting elastic, viscous, and plastic elements. Below, the equations are given that are conventionally represented by them.

The material is assumed incompressible. The Cauchy deviator stress tensor $\mathbf{T}_i$ of the elastic element numbered i is calculated by means of conventional formulas of the nonlinear elasticity theory:

$$\operatorname{dev} \mathbf{T}_i = \operatorname{dev}\left(\rho \sum_{k=1}^{3} \lambda_k^{(i)} \frac{\partial f}{\partial \lambda_k^{(i)}} \mathbf{n}_k^{(i)} \otimes \mathbf{n}_k^{(i)}\right), \tag{1}$$

in which the mass density of the free energy of the medium f depends on the ex-tension ratios of elastic elements:
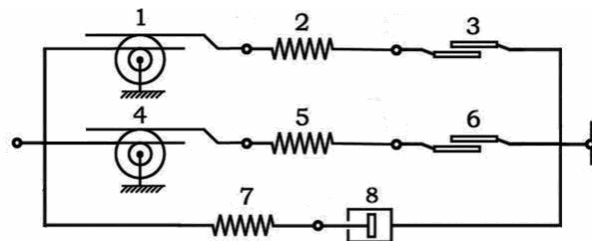
FIG. 1: Considered model of mechanical behavior of rubber

$$f = f(\lambda_1^{(2)}, \lambda_2^{(2)}, \lambda_3^{(2)}, \lambda_1^{(5)}, \lambda_2^{(5)}, \lambda_3^{(5)}, \lambda_1^{(7)}, \lambda_2^{(7)}, \lambda_3^{(7)}) ,$$

where $\lambda_1^{(i)}, \lambda_2^{(i)}, \lambda_3^{(i)}$ and $\mathbf{n}_1^{(i)}, \mathbf{n}_2^{(i)}, \mathbf{n}_3^{(i)}$ are the extension ratios and the eigenvectors of the extension tensor $\mathbf{V}_i$ of the elastic element numbered i. A change in time of the tensor $\mathbf{V}_i$ is calculated using the evolution equation:

$$\frac{2}{v_m}\, \mathbf{Y}_i^{0.5}\, \mathbf{D}_i \mathbf{Y}_i^{0.5} \;=\; \dot{\mathbf{Y}}_i - \mathbf{Y}_i\, \mathbf{W}_{\mathbf{R}}^{\mathrm{T}} - \mathbf{W}_{\mathbf{R}}\, \mathbf{Y}_i\,, \qquad \mathbf{W}_{\mathbf{R}} = \dot{\mathbf{R}}\, \mathbf{R}^{\mathrm{T}}\,.$$

In this equation, the following symbols are used:

$$\mathbf{Y}_i = \mathbf{V}_i^{\frac{2}{v_m}}\,, \qquad v_m > 0\,,$$

where $\mathbf{R}$ is the rotation tensor in the polar decomposition $\mathbf{F} = \mathbf{VR}$ of the deformation gradient of the medium $\mathbf{F}$ into the left tension tensor $\mathbf{V}$ and the rotation $\mathbf{R}$; v_m is the transmission ratio of the m-th transmission element that is connected with the considered elastic element on the left. In this case, the rate of the performance of work in the i-th elastic element is determined according to the formula

$$\mathbf{T}_i \cdot \mathbf{D}_i = \rho \sum_{k=1}^{3} \frac{\partial f}{\partial \lambda_k^{(i)}}\, \dot{\lambda}_k^{(i)} - \frac{\rho\, \dot{\nu}_m}{\nu_m} \sum_{k=1}^{3} \frac{\partial f}{\partial \lambda_k^{(i)}}\, \lambda_k^{(i)} \ln(\lambda_k^{(i)}). \tag{1}$$

Structural deformations of the parts of the elastomer matrix and macroscopic deformations of rubber differ substantially from one another. This difference can be taken into account in calculations with the aid of transmission elements. Due to these elements, the strain rate tensor at the right point of the transmission element increases v_m times as compared to the corresponding tensor at the left point at a simultaneous decrease in the Cauchy stress tensor:

$$\mathbf{D}_m^{\mathrm{left}} = \frac{1}{v_m}\, \mathbf{D}_m^{\mathrm{right}}\,, \qquad \mathbf{T}_m^{\mathrm{left}} = v_k\, \mathbf{T}_m^{\mathrm{right}}\,.$$

The deviator of the Cauchy stress tensor $\mathbf{T}_j$ of the viscous element numbered j is calculated from formulas of the nonlinear viscous fluid theory with the aid of the corresponding strain rate tensor $\mathbf{D}_j$:

$$\mathrm{dev}\,\mathbf{T}_j = 2\eta_j\, \mathbf{D}_j\,. \tag{2}$$

For the n-th plastic element the deviator of the Cauchy stress tensor will be determined from the formulas of the plastic flow theory:

$$\mathbf{D}_n = \sqrt{\frac{\mathbf{D}_n \cdot \mathbf{D}_n}{\mathrm{dev}\mathbf{T}_n \cdot \mathrm{dev}\mathbf{T}_n}}\; \mathrm{dev}\mathbf{T}_n, \tag{3}$$

To close the system, we use the proportional dependence between the strain rate tensors of the plastic element $\mathbf{D}_n$ and of the entire medium $\mathbf{D}$:

$$\sqrt{\mathbf{D}_n \cdot \mathbf{D}_n} = \kappa_n \sqrt{\mathbf{D} \cdot \mathbf{D}} , \qquad (4)$$

where the factor κ_n is the nonnegative function given by the dependence

$$\kappa_n = \begin{cases} 0, & \Phi_n(\mathbf{T}, ...) < g_n , \\ \zeta_n(g_n), & \Phi_n(\mathbf{T}, ...) = g_n . \end{cases}$$

The fluidity function Φ_n, with the aid of which a criterion of the development of plastic deformations in a medium is formed, is the function of the Cauchy tensor of stresses $\mathbf{T}$ operating in the material. Plastic deformation of the medium occurs only when the fluidity function Φ_n has a maximum value during the entire previous history of the existence of the medium:

$$g_n = \max \Phi_n .$$

The entropies of the material and the heat flux $\mathbf{h}$ are calculated according to the formulas of the nonequilibrium thermodynamics:

$$s = -\frac{\partial f}{\partial \theta} , \qquad \mathbf{h} = -c_{\mathbf{h}} \, \mathrm{grad} \, \theta , \qquad (5)$$

where $c_{\mathbf{h}} > 0$ is the thermal conductivity.

3. STEP-BY-STEP METHOD OF DETERMINING CONSTANTS FOR THE MODEL OF THE MECHANICAL BEHAVIOR OF RUBBER

To determine constants in the model considered, experiments with five specimens were used. Each of them was determined as follows. In the first cycle, a specimen is extended at a constant rate $|\dot{\lambda}| = 1/60 \text{ s}^{-1}$. After this, for 60 minutes the process of the relaxation of stresses was observed at a fixed strain of the medium. Thereafter the material was unloaded at a constant strain rate $|\dot{\lambda}| = -1/60 \text{ s}^{-1}$ and the creep of the material was fixed for 30 minutes. After this, the next cycles of deformation were employed. The difference of the subsequent cycles from the first one is that the relaxation of stresses was observed for 30 min instead of 60 min and the maximum extension ratio was smaller than that in the first cycle. Some information on the extension of the material at different cycles of deformation is presented in Table 1.

Such experiments yield a large amount of information on the mechanical properties of the material. On one specimen in one experiment one obtains data on the softening of the medium in the first cycle of deformation (the Patrikeev–Mullins effect), on the viscoelastic properties, and on the relaxation and creep processes.

Table 1: Values of maximum extension ratios of material depending on the cycle number for the specimens tested

No. of a specimen	1st cycle	2nd cycle	3rd cycle	4th cycle	5th cycle	6th cycle	7th cycle
1	1.5	1.25	1.5	–	–	–	–
2	1.75	1.25	1.5	1.75	–	–	–
3	2	1.25	1.5	1.75	2	–	–
4	2.25	1.25	1.5	1.75	2	2.25	–
5	2.5	1.25	1.5	1.75	2	2.25	2.5

The constants of the model can be determined in steps using the information obtained on the previous steps to find new constants.

3.1 The First Step

First, we consider a simple situation where the volume density of the free energy of the material $\omega = \rho f$ is the function of only the extension ratio of the second element:

$$w = w_2 = c_1^{(2)}\left(\sum_{i=1}^{3}(\lambda_i^{(2)})^2 - 3\right) + c_2^{(2)}\left(\sum_{i=1}^{3}(\frac{1}{\lambda_i^{(2)}})^2 - 3\right).$$

This means that within the framework of such an assumption all the elements from the fourth to the eighth one do not exert any influence on the mechanical behavior of the medium. Plastic deformations are accumulated only in the first cycle of deformation. In all the subsequent cycles the medium whose properties are modeled by elements numbered 1, 2, and 3 behaves as an elastic material. We will displace experimental data so that all the cycles except the first one could issue from the coordinate origin. The experimental data transformed in this way (Fig. 2) allow one to determine the elastic properties of the second element.

We will find the constants $c_1^{(2)}$ and $c_2^{(2)}$ of an elastic element and the values of the transmission ratio ν_1 of the first transmission element. We consider that for each specimen the transmission ratio ν_1 has its own value, whereas the constants $c_1^{(2)}$ and $c_2^{(2)}$ are common for all the specimens. To find the constants, we use only the points on experimental curves obtainable after the completion of the relaxation processes. These are the equilibrium points. We consider the relaxation processes to be entirely completed. The theoretical curve must pass through them. Here, we take into account only the points whose extension ratios are smaller than half the maximal one in the first deformation cycle. The passage of the theoretical curve through the remaining equilibrium points will be considered later.
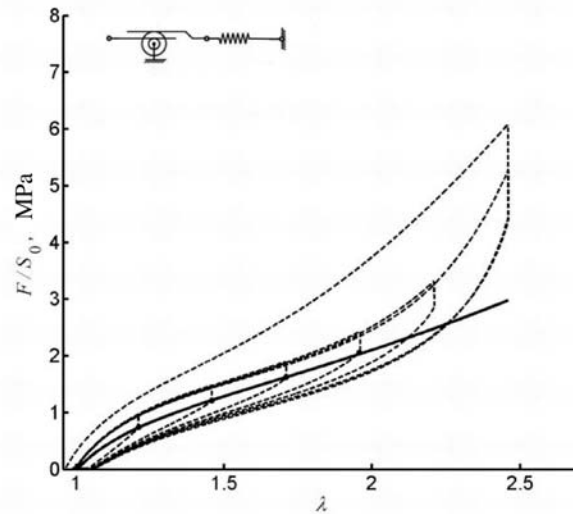
FIG. 2: Experimental data obtained in testing the fifth specimen (given with a shift along the λ axis) — the dashed line, and the theoretical curve determined at the first step of the search for constants — the solid line. The symbols denote: F is the extension force; S_0 is the area of the initial cross section

The process of finding the values of the considered quantities was arranged as follows. For the third specimen we determined the values of the variables $c_1^{(2)}$, $c_2^{(2)}$, and ν_1. For the remaining specimens we found only the values of the variables ν_1 using the found values of the constants $c_1^{(2)}$ and $c_2^{(2)}$ to describe the properties of the elastic element. The third specimen was selected as the basic one for determining elastic properties, since it occupies an intermediate position as to the level of maximum deformations attainable in experiment. Therefore it is likely that we will obtain some average values.

The model used at the first step and the theoretical curve obtained with the aid of this model for the fifth specimen are shown in Fig. 2. Our calculations have shown that the most severe differences between theoretical and experimental data occur precisely on the fifth specimen, since it undergoes the greatest deformations. Therefore, in the present article illustrations are given mainly for the fifth specimen.

3.2 The Second Step

Using the values of the transmission ratio of the first transmission element ν_1 found for different specimens, we represent the parameter ν_1 as a function of maximum deformations for the entire previous history of medium deformation:

$$\nu_1 = \nu_1^{(1)} \exp\left(-\nu_2^{(1)} \max\left(I_V\right)\right) , \tag{6}$$

where the invariant I_V is calculated from the formula

$$I_V = \sqrt{3\mathrm{tr}(\mathbf{V}^2) - \mathrm{tr}(\mathbf{V})^2}\ .$$

We find two more constants in the model: $\nu_1^{(1)}$ and $\nu_2^{(1)}$.

In our opinion the first transmission element must model the coupling between structural stresses in the active part of the binding elastomer nanocomposite and macroscopic stresses of the material. It is natural that this coupling depends on the process of the fracture of aggregates into parts in the process of rubber extension. In the model, this process is taken into account by a decreasing transmission ratio of the first transmission element and is defined by Eq. (6).

3.3 The Third Step

In the model, we take into account the accumulation of irreversible deformations. We will make the considered scheme of mechanical behavior more complex by including into it a plastic element numbered three. The properties of this element are defined by Eq. (4) and by the choice of the functions $\zeta_3(g_3)$ and $\Phi_3(\mathbf{T})$. To find it, we use (in contrast to the previous steps) real rather than displaced curves of the dependence of the extension force on the extension ratio for the specimens investigated:

$$\zeta_3(g_3) = \kappa_0^{(3)} + \kappa_1^{(3)}\exp(\kappa_2^{(3)}g_3), \qquad \Phi_3 = \sqrt{\mathrm{dev}\mathbf{T}\cdot\mathrm{dev}\mathbf{T}}.$$
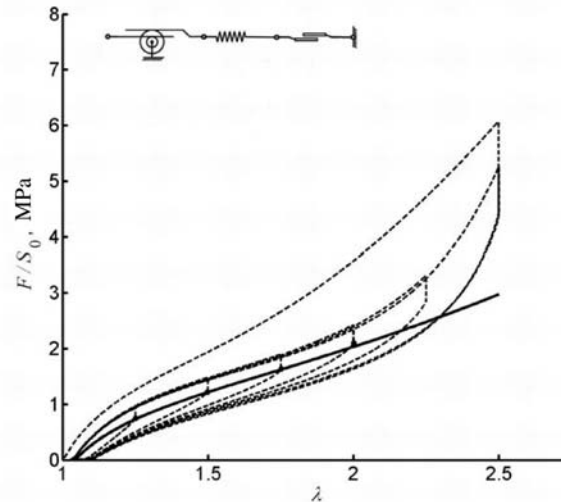

FIG. 3: Experimental data obtained in testing the fifth specimen — the dashed line, and the theoretical curve determined at the third step of the search for constants — the solid line

We will select the values of the constants $\kappa_0^{(3)}$, $\kappa_1^{(3)}$, and $\kappa_2^{(3)}$ in such a way as to obtain in the model an exact description of the values of the residual extension ratio (obtainable after the completion of the creep process) for all the specimens considered.

The model used at the third step and the theoretical curve obtained with the aid of this model for the fifth specimen are shown in Fig. 3.

3.4 The Fourth Step

In constructing a mathematical model of the mechanical behavior of rubber we will resort to the hypothesis that in a material subjected to deformation there occurs the formation of highly robust fibers. These fibers consist of an orientated polymer, and they are formed as a result of the slipping of the polymer chains from the layers near the filler particles into the gaps between the aggregates of particles. At this step we will describe the elastic properties of the fibers that have already been formed (i.e., we consider that the fibers have already been formed as a result of the first loading). We write the potential of the free energy of the medium in the form of the sum $\omega = \omega_2 + \omega_5$, where

$$w_5 \;=\; \begin{cases} 0, & \xi_5 < 0, \\ c_1^{(5)}\xi_5, & \xi_5 \geq 0. \end{cases}$$
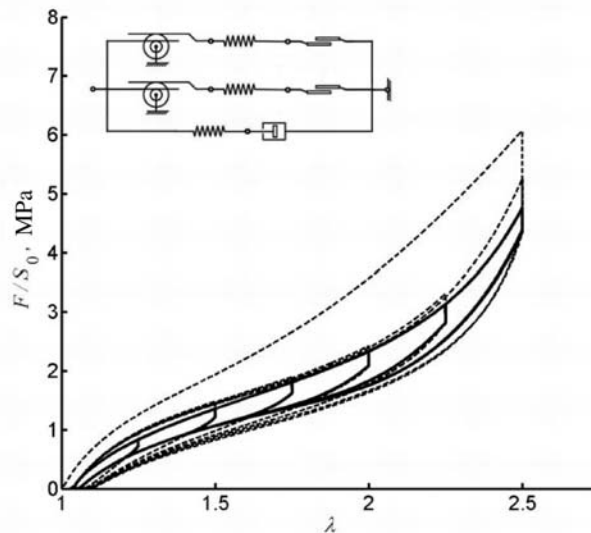
and
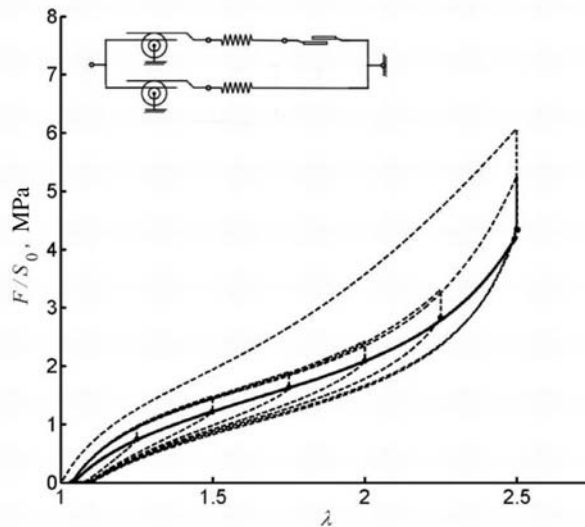
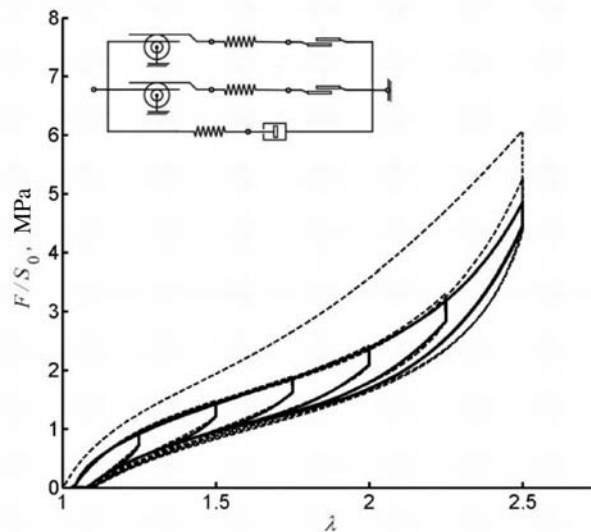**FIG. 4:** Experimental data obtained in testing the fifth specimen — the dashed line, and the theoretical curve determined at the fourth step of the search for constants — the solid line

$$\xi_5 = \left((\lambda_1^{(5)})^2 - 1\right)\left((\lambda_2^{(5)})^2 - 1\right)\left((\lambda_3^{(5)})^2 - 1\right).$$

To select the constant $c_1^{(5)}$ of the fifth elastic element and of the transmission ratio ν_4 of the fourth transmission element, we use all the points on the experimental curve that were obtained on completion of the relaxation processes. The model used at the fourth step and the theoretical curve obtained with the aid of this model for the fifth specimen are shown in Fig. 4.

3.5 The Fifth Step

In the model we will take into account the action of the sixth plastic element that describes the process of the formation of fibers as a result of the motion of polymer chains from the layers into the gaps between the inclusions. The properties of this element are defined by Eq. (4) and by the choice of the function $\zeta_6(g_6)$ and $\Phi_6(\mathbf{T})$. To find them, we use the points on the experimental curve that correspond to the moments of the completion of relaxation processes for the first cycles of deformation in all of the specimens (Fig. 5):

$$\zeta_6(g_6) = \kappa_0^{(6)} + \kappa_1^{(6)} \exp\left(\kappa_2^{(6)} g_6\right), \qquad \Phi_6 = \sqrt{\mathrm{dev}\mathbf{T} \cdot \mathrm{dev}\mathbf{T}} ,$$
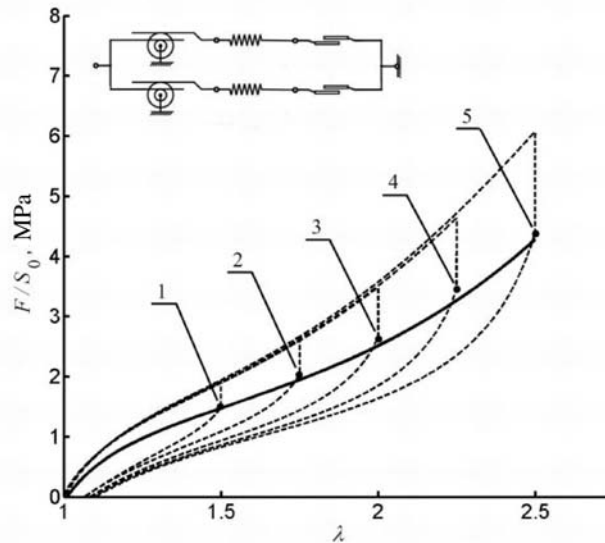
FIG. 5: Experimental data of the first cycles of deformation of specimens — the dashed line. The curves shown by the dashed line refer to the first cycle of loading the specimens. The digits at the points correspond to the numbers of specimens. The solid line shows the theoretical curve of the extension of the material obtained with account for the growth of plastic deformations

where $\mathbf{T}$ is the tensor of the Cauchy stresses operating in the material. We select the values of the constants $\kappa_0^{(6)}$, $\kappa_1^{(6)}$, and $\kappa_2^{(6)}$ in such a way that the calculated curve of the unloading of the first cycle could pass through the selected points. The model used at the fifth step and the theoretical curve obtained with the aid of this model for the fifth specimen are shown in Fig. 5.

3.6 The Sixth Step

We include into the model the elements that allow one to describe the viscoelastic behavior of the material. This can be attained in two ways. The first way presupposes the introduction of several Maxwellian elements into the model. In this case, their behavior must be described by relatively simple expressions.

The second way presupposes the introduction into the model of only one Maxwellian element. But its properties will be defined by substantially nonlinear expressions.

We have selected the second way. We will describe the characteristic features of the viscoelastic behavior of the material with the aid of the seventh elastic and eighth viscous elements.

The potential of the free energy of the medium is presented in the form of the sum $\omega = \omega_2 + \omega_5 + \omega_7$, where

$$w_7 = c_1^{(7)} \left(\sum_{i=1}^{3} (\lambda_i^{(7)})^2 - 3 \right). \tag{7}$$
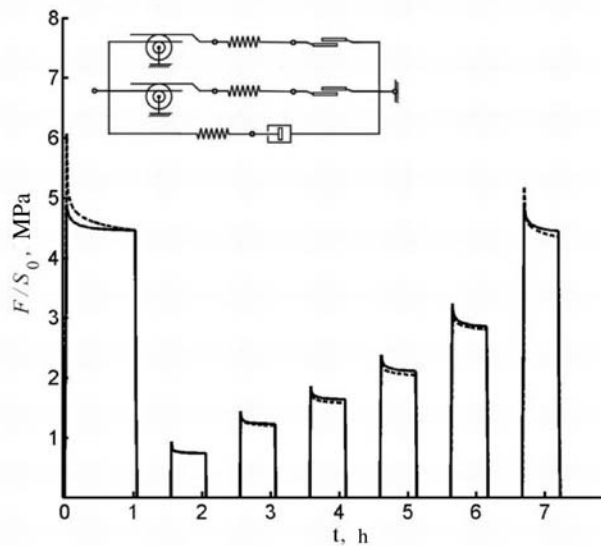

FIG. 6: Experimental data obtained in testing the fifth specimen — the dashed line and the theoretical curve determined at the sixth step of the search for constants

The properties of the viscous element are determined with the aid of Eq. (2) and the following viscosity function:

$$\eta_8 = \eta_0^{(8)} \exp(\eta_1^{(8)} I_V) .$$

The constants $c_1^{(7)}$, $\eta_0^{(8)}$, and $\eta_1^{(8)}$ are selected so that the theoretical curve could coincide with experimental data over the portions of material extension for all the cycles of deformation except the first one. The model used at the sixth step and the theoretical curve obtained with the aid of this model for the fifth specimen are shown in Fig. 6.

3.7 The Seventh Step

We will complicate the mathematical expression for the viscosity function η_8 thus as to satisfactorily describe experimental data not only on material extension, but also on removal of outer loading.

For this purpose, the mathematical expression of the function η_8 is supplemented with still one other term. The constants $\eta_2^{(8)}$, $\eta_3^{(8)}$, and $\eta_4^{(8)}$ are selected so that the theoretical curves could coincide with experimental ones on both extension and removal of loading for all of the cycles except the first one:

$$\eta_8 = \eta_0^{(8)} \exp(\eta_1^{(8)} I_V) + \eta_2^{(8)} (\exp(-\eta_3^{(8)}\mathbf{V} \cdot \mathbf{D}) + I_V \exp(-\eta_4^{(8)}\mathbf{V} \cdot \mathbf{D})) .$$

FIG. 7: Experimental data obtained in testing the fifth specimen — the dashed line, and the theoretical curve with a complicated function of viscosity for a more accurate description of loading and unloading determined at the seventh step of the search for constants — the solid line

The model used at the seventh step and the theoretical curve obtained with the aid of this model for the fifth specimen are shown in Fig. 7.

3.8 The Eighth Step

At the previous two steps we considered the modeling of rapid processes. Now, we must refine theoretical calculations with a view to satisfactorily describe the process of stress relaxation. For this purpose, it is necessary that the numerical value of viscosity during relaxation be much higher than the material viscosity during loading and unloading. We will consider this process separately. For a while we will forget about the already found expression for η_8. For each specimen we have several portions of stress relaxation on deformation of specimens.

During relaxation, the extensions of a specimen are unchanged, and only the extension ratios of the seventh elastic element undergo a change. The values of viscosity η_8 are approximated by the formula

$$\eta_8 = \eta_8^5 \exp\left(bI_V7\right) ,$$

where $I_{V7} = \sqrt{3\mathrm{tr}(\mathbf{V}_7^2) - \mathrm{tr}(\mathbf{V}_7)^2}$. The value of the parameter $b = b(\mathbf{V})$ depends on the specimen extension tensor. For each extension ratio of the material it is not difficult to find its value. After this, we describe its dependence on deformations with the aid of the mathematical expression
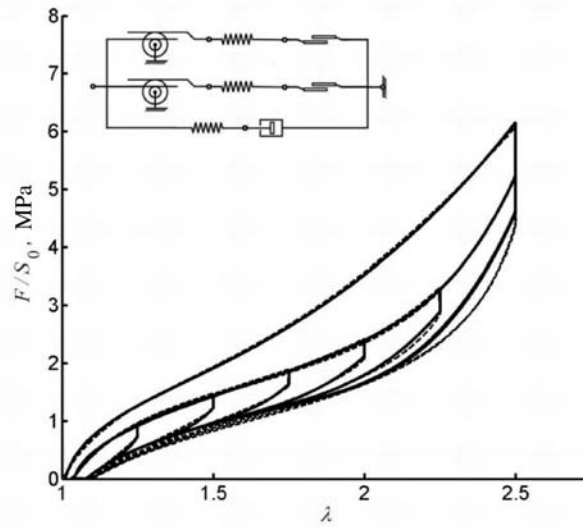

FIG. 8: Experimental data obtained in testing the fifth specimen — the dashed line, and the theoretical curve determined at the eighth step of the search for constants — the solid line

$$b = -\frac{\eta_6^{(8)}}{\exp\left(\eta_7^{(8)} I_V\right)},$$

where $\eta_6^{(8)}$ and $\eta_7^{(8)}$ are constants. The viscosity functions take the form

$$\eta_8 = \eta_5^{(8)} \exp\left(-\frac{\eta_6^{(8)} I_{V7}}{\exp(\eta_7^{(8)} I_V)}\right).$$

The model employed at the eighth step and the theoretical curve obtained with the aid of this model are presented in Fig. 8.

3.9   The Ninth Step

We will unite the rapid and slow relaxation times in the viscosity:

$$\eta_8 = \eta_0^{(8)} \exp(\eta_1^{(8)} I_V) + \eta_2^{(8)}\left(\exp(-\eta_3^{(8)} \mathbf{V} \cdot \mathbf{D}) + I_V \exp(-\eta_4^{(8)} \mathbf{V} \cdot \mathbf{D})\right) +$$
$$+\eta_5^{(8)} \exp\left(\frac{-\eta_6^{(8)} I_{V7}}{\exp(\eta_7^{(8)} I_V)}\right) \exp(-\eta_8^{(8)} I_D),$$

where $I_D = \sqrt{3\mathrm{tr}(\mathbf{D}^2) - \mathrm{tr}(\mathbf{D})^2}$. The constant $\eta_8^{(8)}$ allows one to make the contribution of the last term insignificant at the considered rates of material deformation and to transform this term into the main one (at the expense of the high value of the constant $\eta_5^{(8)}$) in the absence of deformation.

3.10   The Tenth Step

The found dependence of viscosity will be supplemented with still another term to describe the experiment on the first loading:

$$\eta_8 = \eta_0^{(8)} \exp(\eta_1^{(8)} I_V) + \eta_2^{(8)}\left(\exp(-\eta_3^{(8)} \mathbf{V} \cdot \mathbf{D}) + I_V \exp(-\eta_4^{(8)} \mathbf{V} \cdot \mathbf{D})\right) +$$
$$+\eta_5^{(8)} \exp\left(\frac{-\eta_6^{(8)} I_{V7}}{\exp(\eta_7^{(8)} I_V)}\right) \exp(-\eta_8^{(8)} I_D) +$$
$$+\eta_9^{(8)} \exp(\eta_{10}^{(8)} I_V) \exp\left(\eta_{11}^{(8)} \frac{I_V - \max(I_V)}{\max(I_V)}\right),$$

The constants $\eta_9^{(8)}$ and $\eta_{10}^{(8)}$ of the last term in the equation are determined after the first loading. Since the current and maximum extensions of the specimen coincide after the first extension of specimens, the value of the constant $\eta_{11}^{(8)}$ at this stage of deformation cannot be determined. We find the value of the constant $\eta_{11}^{(8)}$ from the condition of the most accurate description of the behavior of the medium in the region of deformations close to the maximum one when the material is subjected to further deformation. As a result, we obtain a theoretical de-

FIG. 9: Experimental data obtained in testing the fifth specimen — the dashed line, and the theoretical curve determined at the tenth step of the search for constants — the solid line

scription of the experiment. A comparison of the experimental and theoretical curves is shown in Fig. 9.

4. CHECKING OF THE FULFILLMENT OF THE DISSIPATION INEQUALITY

The governing equations of the model must lead to automatic fulfillment of the dissipation inequality:

$$\mathbf{T} \cdot \mathbf{D} - \rho(\dot{f} + s\,\dot{\theta}) - \frac{\mathbf{h} \cdot \mathrm{grad}\theta}{\theta} \geq 0. \tag{8}$$

We will prove the validity of inequality (8) for the material the mechanical behavior of which is illustrated by the scheme shown in Fig. 1. We will decompose the value of the scalar product $\mathbf{T} \cdot \mathbf{D}$ using, for the purpose, the rules of constructing the model and performing a number of obvious transformations:

$$
\begin{aligned}
\mathbf{T} \cdot \mathbf{D} &= (\mathbf{T}_1^{\mathrm{left}} + \mathbf{T}_4^{\mathrm{left}} + \mathbf{T}_7) \cdot \mathbf{D} = \mathbf{T}_1^{\mathrm{right}} \cdot \mathbf{D}_B + \mathbf{T}_4^{\mathrm{right}} \cdot \mathbf{D}_D + \mathbf{T}_7 \cdot \mathbf{D}_A = \\
&= \mathbf{T}_1^{\mathrm{right}} \cdot (\mathbf{D}_B - \mathbf{D}_C) + \mathbf{T}_1^{\mathrm{right}} \cdot \mathbf{D}_C + \\
&+ \mathbf{T}_4^{\mathrm{right}} \cdot (\mathbf{D}_D - \mathbf{D}_E) + \mathbf{T}_1^{\mathrm{right}} \cdot \mathbf{D}_E + \\
&+ \mathbf{T}_7 \cdot (\mathbf{D}_A - \mathbf{D}_F) + \mathbf{T}_7 \cdot \mathbf{D}_F = \\
&= \mathbf{T}_1^{\mathrm{right}} \cdot \mathbf{D}_2 + \mathbf{T}_1^{\mathrm{right}} \cdot \mathbf{D}_3 + \mathbf{T}_4^{\mathrm{right}} \cdot \mathbf{D}_5 + \mathbf{T}_4^{\mathrm{right}} \cdot \mathbf{D}_6 + \mathbf{T}_7 \cdot \mathbf{D}_7 + \mathbf{T}_7 \cdot \mathbf{D}_8.
\end{aligned}
$$

A further simplification leads to the result

$$\mathbf{T} \cdot \mathbf{D} = \mathbf{T}_2 \cdot \mathbf{D}_2 + \mathbf{T}_3 \cdot \mathbf{D}_3 + \mathbf{T}_5 \cdot \mathbf{D}_5 + \mathbf{T}_6 \cdot \mathbf{D}_6 + \mathbf{T}_7 \cdot \mathbf{D}_7 + \mathbf{T}_8 \cdot \mathbf{D}_8 =$$
$$= \sum_{k=2,3,5,6,7,8} \mathbf{T}_k \cdot \mathbf{D}_k$$

We have come to the conclusion that the power of the stresses functioning in the medium is equal to the sum of the powers of the operation of stresses in all the elements of the scheme of the mechanical behavior of the medium except for the transmission elements. As a result of this, the dissipation inequality (8) takes the form

$$\sum_{k=2,3,5,6,7,8} \mathbf{T}_k \cdot \mathbf{D}_k - \rho(\dot{f} + s\,\dot{\theta}) - \frac{\mathbf{h} \cdot \mathrm{grad}\theta}{\theta} \geq 0 \,. \tag{9}$$

We substitute the value of the material derivative of the free energy density:

$$\dot{f} = \frac{\partial f}{\partial \theta} \dot{\theta} + \sum_{k=2,5,7} \sum_{i=1}^{3} \frac{\partial f}{\partial \lambda_i^{(k)}} \dot{\lambda}_i^{(k)}$$

into inequality (9) with allowance for (1) and (5). As a result, we obtain the constraint

$$\sum_{n=3,6,8} \mathbf{T}_n \cdot \mathbf{D}_n - \sum_{k=2,5,7} \sum_{i=1}^{3} \frac{\rho\,\dot{\nu}_k}{\nu_k} \frac{\partial f}{\partial \lambda_i^{(k)}} \lambda_i^{(k)} \ln(\lambda_i^{(k)}) + \frac{c_{\mathrm{h}}\mathrm{grad}\theta \cdot \mathrm{grad}\theta}{\theta} \geq 0$$

Using the properties of the viscous (2) and plastic (3) elements, we transform it into

$$\mathbf{T}_8 \cdot \frac{\mathrm{dev}\mathbf{T}_8}{2\eta_8} + \sum_{n=3,6} \mathbf{T}_n \cdot \sqrt{\frac{\mathbf{D}_n \cdot \mathbf{D}_n}{\mathrm{dev}\mathbf{T}_n \cdot \mathrm{dev}\mathbf{T}_n}} \mathrm{dev}\mathbf{T}_n -$$

$$- \sum_{k=2,5,7} \sum_{i=1}^{3} \frac{\rho\,\dot{\nu}_k}{\nu_k} \frac{\partial f}{\partial \lambda_i^{(k)}} \lambda_i^{(k)} \ln(\lambda_i^{(k)}) + \frac{c_{\mathrm{h}}\mathrm{grad}\theta \cdot \mathrm{grad}\theta}{\theta} \geq 0$$

With the aid of the identity

$$\mathbf{A} \cdot \mathrm{dev}\,\mathbf{A} = \mathrm{dev}\,\mathbf{A} \cdot \mathrm{dev}\,\mathbf{A}$$

we obtain the dissipation inequality in the final form:

$$\frac{\mathrm{dev}\mathbf{T}_8 \cdot \mathrm{dev}\mathbf{T}_8}{2\eta_8} + \sum_{n=3,6} \sqrt{\frac{\mathbf{D}_n \cdot \mathbf{D}_n}{\mathrm{dev}\mathbf{D}_n \cdot \mathrm{dev}\mathbf{T}_n}} \ \mathrm{dev}\mathbf{T}_n \cdot \mathrm{dev}\mathbf{T}_n -$$

$$- \sum_{k=2,5,7} \sum_{i=1}^{3} \frac{\rho\,\dot{\nu}_k}{\nu_k} \frac{\partial f}{\partial \lambda_i^{(k)}} \lambda_i^{(k)} \ln(\lambda_i^{(k)}) + \frac{c_{\mathrm{h}}\,\mathrm{grad}\theta \cdot \mathrm{grad}\theta}{\theta} \geq 0 \tag{10}$$

Since the viscosity η_6, the parameters ν_k, and the thermal conductivity c_h are positive, the dissipation inequality (10) will be valid provided the following constraints are fulfilled:

$$- \sum_{k=2,5,7} \sum_{i=1}^{3} \frac{\rho \, \dot{\nu}_k}{\nu_k} \frac{\partial f}{\partial \lambda_i^{(k)}} \lambda_i^{(k)} \ln(\lambda_i^{(k)}) \geq 0 \, . \tag{11}$$

For the fourth element the value of the transmission number ν_k is constant. This means that for it $\dot{\nu}_4 = 0$. For the second transmission element the transmission number ν_2 is a nonincreasing function in time. Therefore the constant $\dot{\nu}_k \leq 0$ holds. Thus, to check the fulfillment of inequality (11) we are to make sure that the following condition is valid:

$$\sum_{i=1}^{3} \frac{\partial f}{\partial \lambda_i^{(2)}} \lambda_i^{(2)} \ln(\lambda_i^{(2)}) \geq 0.$$

We substitute into this expression the specific form of the free energy potential of the material considered:

$$\sum_{i=1}^{3} \frac{\partial f}{\partial \lambda_i^{(2)}} \lambda_i^{(2)} \ln(\lambda_i^{(2)}) = \sum_{i=1}^{3} 2 \left(c_1^{(2)} (\lambda_i^{(2)})^2 - \frac{c_2^{(2)}}{(\lambda_i^{(2)})^2} \right) \ln(\lambda_i^{(2)}) =$$

$$= 2c_1^{(2)} \sum_{i=1}^{3} \left((\lambda_i^{(2)})^2 - 1 \right) \ln(\lambda_i^{(2)}) + 2c_1^{(2)} \sum_{i=1}^{3} \ln(\lambda_i^{(2)}) +$$

$$+ 2c_2^{(2)} \sum_{i=1}^{3} \left(1 - \frac{1}{(\lambda_i^{(2)})^2} \right) \ln(\lambda_i^{(2)}) - 2c_2^{(2)} \sum_{i=1}^{3} \ln(\lambda_i^{(2)}) \geq 0 \, .$$

In an incompressible material the product $\lambda_1^{(2)} \lambda_2^{(2)} \lambda_3^{(2)}$ is equal to unity. As a result, we obtain the final expression:

$$2c_1^{(2)} \sum_{i=1}^{3} ((\lambda_i^{(2)})^2 - 1) \ln(\lambda_i^{(2)}) + 2c_2^{(2)} \sum_{i=1}^{3} (1 - \frac{1}{(\lambda_i^{(2)})^2}) \ln(\lambda_i^{(2)}) \geq 0.$$

It is evident that it is always satisfied. Consequently, the dissipation inequality always holds as we set out to prove.

5. CONCLUSIONS

A method to seek for model constants in steps for describing the viscoelastic properties of rubbers is suggested. The system of governing equations takes into account the characteristic features of the behavior of a material on the structural level of the medium. The theoretical results obtained rather accurately describe the behavior of rubber.

ACKNOWLEDGEMENT

REFERENCES

Drozdov, A. D. and Dorfman, A., Finite viscoelasticity of filled rubbers: the effect of preloading and thermal recovery, *Cont. Mech. Thermodyn.*, vol. 14, pp. 337–361, 2002.

Drozdov, A. D. and Dorfman, A., A constitutive of particle-reinforced rubbers, *Mechanica*, vol. 39, pp. 245–270, 2004.

Govindjee, S. and Simo, J. C., Mullins' effect and the strain amplitude dependence of the storage modulus, *Int. J. Solid Struct.*, vol. 29, pp. 1737–1751, 1992.

Govindjee, S. and Reese, S., A presentation and comparison of two large deformation viscoelasticity models, *J. Eng. Mater. Tech.*, vol. 119, pp. 251–255, 1997.

Haupt, P., Lion, A., and Backhaus, E., On the dynamic behaviour of polymers under finite strains: constitutive modeling and identification of parameters, *Int. J. Solid. Struct.*, vol. 37, pp. 3633–3646, 2000.

Holzapfel, G. A. and Simo, J. C., A new viscoelastic constitutive model for continuous media at finite thermomechanical changes, *Int. J. Solid Struct.*, vol. 33, pp. 3019–3034, 1996.

Holzapfel, G. A., On large strain viscoelasticity: continuum formulation and finite element applications to elastomeric structures, *Int. J. Numer. Meth. Eng.*, vol. 39, pp. 3903–3926, 1996.

Klüppel, M., The role of disorder in filler reinforcement of elastomers on various length scales, in: *Advances in Polymer Science*, vol. 164, pp. 1–86, 2003.

Lion, A., A physically based method to represent the thermomechanical behaviour of elastomers, *Acta Mech.*, vol. 123, pp. 1–25, 1997a.

Lion, A., On the large deformation behaviour of reinforced rubber at different temperatures, *J. Mech. Phys. Solids*, vol. 45, pp. 1805–1834, 1997b.

Lion, A., Thixotropic behaviour of rubber under dynamic loading histories: experiment and theory, *J. Mech. Phys. Solids*, vol. 46, pp. 895–930, 1998.

Meier, J. G. and Klüppel, M., Carbon black networking in elastomers monitored by dynamic mechanical and dielectric spectroscopy, *Macromolec. Mater. Eng.*, vol. 293, pp. 12–38, 2008.

Miehe, C. and Keck, J., Superimposed finite elastic-viscoelastic-plastoelastic stress response with damage in filled rubbery polymers. Experiments, modelling and algorithmic implementation, *J. Mech. Phys. Solids*, vol. 48, pp. 323–365, 2000.

Novokshanov, R. S. and Rogovoi, A. A., Evolution governing relations for finite viscoelastic deformations, *Izv. Ros. Akad. Nauk, Mekh. Tverd. Tela*, vol. 40, no. 4, pp. 122–140, 2005.

Palmov, V. A., Comparison of different approaches in viscoelasticity for large strain, *ZAMM*, vol. 80, pp. 801–806, 2000.

Palmov, V. A., A comparison of the methods of decomposition of deformation in nonlinear viscoelasticity and elastoplasticity, in: *Elasticity and Inelasticity (a volume of papers dedicated to the 90th birthday of A. A. Il'yushin)*, Moscow: MGU Press, 2001, pp. 81–87.

Reese, S. and Govindjee, S., A theory of finite viscoelasticity and numerical aspects, *Int. J. Solid Struct.*, vol. 35, pp. 3455–3482, 1998.

Rogovoi, A. A., Governing relationships for finite elastic-inelastic deformations, *Prikl. Mekh. Tekh. Fiz.*, vol. 46, no. 5, pp. 138–149, 2005.

Svistkov, A. L. and Lauke, B., Differential governing equations of incompressible media on finite deformations, *Prikl. Mekh. Tekh. Fiz.*, vol. 50, no. 3, pp. 158–170, 2009.

Simo, J. C., On a fully three-dimensional finite-strain viscoelastic damage model: formulation and computational aspects, *Comput. Meth. Appl. Mech. Eng.*, vol. 60, pp. 153–173, 1987.

ANALYSIS OF JUTE FIBER-REINFORCED EPOXY/VAc-EHA/HMMM IPN COMPOSITE PLATE

R. K. Misra[1][*] & Chandan Datta[2]

[1]*Department of Mechanical Engineering, KIIT University, Bhubaneswar-751024, Orissa, India*

[2]*Department of Polymer Engineering, Birla Institute of Technology, Mesra, Ranchi-835215, India*

[*]Address all correspondence to R. K. Misra E-mail: mishrark_kanpur@yahoo.com

Jute fiber-reinforced semi-IPN and full-IPN Epoxy/VAc-EHA/HMMM IPN composite plates have been prepared in a laboratory at different volume fractions of VAc-EHA for the evaluation of mechanical properties. An epoxy solution was blended with VinylAcetate-2-Ethylhexylacrylate (VAc-EHA) resin in an aqueous medium at varying weight fractions of VAc-EHA. It has been observed that as soon as the percentage of the VAc-EHA increases, the ultimate tensile strength and modulus of elasticity of a jute fiber-reinforced semi-IPN and full-IPN composite plate decreases. A jute fiber-reinforced full-IPN composite plate is compact and harder than a jute fiber-reinforced semi-IPN composite plate.

KEY WORDS: *jute fiber, epoxy, vinylacetate-2-ethylhexylacrylate, full-IPN, semi-IPN*

1. INTRODUCTION

The importance and popularity of fiber-reinforced epoxy composites are due to their unusually high strength and stiffness for a given weight of material. In recent years, greater emphasis has been rendered in the development of fiber-filled epoxy composites based on natural fibers with a view to replace solely or in part in various applications.

Natural fibers such as jute, coir, banana, and bamboo (Rana et al., 1997, 2003; Monteiro et al., 2008; Idicula et al., 2005; Thwe and Liao, 2002) have many advantages as compared to synthetic fibers. Their low cost, lower density, friendly to environment, and renewable nature make them attractive for use as a reinforcing material in the fiber-filled composites. Compared to other natural fibers, jute fibers are economical and easily available in tropical countries. Workable tensile modulus and a nonabrasive nature of the jute fiber (Corrales et al., 2007) permit higher

fiber loading in the composite without the fear of extensive damage to compounding and molding equipment that occurs when much harder glass fiber is used. Therefore, research and development are continued to explore its applications. Jute fiber as reinforcement in polymer composites is one of them (Gassan and Bledzki, 1999). In 1985, Kishore (1985) used jute as a reasonable core material in jute-glass hybrid laminates.

In this paper, unmodified liquid Diglycidylether of bis-phenol A (DGEBA) resin has been selected. In order to impart greater heat resistance and flame retardance, an epoxidized novolac (EPN) resin was prepared in a laboratory to use along with DGEBA resin. Epoxy resins are brittle materials having fracture energy of about two orders of magnitude lower than engineering thermoplastic and three orders lower than metals. This inherent brittleness causes poor damage tolerance to impact of the composites made from epoxy resins. Hence investigation into the possibilities of modification of epoxy resin blend to impart fracture toughness was warranted. A copolymer of vinyl acetate and 2-ethylhexylacrylate was used for this purpose. The system was made full–IPN by using of Hexa Methoxy Methyl Melamine (HMMM) as crosslinker.

2. EXPERIMENTAL STUDIES

2.1 Materials

Two types of epoxy resins were employed. One was unmodified liquid diglycidyl ether of bisphenol A (Ciba Specialty Chemicals, India, Araldite GY 250) with a furnished value of equivalent weight per epoxide group of 185–192. It was obtained from local market (softening point 84°C, by the Ring & Ball Method).The other was an epoxidized novolac resin synthesized in our laboratory.

Epichlorohydrin was used for epoxidation of novolac and was purchased from S. D. Fine Chemicals, India. Diethylenetriamine, m-phenylene diamine (MPDA) and diamino diphenylsulphone (DPDS) were used in preparation of modified hardeners for the epoxy resins and were also purchased from S.D. Fine Chemicals, India.

Vac-EHA copolymer was in emulsion form. It was obtained from Macromoles, India. Hexa methoxy-methyl-melamine (HMMM) was prepared in the laboratory using a standard procedure (Melter, 1981). The nonionic surfactant, Triton X-100 was purchased from Aldrich (Milwaukee, WI). Jute fiber was extracted from the Jute Fabric. The Jute Fabric was procured from Fort Gloster, India.

2.2 Preparation of Liquid Eutectic Mixture of MPDA, DPDS, and Diglycidyl Ether of Bisphenol A (DGEBA) Adduct (Hardener H-1)

Liquid eutectic mixture of m-phenylene diamine (MPDA) and diamino diphenylsulphone (DPDS) was charged into a three-neck flask fitted with a stir and was

warmed to about 75°C. The liquid DGEBA epoxy resin was slowly added at 46% weight so that the temperature of the resulting exothermic reaction was always kept at around 100°C. The reaction was continued for 3 h. Subsequently the heating was discontinued and when the temperature of the reaction mass had dropped to 55°C, phenol (2% by weight) was added as a cure accelerator, and the thus-obtained blackish liquid was used without further modification after filtration. This liquid has been given "Hardener H-1" name.

2.3   Cyanoethylation of Diehtylene Triamine (Hardener H-2)

The use of a cyanoethylated derivative of diehtylene triamine (DETA) as the second hardener system was to take advantage of the system better wetting ability to jute fiber. Moreover, these water-soluble curing agents obtained by the reaction of DETA with acrylonitrile (cyanoethylation) are of reduced reactivity, i.e., a greater pot life and dependence on the extent of the modification; degree of reactivity can be regulated.

  Based on the desired degree of modification as determined by the acrylonitrile, DETA mole ratio, a pre-calculated quantity of acrylonitrile was charged into a three-neck flask fitted with a stirrer. The desired quantity of DETA was then added in a gradual slow manner. As the cyanoethylation was exothermic and reversible, the whole system was immersed in an ice bath so as to maintain the reaction system at a constant temperature of 20°C throughout the reaction, which proceeded for 4 h with a concomitant rise in viscosity of the reaction mixture. Our hardener H2, a highly modified (cyanoethylated) DETA, was used without further modification. It had a room temperature viscosity of 100 centipoises. With DGEBA, it gave a pot life of in excess of 2.5 h in 50 g batch. After that, adduct was hydrolyzed with NaOH for making it function as a novel curing agent.

2.4   Preparation of Composites

The individual polymers were first separately diluted with distilled water and stirred well to maintain a solid content of 50% by weight for convenience. Then a weighed amount of EPN and DGEBA (50:50) was taken in a three-neck, round–bottom flask. VAc-EHA copolymer was then accurately weighed and introduced into the flask. The mixed hardeners (H1:H2 = 5:1) of the epoxy are added at this mixture at 25% by weight. The contents of the flask were then stirred well to give a homogeneous mixture. When the formation of bubbles ceased, the viscous mass was applied on both sides of jute fabric by hand lay-up technique. The green laminates were squeezed between two Mylar films using pressure of a hand roller so as to minimize voids and to avoid accumulation of excess matrix resin as far as possible. The hand-pressed laminates free from excess resin were allowed to cure. It was then initially kept at room temperature for about 24 h, and then heated in an oven at 80°C for 4 h, followed by further heating at 150°C for 1 h, and finally post cured in an oven at 80°C for 6 h. The samples of semi-IPNs thus obtained

are referred to as S5, S10, S15, and S20 where S denotes semi and 5, 10, 15, and 20 denotes the percentage of VAc-EHA in the IPNs.

In order to get full IPN, a cross linker for the acrylic copolymer, namely HMMM, was added to the mixture at the final stage. In all cases, the concentration of HMMM was kept constant at 20% by weight based on VAc-EHA copolymer. All other operations were identical to those followed for semi-IPNs. The samples of full-IPNs are referred to as F5, F10, F15, and F20 where F denotes full and 5, 10, 15, and 20 denotes the percentage of VAc-EHA in the IPNs.

2.5 Tensile Properties

An Instron universal tensile testing machine (Instron 3366, U.K.) was used for measuring the tensile properties like tensile strength, modulus. ASTM D638 method was followed. A crosshead speed of 5 mm/min was maintained. All testing were conducted under ambient conditions in an environmentally controlled room. The data reported are averages of at least six measurements, and typically scattering range of the results was ±5%.

3. RESULTS AND DISCUSSION

The mechanical properties of both semi-IPNs (where only epoxy was cross linked) and full-IPNs (where both epoxy and VAc-EHA were cross linked) had been studied as a function of blend ratios of epoxy and VAc-EHA.

The mode of change of ultimate tensile strength, transverse and longitudinal moduli of elasticity at different percentage of the VAc-EHA of the semi-IPNs and full-IPNs had been compared and shown in Figs. 1–3. The influence of cross-link-
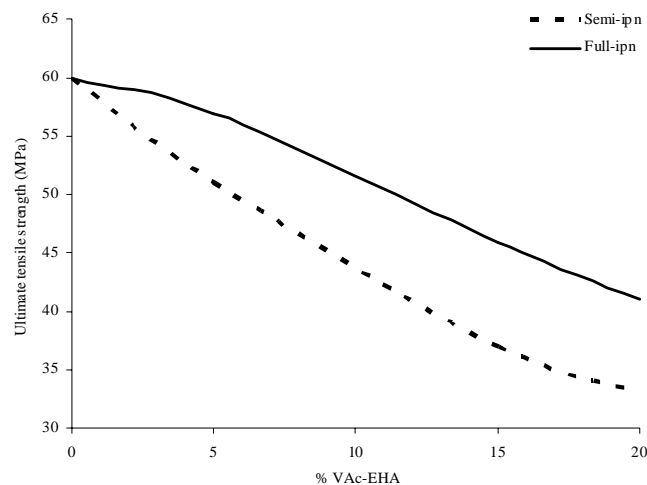
FIG. 1: Ultimate tensile strength of the jute fiber-reinforced Epoxy/VAc-EHA/HMMM IPN composite at different percentage of the VAc-EHA
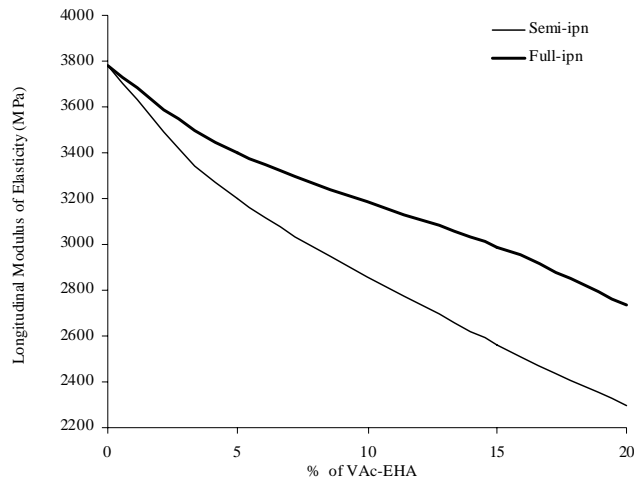
FIG. 2: Longitudinal modulus of elasticity of the jute fiber-reinforced Epoxy/VAc-EHA/HMMM IPN composite at different percentage of the VAc-EHA

ing of the dispersed network of epoxies was quite evident from the figures. In both the cases of semi-IPNs and full-IPNs, there was a reduction in ultimate tensile strength (UTS) and modulus with an increase in the VAc-EHA content. But the difference between semi-IPN and full-IPN increases as soon as the percentage of the VAc-EHA increases. This decreasing trend might be attributed to the following probable reasons
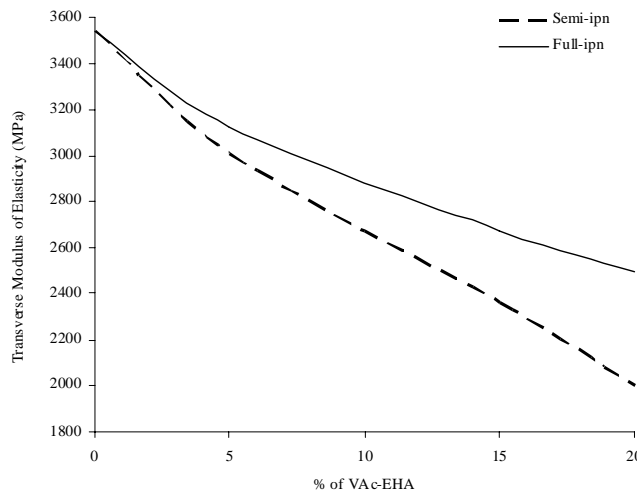
FIG. 3: Transverse modulus of elasticity of the jute fiber-reinforced Epoxy/VAc-EHA/HMMM IPN composite at different percentage of the VAc-EHA
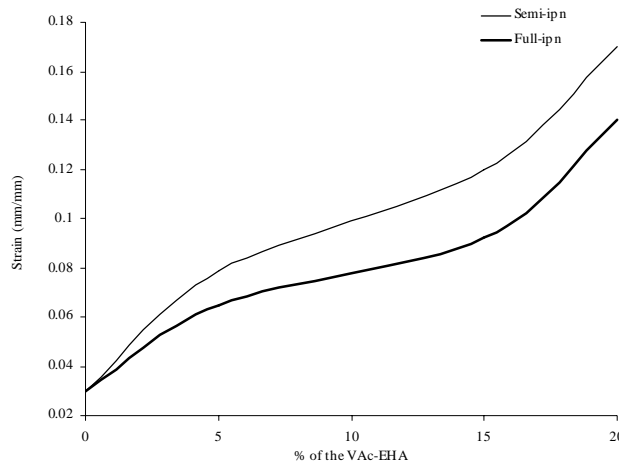
FIG. 4: Strain of the jute fiber-reinforced Epoxy/VAc-EHA/HMMM IPN composite at different percentage of the VAc-EHA

- Reducing the possibility of complete curing sites of epoxies matrix by shielding the reactive sites of epoxies by the dispersed VAc-EHA matrix.
- Another important reason might be the plasticizing that influences the dispersed VAc-EHA domain.

It was observed that full-IPNs of Epoxy/VAc-EHA systems had higher UTS and the modulus of elasticity than semi-IPNs. This could be possibly explained by the fact that the VAc-EHA moieties have a much higher free volume, and there was ample scope of interpenetration by linear chains of VAc-EHA copolymer, hence in the case of full-IPNs the cross links within the chains make them more compact.

Figure 4 shows the strain of the jute fiber-reinforced Epoxy/VAc-EHA/HMMM IPN composite at different percentage of the VAc-EHA. By virtue of a higher extent of interpenetration, strain percentage of semi-IPNs is higher than that of full-IPNs. The curve displays the tendency of necking as the VAc-EHA copolymer content gradually increases. Thus, the change in fracture mechanics from a brittle nature to a ductile one is due to an increase in plastic deformation.

Table 1 shows the tensile strength (TS) of semi-IPN and full-IPN at different percentage of the VAc-EHA. At 0% of the VAc-EHA, TS of semi-IPN and full-IPN is same. But as soon as the percentage of the VAc-EHA increases the tensile strength of full-IPN decreases at a slower rate compared to semi-IPN.

After introducing the VAc-EHA, tensile strength of the jute fiber-reinforced semi-IPN composite decreases at a faster rate as compared to full-IPN. In full-IPN both epoxy and VAc-EHA were cross linked. Due to cross link of epoxy and VAc-EHA, a jute fiber-reinforced full-IPN composite plate becomes harder than a jute fiber-reinforced semi-IPN (where only epoxy was cross linked) composite

TABLE 1: Tensile properties of the jute fiber reinforced Epoxy/VAc-EHA/HMMM IPN composite

Code	Semi-IPN					Full-IPN				
	S0	S5	S10	S15	S20	F0	F5	F10	F15	F20
%VAc-EHA	0	5	10	15	20	0	5	10	15	20
T.S. (MPa)	60	51	48	37	33	60	57	54	46	41

plate. A jute fiber-reinforced semi-IPN composite plate is soft. Therefore, a jute fiber-reinforced semi-IPN composite plate dissipates more energy compared to a jute fiber-reinforced full-IPN composite plate.

4. CONCLUSIONS

Jute fiber-reinforced semi-IPN (where only epoxy was cross linked) and full-IPN (where both epoxy and VAc-EHA were cross linked) Epoxy/VAc-EHA/HMMM IPN composite plates have been prepared in a laboratory at different volume fractions of VAc-EHA for the evaluation of mechanical properties. Theoretical static and dynamic analyses of the composite plate have also been presented in this work.

As soon as the percentage of the VAc-EHA increases, the ultimate tensile strength and modulus of elasticity of jute fiber-reinforced semi-IPN and full-IPN composite plates decrease. The tensile strength and modulus of elasticity of the jute fiber-reinforced full-IPN composite plate decreases at a slower rate compared to a jute fiber-reinforced semi-IPN composite plate. In a jute fiber-reinforced semi-IPN composite plate, only epoxy was cross linked as compared to a jute fiber-reinforced full-IPN composite plate where both epoxy and VAc-EHA were cross linked. Therefore, a jute fiber-reinforced full-IPN composite plate was compact and harder as compared to jute fiber-reinforced semi-IPN composite plate. Due to this reason damping properties of the jute fiber-reinforced semi-IPN composite plate is better than a jute fiber-reinforced full-IPN composite plate. And the extent of interpenetration of VAc-EHA the strain percentage of semi-IPNs are also higher than those of full-IPNs.

REFERENCES

Corrales, F., Vilaseca, F., Llop, M., Giron'es, J., Mendez, J. A., and Mutje, P., Chemical modification of jute fibers for the production of green-composites, *J. Hazard. Mater.*, vol. 144, pp. 730–735, 2007.

Gassan, J. and Bledzki, A. K., Possibilities for improving mechanical properties of jute/epoxy composites by alkali treatment of fibers, *Comput. Sci. Technol.*, vol. 59, pp. 1303–1309, 1999.

Idicula, M., Malhotra, S. K., Joseph, K., and Thomas, S., Dynamic mechanical analysis of randomly oriented intimately mixed short banana/sisal hybrid fiber reinforced polyester composites, *Comput. Sci. Technol.*, vol. 65, pp. 1077–1087, 2005.

Kishore, M. R., Jute-glass sandwich composites, *J. Reinf. Plast. Compos.*, vol. 4, pp. 186–194, 1985.

Melter, Y. L., Water Soluble Polymers Development since 1978; Park Ridge, NJ: Noyes Data Corporation, 1981.

Monteiro, S. N., Terrones, L. A. H., and D'Almeida, J. R. M., Mechanical performance of coir fiber/polyester composites, *Polym. Test*, vol. 27, pp. 591–595, 2008.

Rana, A. K., Mandal, A., and Bandyopadhyay, S., Short jute fiber reinforced polypropylene composites: effect of compatibiliser, impact modifier and fiber loading, *Comp. Sci. Technol.*, vol. 63, pp. 801–806, 2003.

Rana, A. K., Mandal, A., Mitra, B. C., Jacobson, R., Rowell, R., and Banerjee, A. N., Short jute fiber-reinforced polypropylene composites: effect of compatibilizer, *J. Appl. Polym. Sci.*, vol. 69, pp. 329–338, 1997.

Thwe, M. M. and Liao, K., Effects of environmental aging on the mechanical properties of bamboo-glass fiber reinforced polymer matrix hybrid composites, *Composites A*, vol. 33, pp. 43–52, 2002.

STUDY OF ELASTIC AND STRENGTH PROPERTIES OF HYBRID AND GRADIENT POLYMER COMPOSITES

A. M. Kuperman,[*] R. A. Turusov, & A. Ya. Gorenberg

N. N. Semenov Institute of Chemical Physics, Russian Academy of Sciences, Moscow, Russia

[*]Address all correspondence to A. M. Kuperman E-mail: viva@chph.ras.ru

The paper deals with the properties of hybrid (HPC) and gradient (GPC) polymer composites depending on the ratio of the content of different fibers. The major factor governing the regularities of the mechanical behavior of composites is the ratio of ultimate strains of reinforcing fibers. Synergy effects of increasing deformability of carbon fibers under tension and organic fibers under compression in a glass-fiber-reinforced (GFR) matrix are observed. Gradient materials with a nonuniform structure enable one to assign a law of variation of the material stiffness, which gives an optimal stress distribution in a whole product under loading.

KEY WORDS: *hybrid and gradient polymer composites, elastic and strength properties*

Creation of hybrid (HPC) and gradient (GPC) polymer composites combining two and more types of fibers (glass, organic, carbon, boron) is a promising trend in the development of modern technical equipment since it extends the capabilities of creating materials with the specified properties (Gunyaev et al., 1976, 1977; Rumyantsev et al., 1981; Complex, 1982).

The present paper is aimed at investigation of elastic and strength characteristics of unidirectional HPC depending on the volumetric ratio and structural position of reinforcing fibers of different types.

In creating HPC we strived for obtaining specimens with a mixed but, if possible, more uniform structure. For this purpose we used reinforcing threads with low linear density: 55 tex "E" and "S" glass fibers, 29 tex SVM aramide organic fibers (analog of Kevlar), 400 tex KBSN boron fibers (this is a yarn composed of seven boron fibers enclosed in a glass braid). Carbon fibers with a linear density of 25 tex were removed from the LU-3 carbon fiber tape. Bobbins with two types of fibers were placed on the bobbin holder, then they were wound off at a given proportion and the fibers simultaneously run through the impregnation-tension tract. The EDT-10 epoxy diane resin (analog of DGEBA) was used as a binder.

Individual unidirectional rings were wound over sectional steel mandrels 150 mm in diameter, which were assembled into a block consisting of 12 mandrels; each mandrel was 10 mm wide. The mandrels for tension rings consisted of two half-disks that were used in testing of rings. Longitudinal reciprocal motion of impregnated threads along a 10-mm mandrel was executed with the help of a calm-type feed-eye. The winding parameters were: winding speed of 8 m/min, tension of 1.5–2 kg, winding pitch of 1.2 mm/rev, and binder temperature of 50°C. The time of winding was determined by the required thickness of rings. For the specimens tested under tension and compression the thickness was 1.5–2.5 mm (that equaled two double passes of the feed-eye with impregnated threads). Moreover, one ring with a threefold thickness was wound in order to determine the content of the binder and the porosity of specimens. The cure regime was: 2 h at 120°C and 6 h at 160°C. The obtained composites had about 40 vol.% of binder.

The specimens were tested under tension at the 1958U-10-1 test machine (analog of the Instrone) with a maximum load of 10 tons. The strain rate was 15 mm/min. The outer surface of compression specimens was polished, then the specimens were removed from the mandrel and tested with the aid of a 72-cam test devise (developed at the "Stekloplastic" Scientific and Production Association) that provided a uniform field of loading. As a result of experiments, the tension and compression diagrams of the ring specimens σ–ε were obtained; these diagrams allowed one to determine elastic and strength properties of specimens and describe the processes in the specimens under loading.

The most important factor that affects the character of the mechanic behavior of HPC, especially in tension, is the value of ultimate strains of reinforcing fibers. Organic/glass and boron/carbon fiber reinforced plastics were studied as HPC, in which the fibers with close strain characteristics are combined. It was shown that the mechanic behavior of such materials in tension, compression, bending, and shear generally agree with the additivity concept, i.e., the ideas of proportional contribution of each component to mechanical characteristics of HPC. The diagrams given in Fig. 1 are mainly linear. Fibers of different types break down virtually simultaneously. Of course, in combining various fibers the dispersion of ultimate strains increases thus affecting the strength of HPC.

Another character of regularities is observed in investigation of HPC combining fibers of different deformability. Under tension of glass/carbon, organic/carbon and boron/glass fiber reinforced plastics, the fibers do not break simultaneously. In this case, the ultimate strain of composites is determined, mainly, by deformation of those fibers whose volumetric content prevails. We denote low-modulus reinforcing fibers by subscript 1 and high-modulus ones by subscript 2.

In the case of a low content of the fibers with high modulus E_2 (and low elongation $\bar{\varepsilon}_2$), the ultimate strain of the composite is equal to the ultimate strain of low-modulus fibers $\bar{\varepsilon}_1$, and its strength σ_{c1} is found from the following equation:

$$\sigma_{c1} = \bar{\varepsilon}_1(E_m V_m + \bar{E}_1 V_1). \tag{1}$$
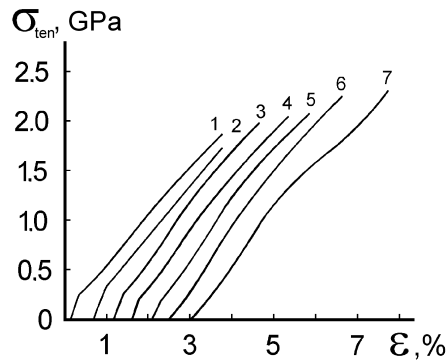
FIG. 1: Stress-strain curves $\sigma-\varepsilon$ of organic/glass FRP ring specimens composed of VMP glass fibers and SVM organic aramide fibers. The ratios of organic to glass fiber sections are: 1) 100:0; 2) 84:16; 3) 68:32; 4) 51:49; 5) 33:67; 6) 16:84; 7) 0:100

In the case of a high content of the fibers with high modulus E_2 (and low elongation $\bar{\varepsilon}_2$), the ultimate strain of the composite is equal to the ultimate strain of fibers $\bar{\varepsilon}_2$ and its strength $\sigma_{c(1+2)}$ is calculated by the formula

$$\sigma_{c(1+2)} = \bar{\varepsilon}_2(E_m V_m + \bar{E}_1 V_1 + E_2 V_1).\tag{2}$$

The portion of strength introduced by the matrix $\varepsilon\ E_m V_m$ can be neglected since it does not exceed 2–3% of the strength of fibers.

The mechanism of destruction of HPC changes on reaching some critical ratio of fibers with different moduli μ_{cr2}, which can be found from

$$\frac{\bar{\varepsilon}_2 \cdot \bar{E}_2}{\bar{\varepsilon}_1 + \bar{\varepsilon}_2(\bar{E}_2 - \bar{E}_1)}\ .\tag{3}$$

Figure 2 gives the stress-strain curves of glass/carbon FRP. The curves are presented for HPC with different content of high-modulus fibers. In this case, μ_{cr2} calculated by formula (3) is about 25 vol.%. In the initial section of stress-strain curves (section I), glass and carbon fibers in HPC deform simultaneously. The slope of the curves corresponds to the elasticity modulus obtained from additivity principles. Carbon fibers begin to break down at a relative deformation of 0.7–1.0% (~600 MPa). When the content of carbon fibers exceeds μ_{cr2} (curves 1 and 2) complete destruction of ring specimens takes place.

With the content of carbon fibers below some critical value Åcr2, nonlinear sections II (curves 3–6) appear on the diagrams $\sigma-\varepsilon$. These nonlinear sections indicate the destruction of carbon fibers in the glass-fiber-reinforced plastic matrix, finally, to the segments of a "critical" length. Nonlinear sections II terminate at deformation ε equal to about 2%. Then virtually linear sections III (curves 3–7) are observed: only glass fibers carry the load at the stage. The elasticity moduli and
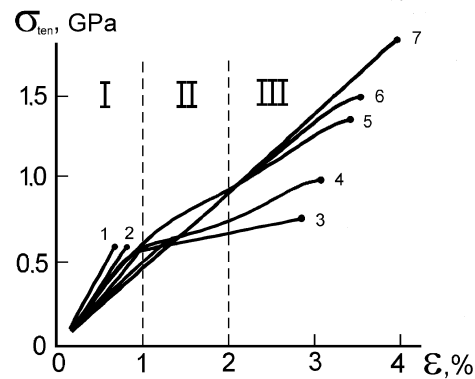
FIG. 2: Stress-strain curves $\sigma-\varepsilon$ of glass/carbon FRP ring specimens (the numbers of curves correspond to the ratios given in Table 1)

strength of specimens in this section are determined by volume fractions of the components. Destruction of such HPC occurs at deformation ε_1 equal to 3–4%.

Table 1 gives the values of the elasticity modulus, strength, and ultimate strain obtained from stress-strain curves of glass/carbon FRP.

The elasticity modulus of ring specimens in the first section of the diagram $E_{(1+2)}^{I}$ is linearly dependent on the ratio of fibers with different moduli, which corresponds to the additivity principle. It consists of two components introduced, correspondingly, by glass and carbon fibers E_1^{I} and E_2^{I}. The values of these components are tabulated in columns 4 and 5 of Table 1: they are calculated from

TABLE 1: Characteristics of fibers in glass/carbon fiber reinforced plastics obtained from the stress-strain curves $\sigma-\varepsilon$

No.	Volumetric ratio of fibers, %		Elasticity modulus, E, GPa				Tensile strength, GPa		Ultimate strain, %	
	1	2	3	4	5	6	7	8	9	10
	V_1	V_2	E_{1+2}^{I}	E_2^{I}	E_1^{I}	E_1^{III}	σ_1	σ_2	ε_1	ε_2
1	0	100	90	90	–	–	–	1.15	–	0.7
2	22	78	75	65	10	–	–	1.33	–	0.8
3	42	58	68	49	19	10	3.12	1.45	2.9	0.9
4	59	41	65	38	27	30	2.88	1.39	3.1	1.0
5	74	26	60	25	35	35	3.15	1.53	3.4	1.2
6	88	12	50	10	40	40	2.84	–	3.5	1.5
7	100	0	46	–	46	46	3.05	–	3.9	–

elasticity moduli and relative contents of the fibers in the composite. Comparison of them with the values of the elasticity modulus on the linear section III of the diagrams E_1^{III} (column 6) shows that after destruction of carbon fibers the elasticity modulus of the material is entirely determined by the elasticity modulus of glass fibers.

Under repeated loading of the specimens, the curves σ–ε are absolutely linear and have the elasticity modulus typical of the third section of the diagrams. No changes are observed in the shape of the curves under multiple (up to 10 times) loading of the specimens. Evidently, carbon fibers do not have additional failure under repeated reloading.[*]

It should be noted that the strength of glass fibers in glass/carbon FRP (after destruction of carbon fibers in the glass-fiber-reinforced matrix) turns to be the same as in unidirectional GFRP (column 7 in Table 1).

The analysis of stress-strain curves σ–ε under tension shows that with an increase in the content of fibers the apparent ultimate strain of carbon fibers increases from 0.7 to 1.5%. A substantial increase in the strain of carbon fibers in glass/carbon fiber reinforced plastic is the "synergy effect" and it is caused by multiple destructions of fibers and appearance of gaps between them.

The nonlinear section II on the stress-strain curves can be treated as the "pseudoplasticity" section caused by gradual fragmentation of carbon fibers and their separation from the matrix. In this case, as is seen, fracture energy increases greatly compared with carbon filled fiber reinforced plastic. Such materials could be of considerable utility in the places of constructions with an increased concentration of stresses.

Figure 3 presents the tensile strength of unidirectional GPC specimens as a function of the ratio of the quantity of two types of fibers. The data are presented for both organic/glass fiber reinforced plastics composed of the fibers with close values of ultimate strains and for GPC based on the fibers with different deformabilities. In the first case, the dependence is linear, whereas in the second case we observe minima which show a deviation of the material strength from the additivity principle. The positions of the minima correspond to μ_{cr1}.

The compression strength of composite materials slightly depends on deformability of elementary fibers. Destruction of HPC occurs, in an ideal case, due to the buckling of the fibers. This indicates that strength of the material is determined, first of all, by the stiffness of reinforcing elements, density of their packing, elasticity modulus, and strength of the polymer matrix, as well as by the shape of specimens and test conditions.

Boron- and glass fiber reinforced plastics possess the highest compression strength since, in this case, a high elasticity modulus is combined with a large diameter of

---

[*]Our data on measurement of electrical conductance of glass-carbon-filled plastic come into conflict with these results. Stable values of electrical conductance were observed only in 5–6 loading–unloading cycles.
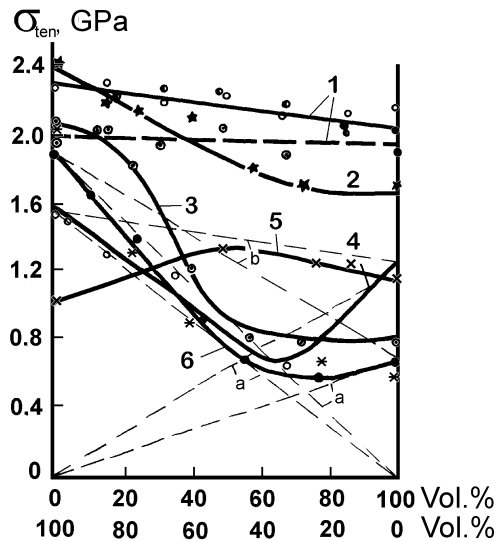
FIG. 3: Tensile strength of HPC as a function of the volumetric ratio of different types of fibers. 1) 1) aramid organic fibers + "S" glass fibers; 2) aramid organic fibers + "E" glass fibers; 3) aramid organic fibers + carbon fibers; 4) "S" glass fibers + boron fibers; 5) carbon fibers + boron fibers; 6) "S" glass fibers + carbon fibers

fibers (90–200 μm for boron fibers and 12–100 μm for glass fibers). Moreover, these fibers are virtually isotropic and have high stiffness and transversal and shear strengths.

Organic fiber reinforced plastics have a very low compressive strength (about 10 times lower than the tensile strength). A high degree of anisotropy of the fibers and their low transversal strength govern early buckling of organic fibers in the material. That is why it is very important to improve the mechanical behavior of carbon and organic fiber reinforced plastics under compression.

Experimental investigation of HPC based on combination of fibers of different types showed that, in most cases, compression strength of materials depends on the volume fiber content (Fig. 4).

Compressive stress-strain curves of materials are also virtually linear; the elasticity modulus remains constant under multiple loading (to 10 times) of the specimens (Fig. 5).

This indicates that carbon and organic fibers within glass fiber or boron fiber matrices do not buckle under the strains and, correspondingly, under the stresses of two-three times higher as compared to carbon and organic fiber reinforced plastics. This synergy effect allows one to have practically additivity principles for the compressive strength of HPC with various ratios of fibers of different moduli (Fig. 6).
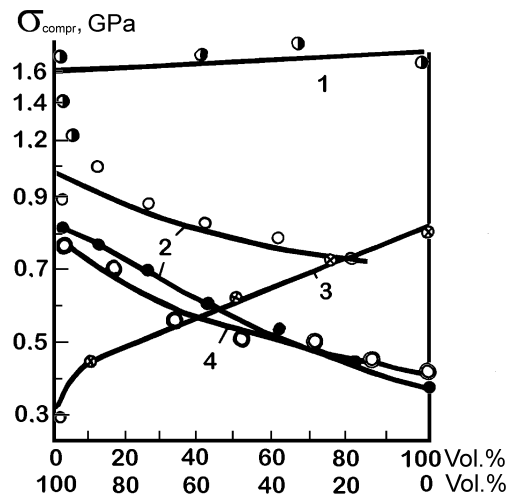
FIG. 4: Compressive strength of HPC vs. volume fractions of various types of fibers. 1) "S" glass fibers + boron fibers; 2) "S" glass fibers + carbon fibers; 3) aramid organic fibers + boron fibers; 4) aramid organic fibers + "S" glass fibers

Figure 7 sums up (in relative units) the obtained experimental data on the properties of HPC based on the combination of four types of fibers with different moduli. It also illustrates the regularities of variation of the elasticity modulus and tensile, compression, bending, and shear strength and density of materials as a function of a relative content of two types of fibers.
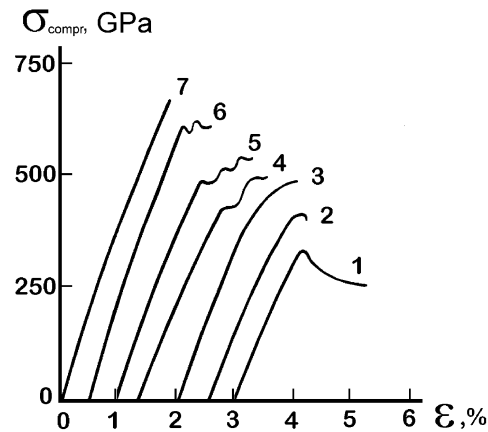
FIG. 5: Compressive stress-strain curves of glass/carbon fiber reinforced plastics (the numbers of the curves correspond to the ratios in Table 1)
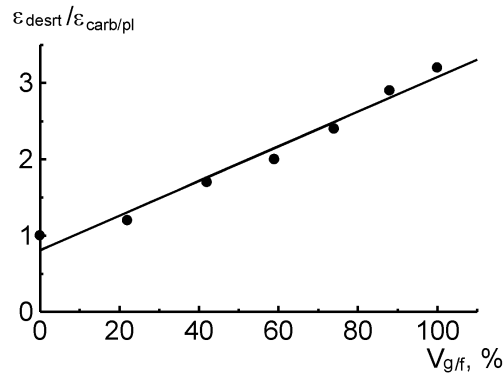
FIG. 6: Increase of deformability of glass/carbon fiber reinforced plastics with increasing glass fiber content

The elasticity modulus and density of materials, their compression strength, and tensile strength of HPC based on the combination of fibers with close values of the ultimate strain can be easily controlled by the ratio of the amount of fibers according to the additivity principle. A deviation from this principle is observed with a considerable difference in the deformabilities of the fibers

$$\alpha - \frac{\gamma}{\gamma_0}, \frac{E}{E_0}, \frac{\sigma_{ten}}{\sigma_0}, \frac{\sigma_{compr}}{\sigma_0}, \frac{\sigma_{bend}}{\sigma_0}, \frac{\tau_{sh}}{\tau_0}.$$

We give some examples of the most rational combination of fibers with different moduli in HPC:

- a combination of glass and organic fibers allows one, on the one hand, to obtain materials with higher compression and shear stresses (compared with organic fiber reinforced plastics) and, on the other hand, to improve specific characteristics of a hybrid system (compared with glass-fiber-reinforced plastics);
- HPC based on the combination of glass and carbon fibers have a higher elasticity modulus compared with glass fiber reinforced plastics. In this case, specific characteristics of materials are retained in compression and slightly decrease in tension. Destruction energy of the specimens increases;
- addition of boron fibers into glass fiber reinforced plastics gives a substantial increase in the elasticity modulus of HPC. In this case, compression strength of materials increases (or remains the same);
- a combination of boron and high-modulus carbon fibers gives an improvement of absolute and specific characteristics of the material (tensile strength, elasticity modulus) compared with both types of monofilament compositions.
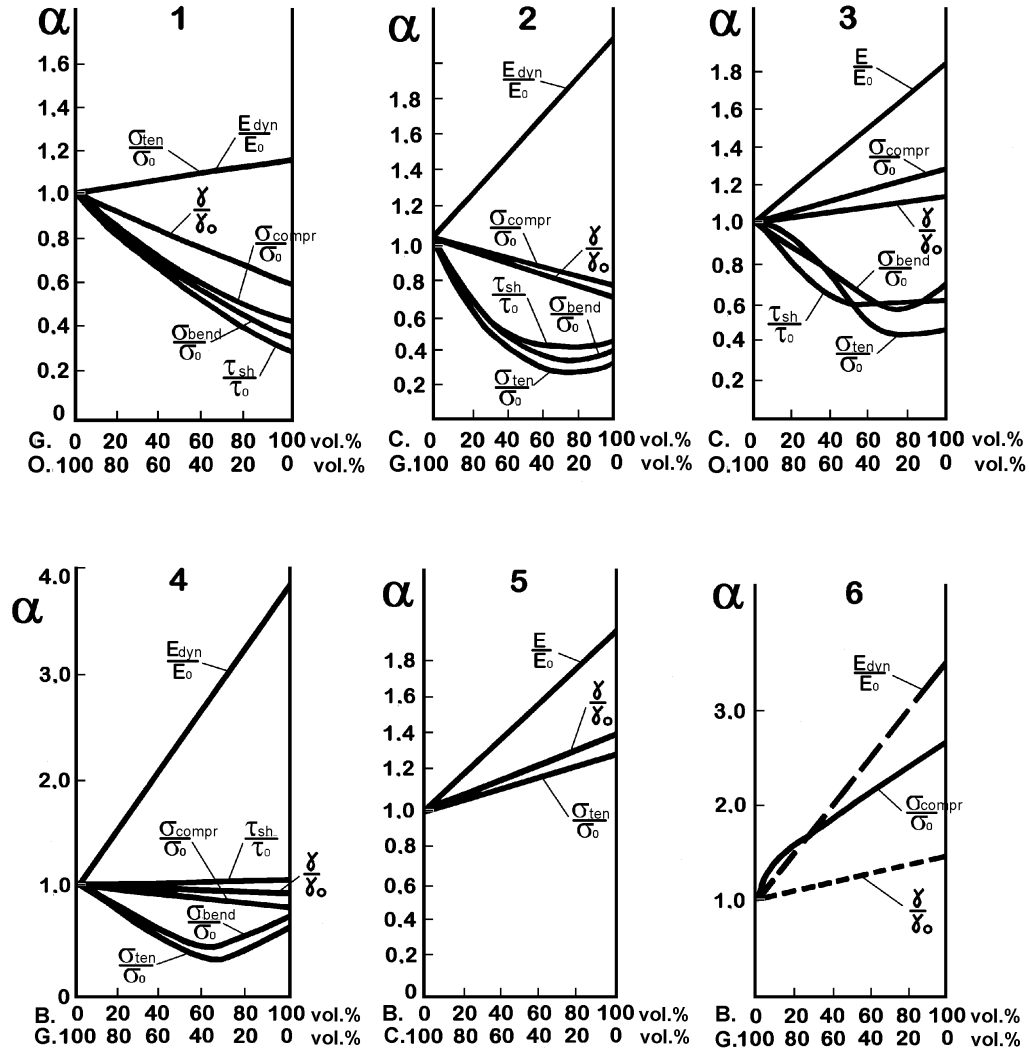
FIG. 7: Relative variation of HPC characteristics (α) as a function of the volume ratio of two types or the fibers (v): glass/organic fiber reinforced plastic (1), glass/carbon fiber reinforced plastic (2), organic/carbon fiber reinforced plastic (3), boron/glass fiber reinforced plastic (4), boron/carbon fiber reinforced plastic (5) and boron/organic fiber reinforced plastic (6) (B – boron; C — carbon; G — glass; O — organic)

With the hybridization principle there arises a possibility to formulate and solve a very important problem. A certain law of variation of material stiffness over the product cross section, which provides an optimum stress field in loading of the entire product, can be specified for some elements of the construction. As an example, we can mention super-flywheels and thick-walled glass-fiber-reinforced pressure shells. In both cases, a linear increase of the elasticity modulus of the material with an increase in the product radius is very efficient; this can be easily achieved by variation of the content of carbon fibers in glass-fiber or organic-fiber plastics.

For materials operating under bending such gradient structure of the composite allows one to change the position of the neutral axis, and to increase the material strength due to the preferred position of aramid fibers in the tension zone and glass fibers in the compression zone.

For studying the elastic and strength characteristics of composites, unidirectional plates of different structures were produced (see Fig. 8):

1) uniform carbon-, glass- and organic fiber reinforced plastics;
2) two-layered plates composed of organic/carbon and organic/glass fiber reinforced plastics;
3) gradient structures where the ratio of organic and glass (carbon) fibers changed gradually.

To obtain the above plates, we produced veneer shits based on three types of fibers and the EFNB epoxy phenol binder were manufactured. Six-layered laminate with a required structure was composed of them, the laminate was pressed at 160°C. The plates had the thickness $h = 2$–3 mm, the width $b = 10$ mm, and the fiber volume content of about 50 vol.%.

Bending tests of the specimens were performed with the aid of the three-point loading scheme. To determine the elasticity modulus E the distance between the supports l was 100 mm ($l/h = 40$). The calculations were performed with the well-known formula $E = \frac{1}{4}\frac{1}{b}\frac{F}{\omega}\left(\frac{l}{h}\right)^3$, were $\frac{F}{\omega}$ is the ratio of the applied force to the specimen bending deflection. The bending strength of the plates σ was determined with the distance between the supports $l = 40$ mm ($l/h = 16$) from the conventional formula $\sigma = \frac{3}{2}\frac{Pl}{bh^2}$. However the formula was derived for the materials with homogeneous structures; therefore, the strengths of the tested specimens were correlated by comparing the ultimate loads P or P/h. The specimens were turned over thus changing the tensile and compression zones under three-point bending.

Table 2 presents some results of the investigation. We should mention the possibility of varying the elasticity modulus of specimens within a wide range. The strength of heterogeneous and gradient structures turned to be much (1.5 fold) higher than that of uniform structures, which is likely related to a nonuniform

Uniform structures

Glass fiber reinforced   Organic fiber reinforced   Carbon fiber reinforced

Two-layer plastics

Gradient structures
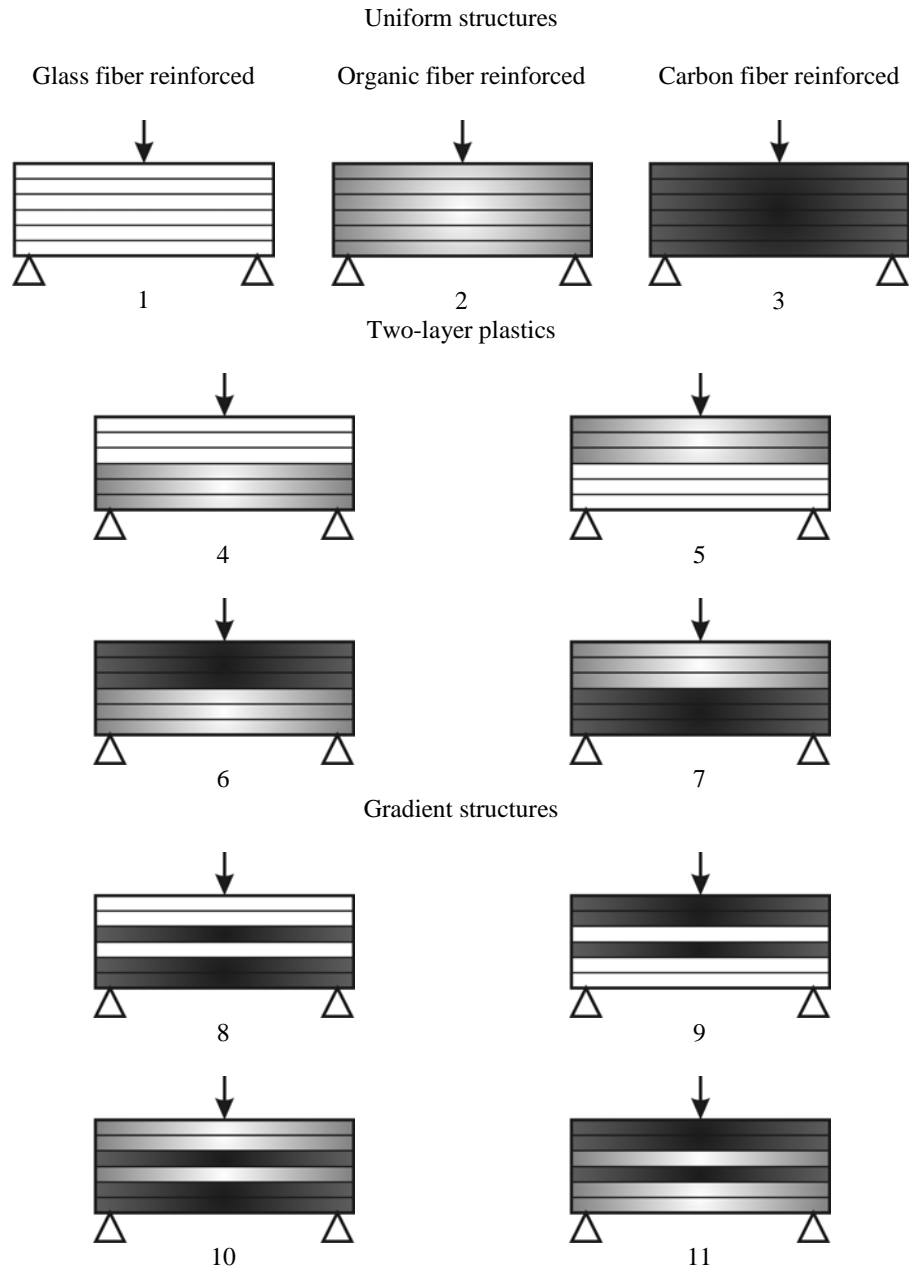
FIG. 8: The sketches of the structures and loading conditions of uniform and nonuniform composite specimens: 1, 2, 3) glass-, organic- and carbon fiber reinforced plastics, respectively; 4, 5) organic/glass fiber reinforced plastics; 6, 7) organic/carbon fiber reinforced plastics; 8, 9 and 10, 11) gradient structures of glass/carbon and organic/carbon fiber reinforced plastics, respectively

TABLE 2: Elastic and strength characteristics of unidirectional composites with uniform and gradient structures under bending

No.	Material	E, GPa ($l/h \approx 40$)	h, mm	P, kg ($l/h \approx 20$)	P/h, kg/mm	σ, GPa ($l/h \approx 16$)
1	Carbon-fiber reinforced plastic	75	2.35	47.3	20.1	0.51
2	Glass fiber reinforced plastic	42	2.37	47.6	20.1	0.51
3	Organic fiber reinforced plastic	49	2.10	31.1	17.7	0.50
Two-layered plates						
4	Organic/glass fiber reinforced	71	2.13	62.3	29.2	0.82
5	plastic	52		46.4	21.8	0.61
6	Organic/carbon fiber reinforced	44	2.25	61.2	27.2	0.73
7	plastic	69		56.3	25.0	0.67
Gradient structures						
8	Glass/carbon fiber reinforced	54	2.62	81.1	30.9	0.71
9	plastic	44		67.9	25.9	0.59
10	Organic/carbon fiber reinforced	54	2.50	84.5	33.8	0.81
11	plastic	40		68.0	27.2	0.65

stress field that is to be calculated. We observed regularities typical of the hybrid structures, namely, the characteristics of materials are improved by introduction of organic (aramid) fibers into the tension zone and of glass fibers into the compression zone.

Gradient composites substantially extend the potentials of polymer composite materials. Practically all "natural constructions" (trunks and stems of plants, bones, protecting needles of plants and animals, beaks and flags of birds, etc.) have the same structure. It is evident that we are far behind the nature in this problem and we have an enormous reserve for improving the operating characteristics of artificial products.

ACKNOWLEDGEMENT

REFERENCES

Complex of Works on Development and Introduction into National Economy of Hybrid Polymer Composite Materials. For official use only. 3/5263-66. Institute of Chemical Physics of the Academy of Sciences of the USSR, Moscow, 1982.

Gunyaev, G. M., Rumyantsev, A. F., Avrasin, Ya. D., and Goryushkin, V. A., *Three-Component Composite Plastics. Nonmetal Composite Materials*, ONTI, VIAM, 1974, 1977, Issue II.

Gunyaev, G. M., Rumyantsev, A. F., Rabotnov, Yu. N., and Stepanychev, E. N., Polyfiber composite materials, *Plastmassy*, no. 9, pp. 31–33, 1976.

Rumyantsev, A. F., Gunyaev, G. M., Felkova, N. N., Stepanychev, E. N., and Mamudov, I. M., Optimization of the composition and reinforcement structure of bi- and three-component composite materials. In: *Composites*, Moscow: Nauka Press, 1981.

TABLE OF CONTENTS FOR VOLUME 1

Composites: Mechanics, Computations, Applications
An International Journal

AUTHOR INDEX FOR VOLUME 1

Composites: Mechanics, Computations, Applications
An International Journal

SUBJECT INDEX FOR VOLUME 1

Composites: Mechanics, Computations, Applications
An International Journal